

**A STUDY OF MARINE CSEM SURVEY
GEOMETRY FOR SEABED LOGGING**

NAZABAT HUSSAIN

MASTER OF SCIENCE
ELECTRICAL AND ELECTRONIC
ENGINEERING

UNIVERSITI TEKNOLOGI PETRONAS

SEPTEMBER 2011

STATUS OF THESIS

Title of thesis

A study of Marine CSEM Survey Geometry for Seabed Logging

I NAZABAT HUSSAIN

hereby allow my thesis to be placed at the Information Resource Center (IRC) of Universiti Teknologi PETRONAS (UTP) with the following condition:

1. The thesis becomes the property of UTP.
2. The IRC of UTP may make copies of the thesis for academic purpose only.
3. This thesis is classified as

☐

Confidential

☒

Non-confidential

If this thesis is confidential, please state the reason:

The contents of the thesis will remain confidential for _____ years.

Remarks on disclosure:

Endorsed by

Signature of Author

Permanent address

MA 248, St. No 24 Dhoke

Syedra Rawalpindi

Pakistan

Date: 13 Sept 2011

Signature of Supervisor

Name of Supervisor

Assoc. Prof. Dr. Mohd. Noh Karsiti

Date: 13 Sept 2011

UNIVERSITI TEKNOLOGI PETRONAS

A STUDY OF MARINE CSEM SURVEY GEOMETRY FOR SEABED LOGGING

by

NAZABAT HUSSAIN

The undersigned certify that they have read and recommended to the post graduate studies program for acceptance this thesis for the fulfillment of the requirement for the degree stated.

Signature: _____

Main Supervisor: Assoc. Prof. Dr. Mohd. Noh Karsiti

Signature: _____

Co-supervisor: Dr. Zainal Arif Burhanudin

Signature: _____

Head of Department: Dr. Nor Hisham Bin Hamid

Date: 13 Sept 2011

A STUDY OF MARINE CSEM SURVEY GEOMETRY FOR SEABED LOGGING

by

NAZABAT HUSSAIN

A Thesis

Submitted to the Postgraduate Studies Program

as a Requirement for the Degree of

MASTER OF SCIENCE

DEPARTMENT OF ELECTRICAL AND ELECTRONIC ENGINEERING

UNIVERSITI TEKNOLOGI PETRONAS

BANDAR SERI ISKANDAR

PERAK

September 2011

DECLARATION OF THESIS

Title of thesis

A Study of Marine CSEM Survey Geometry for Seabed Logging

I NAZABAT HUSSAIN

hereby declare that the thesis is based on my original work except for quotations and citations which have been duly acknowledged. I also declare that it has not been previously or concurrently submitted for any other degree at UTP or other institutions.

Witnessed by

Signature of Author

Permanent address:
MA 248, St. No 24 Dhoke
Syedani Rawalpindi
Pakistan
Date: 13 Sept 2011

Signature of supervisor
Name of Supervisor

Assoc. Prof. Dr. Mohd. Noh Karsiti

Date: 13 Sep 2011

DEDICATION

I dedicate this research work to beloved and last Messenger of Mercy, Prophet Muhammad (صلى الله عليه و آله وسلم), to His family, to His companions (رضوان الله عليه (اجمعين), to my honorable sheikh “*Israr-ul-Haq*” and my beloved parents.

I also dedicate this research work to my wife, to my beloved daughter Mahrukh, to my sibling and to my nieces and nephews. I also dedicate my work to my supervisor, to my co supervisor, to Norashikin Yahya and Noor Hazrain on practical support. I also dedicate to all my friends and family who have always been a great moral and practical support and a source of security and joy in my life.

ACKNOWLEDGEMENT

The foremost thank to Almighty Allah who give me the patience, environment and the intellectual ability to complete this research work. I would like to thank my supervisor, Dr. Mohd Noh B. Karsiti and co-supervisor, Dr. Zainul Arif Burhanudin on their help and guidance, which they provided me with great patience and diligence. I would also like to thank Norashikin Yahya, Asif Iqbal, Bilal Munir Mughal and Aamir Malik on their moral and practical support throughout the degree.

I would like to acknowledge the department of Electrical and Electronic Engineering for providing the good and comfortable working environment. I would like to acknowledge the staffs of Electrical and Electronic engineering Department who had assisted me in my research work. I would like to thank EM exploration group from Universiti Teknologi PETRONAS who have created a nice environment for discussion on marine CSEM geophysical survey, without it completion of this research work would not be possible.

In the same time, I would like to thank my all dear friends Mr. Asif Ali Waggan, Mr. Haseeb Dilshaad, Mr. Aamir Amin, Mr. Mubashir, Mr. Asim Qureshi, Mr. Sohail Safder, Mr. Muhammad Imran Khan and Mr. Usman Khalid. They have been a source of love and joy during my studies at Universiti Teknologi PETRONAS (UTP). I would like to acknowledge Universiti Teknologi PETRONAS (UTP), Malaysia for providing me the monetary resources and infrastructure to complete this research work.

Finally I would like to acknowledge to my Mother, wife, to Nabila Akhter, to my siblings, my nephews and my in-laws for reminding me there are more important things in life than my study.

ABSTRACT

In recent years marine Controlled Source Electromagnetic (CSEM) method is being used for hydrocarbon exploration in deeper water. The marine CSEM is preferred over seismic due to its ability to differentiate reservoir of resistive hydrocarbon and conductive saline fluids. In marine CSEM method, however, the survey data is highly dependent on source-receiver position and orientation. Furthermore, real geological conditions are extremely varied and it is rarely possible to turn the survey data into reliable picture of geological structure using virtual simulation. Consequently, it is important to understand EM field behavior for various geological models and source-receiver position to improve virtual simulation process. The aforementioned aspect studied through comprehensive forward modeling is an alternate to real time geophysical surveys. In this research, a forward modeling algorithm is employed as a *staggered-grid* finite difference solution to the total-electric field Maxwell's equations. Solution are achieved through (i) an optimal grid technique that extends the boundaries of the mesh outward from the region of interest using a minimal number of nodes, and (ii) a direct matrix solution technique that allows for simultaneous solution for all sources. The forward modeling algorithm is applied on 1D and 2D geological models implemented using MATLAB. Results obtained provide qualitative understanding of electromagnetic signal propagation through different stratified media with various source positions and orientation. 1D forward modeling is used to find optimal frequency for specific depth and for studying effects of speed variation of dipole source. The 2D forward modeling is used to understand EM field behavior for resistive hydrocarbon and conductive saline fluid reservoirs. Furthermore, inaccuracy due to improper survey geometry such as dipping effect is also analyzed and discussed. In essence, forward modeling was applied to various scenarios and obtained results were accurately matched with previously published work of real time survey. This is a significant step towards the improvement in confidence modeling which in turn can potentially help to reduce surveying cost.

In compliance with the terms of the Copyright Act 1987 and the IP Policy of the university, the copyright of this thesis has been reassigned by the author to the legal entity of the university,

Institute of Technology PETRONAS Sdn Bhd

Due acknowledgement shall always be made of the use of any material contained in, or derived from, this thesis.

© Nazabat Hussain, August 2011

Institute of Technology PETRONAS SdnBhd

All rights reserved.

TABLE OF CONTENTS

Abstract	vi
Chapter	
1. INTRODUCTION	
1.1 Geophysical Survey	1
1.2 Electromagnetic Geophysical Surveys.....	1
1.3 Geophysical Modeling	3
1.4 Marine Controlled Source EM Method.....	4
1.5 Problem Statement	7
1.6 Research Objective and Contribution.....	8
1.7 Thesis Organization	8
2. EM METHODS IN GEOPHYSICS	
2.1 History.....	11
2.2 Basic Principles of EM induction	12
2.2.1 Field Governing Equations	12
2.2.2 Quasi-Static Equations	15
2.3 Skin depth, Wavelength and Phase Velocity	16
2.3.1 Skin Depth	16
2.3.2 Wavelength	19
2.3.3 Phase Velocity	20
2.4 Horizontal Electric Dipole	21
2.4.1 Auxiliary Potential Functions	23
2.4.2 Infinitesimal Dipole	26
2.5 Reflection and Refraction	29
2.6 Forward Modeling.....	31
2.7 Summary	32
3. ONE DIMENSIONAL NUMERICAL SOLUTION	
3.1 Introduction.....	35
3.2 Finite Difference Scheme for 1D Model.....	36
3.3 Stability and Accuracy of FD method.....	41
3.4 1D Forward Modeling.....	41
3.4.1 1D Isotropic Geological Model.....	42
3.4.2 Numerical Results of Isotropic geological Model	43
3.4.3 1D Anisotropic Geological Model.....	46
3.4.4 Numerical Results of Anisotropic geological Model	47
3.5 Summary	48

4. TWO DIMENSIONAL FORWARD MODELING USING FINITE DIFFERENCE METHOD	
4.1 Introduction.....	49
4.2 EM Field Equations	50
4.3 Signal Propagation in 2D Model.....	53
4.4 FD Scheme for 2D Geological Model	54
4.5 Far Field Region and 2D Modeling	58
4.6 Single Interface Model	59
4.7 Numerical Results for Single Interface Model	61
4.8 Multi-Interface Geological Model	63
4.9 Numerical Results for Multi-Interface Model	65
4.10 Summary	67
5. SOURCE DIPOLE DIPPING AND OPTIMAL MOVING SPEED	
5.1 Introduction.....	69
5.2 Controlled Source Orientation	70
5.3 Numerical Modeling for Dipping Dipole Source	72
5.3.1 Numerical Modeling for GMD-I.....	72
5.3.2 Numerical Results for GMD-I	73
5.3.3 Numerical Modeling for GMD-II	74
5.3.4 Numerical Results for GMD-II	75
5.4 Phase Velocity in Conductive Medium	79
5.5 FD Scheme in Spatial and Temporal Domain	80
5.6 Isotropic Media for Modeling in Temporal Domain.....	84
5.7 Numerical Results	85
5.8 Summary	86
6. CONCLUSSION AND FUTURE WORK	87
LIST OF PUBLICATIONS	
1. 1D Forward Modeling of Marine CSEM Survey for Seabed Logging.	
2. 1D Modeling of Controlled-Source Electromagnetic(CSEM) Data using Finite Element Method for Hydrocarbon Detection in Shallow Water.	
3. Mapping of Hydrocarbon with Marine EM Method using 2D Forward Modeling.	
4. Forward Modeling of Infinitesimal Dipole Dipping Effects in Marine CSEM Survey	
5. Forward Modeling to Study topography Effects on EM Signal Using FEM	
6. Finite Difference Approximation to calculate Optimal Speed of Mobile Source in Marine CSEM Survey	

REFERENCES

APPENDICES

- A. ALGORITHM FOR 1D GEOLOGICAL MODEL
- B. ALGORITHM FOR SINGLE INTERFACE GEOLOGICAL MODEL
- C. ALGORITHM FOR MULTI INTERFACES GEOLOGICAL MODEL
- D. ALGORITHM FOR DIPPING EFFECTS IN 2D GEOLOGICAL
MODEL
- E. ALGORITHM FOR 1D FTCS SCHEME

LIST OF FIGURES

Figure 1.1	Flow Diagram of EM Geophysical Modeling	3
Figure 1.2	Layout of Marine CSEM Survey.....	4
Figure 2.1	Phasor Diagram	17
Figure 2.2	Skin Depth	19
Figure 2.3	Phase Velocity	21
Figure 2.4	Dipole Distributed Field	22
Figure 2.5	Geometrical arrangement of Infinitesimal Dipole.....	27
Figure 2.6	Radiation Pattern of Infinitesimal Dipole.....	28
Figure 2.7	Reflections and Refraction.....	29
Figure 2.8	Flow Diagram of Forward Modeling	32
Figure 3.1	FD Scheme	37
Figure 3.2	1D results of MVO comparison	37
Figure 3.3	Isotropic Geological Model.....	43
Figure 3.4	Numerical Results of 1D isotropic Model (Layer-I)	44
Figure 3.5	Numerical Results of 1D isotropic Model (Layer-II).....	45
Figure 3.6	Numerical Results of 1D isotropic Model (Layer-III)	45
Figure 3.7	Numerical Results of Phase for 1D Isotropic Model.....	45
Figure 3.8	1D anisotropic Model.....	46
Figure 3.9	Magnitude Response of 1D anisotropic Model	47
Figure 3.10	Phase Response of 1D anisotropic Model	48
Figure 4.1	Propagation Path Model	50
Figure 4.2	Discretization of 2D media.....	55
Figure 4.3	Boundary Conditions for 2D solution region	57
Figure 4.4	Skin Depth versus Frequency.....	58
Figure 4.5	Total Penetration Depth.....	59
Figure 4.6	2D results of MVO comparison	59
Figure 4.7	Single Interface Model	60
Figure 4.8	MVO for Single Interface Model	62
Figure 4.9	PVO for Single Interface Model.....	62
Figure 4.10	Multi Interface Model.....	64
Figure 4.11	MVO and PVO for Multi-Interface Model	66
Figure 5.1	Dipole Orientation in marine CSEM survey	70
Figure 5.2	Dipping of Source Dipole.....	71
Figure 5.3	2D Geological Model of Dipping-1	73
Figure 5.4	Numerical Results of GMD-I.....	73
Figure 5.5	2D Geological Model of Dipping-1	74
Figure 5.6	MVO and PVO response of HED-I.....	77
Figure 5.7	MVO and PVO response of HED-II	77
Figure 5.8	MVO and PVO response of HED-III	77
Figure 5.9	MVO and PVO response of HED-IV	78
Figure 5.10	MVO and PVO response of HED-V	78
Figure 5.11	View of inline profiling technique.....	79
Figure 5.12	Discretization in space and time domain	82

Figure 5.13	1D isotropic geological model.....	84
Figure 5.14	Numerical Results for 1D Isotropic Model	85

LIST OF TABLES

Table 2.1	Wavelength of Wave in Conductive Medium	20
Table 3.1	EM parameters of 1D an-isotropic Model.....	44
Table 3.2	EM parameters of Numerical Results for 1D Isotropic Model.....	47
Table 4.1	EM parameters for Single Interface Mode	61
Table 5.1	Maximum Penetration Depth.....	75
Table 5.2	Maximum penetration depth of EM wave in conducting medium	82
Table 5.3	Stability Factor.....	83
Table 5.4	Separation distance between p_1 and p_2 at certain speed of dipole	86

*“Imagination is more important than knowledge. Knowledge is limited.
Imagination encircles the world”*

Albert Einstein

LIST OF SYMBOLS

σ	Electrical conductivity (S/m)
μ	Magnetic permeability (H/m)
ϵ	Electric permittivity (F/m)
\mathbf{J}_s	External Source current density (A/m ²)
\mathbf{J}_s^m	Magnetic source current density (A/m ²)
\mathbf{J}_s^e	Electric source current density (A/m ²)
\mathbf{J}_c	Conduction current density (A/m ²)
\mathbf{E}	Electric field intensity (V/m)
\mathbf{D}	Electric field density (W/m ²)
\mathbf{B}	Magnetic field density (C/m ²)
\mathcal{H}	Magnetic field intensity (A/m ²)
α	Attenuation constant (N/m)
β	Phase constant (r/m)
γ	Propagation constant
λ	Wave length (m)
η	Intrinsic impedance (Ohm)
k	Wave number
i	Imaginary Unit
ω	Radial frequency (Radial/Sec)
φ	Zenith angle/dipping angle
ψ	Vector field
θ	Azimuth angle, phase angle
$\int dl$	Line integral
$\iint ds$	Surface integral
$\iiint dv$	Volume integral
Π_e	Auxiliary potential vector for magnetic field
Π_h	Auxiliary potential vector for electric field
C_p	Phase velocity
ϑ_e	Electric scalar potential
ϑ_m	Magnetic scalar potential
e	Exponential function
$r(x, y, z)$	Rectangular coordinates
$r(r, \theta, \phi)$	Spherical coordinates
\hat{a}_n	Unit vector
θ_i	Incident angle
θ_r	Reflected angle
$\theta_{r'}$	Refracted angle
\mathbf{E}_i	Incident electric field
\mathbf{E}_r	Reflected electric field

\mathbf{E}_r	Refracted electric field
Δh_z	Delta; change in z
$\Delta E_z _{s(i+1/2)}^{+z}$	Forward difference along z-axis
$\Delta E_z _{s(i-1/2)}^{-z}$	Backward difference along z-axis
\hat{e}	Known Electric/magnetic field
\hat{e}^a	Unknown Electric/Magnetic field
d_h	Horizontal difference
d_w	Seawater depth
d_r	Dipole free end height from traverse line
d_m	Source feeding point
d_s	Dipole height from seafloor
Δ	Delta, Laplacian operator,
∇	Nabla, gradient, divergence, curl operator
\mathbf{M}	Coefficient matrix, diagonal matrix
\mathbf{b}	Boundary Conditions
l	Length of Dipole
$\mathbf{J}_{s(s)}^m$	Surface Current Density of magnetic current source
$\mathbf{J}_{s(s)}^e$	Surface Current Density of electric current source
\mathbf{I}_s^m	Electric current of the source (C/Sec)
\mathbf{I}_s^m	Magnetic Current of the source (C/Sec)
q	Charge density (C)
q^s	Charge Density of external Source (C)

LIST OF ABBREVIATIONS

CSEM	Controlled Source Electromagnetic Method
EM	Electromagnetic
FD	Finite Difference
FE	Finite Element
FTCS	Forward Time Central Space
GMD-I	Geological Model of Dipping II
GMD-II	Geological Model of Dipping II
HED	Horizontal Electric Dipole
HMD	Horizontal magnetic Dipole
IE	Integral Equation
MOSES	Magnetometer Off-Shore Electrical Sounding
MT	Magneto-Telluric
MVO	Magnitude Verses Offset
SBL	Seabed Logging
TE	Transverse Electric
TM	Transverse Magnetic
VED	Vertical Electric Dipole
VMD	Vertical Magnetic Dipole

CHAPTER 1 INTRODUCTION

1.1 Geophysical Survey

Geophysical surveys are used to map the reserves of geothermal, mineral hydrology and aquifers in subterranean region. These surveys are based on the study of physical fields that pass through the earth interior. Such fields are gravity, magnetic, seismic and electromagnetic wave fields. In petroleum industry the major concern of geophysical surveys is to find and evaluate the hydrocarbon reserves in subterranean region prior to drilling operation. Previously the most effective and widely used method for the search of petroleum reserves has been seismic survey [1]. In seismic survey, elastic waves are generated by explosion and propagated through the earth interior. The propagated signal reflected back from deep geological structure that contains the information of earth physical properties.

Over the last few decades, the search of oil and gas reserves has been extended from land and shallow water to deep water [2], [3]. However in deep sea, there are marine geological terranes in which the interpretation of seismic data is difficult [3]. Consequently, the results are ambiguous to differentiate between reservoirs filled with hydrocarbon or saline fluids.

1.2 Electromagnetic Geophysical Surveys

Electromagnetic (EM) Geophysical surveys have been used for a long time in the study of subsurface spatial distribution of earth physical properties. The methods are based on the study of physical EM field that passes through the earth. As the EM waves propagate through the earth layers of different conductivity the speed and amplitude of the wave change according to Maxwell's law. In marine environment, EM geophysical surveys are used in addition to than seismic surveys because of its

ability to differentiate between reservoirs saturated with resistive hydrocarbon or conductive saline fluids.

The immediate objective of EM geophysical survey is to obtain information about the electrical properties of interior spatial distribution of earth physical properties [4]. In this method, the EM field is being propagated through earth interior and it will be reflected back from deep non-homogeneous earth structure. The reflected field contains the information of earth hidden properties. The major applications of EM geophysical surveys are to explore petroleum reserves, aquifers and contaminants. These surveys are conducted by using low frequency signal in the range of 0.1 Hz to 10 Hz [5]. The EM geophysical survey data is obtained for several source-receiver positions and at number of frequencies. The strength of signal penetration into the earth can be controlled via two parameters, namely frequency of the EM source and source-receiver positions [6]. The EM geophysical surveys are performed in frequency domain in which transmitter emits a sinusoidal time varying current at a specific frequency. To map earth geology in deep the source-receiver separation distance should be large enough in-comparison to the target depth. Different types of EM methods are used depending on the application as each method has their advantages and disadvantages. The Maxwell's equation for EM field solved by Stefanescu (1942), specifically for geophysical exploration problems [7].

The EM geophysical surveys are classified into two major types as active and passive [8]. The passive geophysical techniques utilize the study of naturally occurring field's known as Magneto-telluric (MT) survey [5]. The *magneto-hydrodynamic* process in earth generates the greater part of earth magnetic field and interaction of this field with solar wind generates natural EM fields. The basic principles of MT methods are defined by Vozoff (1972) [9], Kaufman and Keller (1981) [10]. The MT techniques are most suitable for the study of the earth Crust and Mantle in the ranges of 60 km to 200 km. However, MT geophysical surveys provide poor resolution about conductivity contrast of Crust and Lithosphere [2].

Active geophysical surveys utilize man-made EM source and these sources are also called active source. All of the EM survey methods that utilize an active source are referred to controlled source EM methods [11]. One of the simplest EM methods

is direct current (dc) resistivity method. The dc method induced dc signal into the earth using source electrodes and measure the potential difference with other electrodes [2]. The dc method was developed by Schlumberger brothers who conducted the first resistivity survey for the determination of seabed structure [2].

1.3 Geophysical Modeling

Modeling of geophysical survey is a procedure of converting survey data into physical properties (inversion) or physical properties into synthetic data (forward modeling). Forward modeling is done by first constructing geological models of define electrical properties then a numerical formulation is applied to calculate artificial geophysical data. On the other hand, reverse modeling (inversion) involves a real time survey and conversion of survey data into physical property distribution to form a geological model [6]. The conventional approach for reverse modeling is to construct several geological models in order to generate synthetic data and to compare it with survey data.

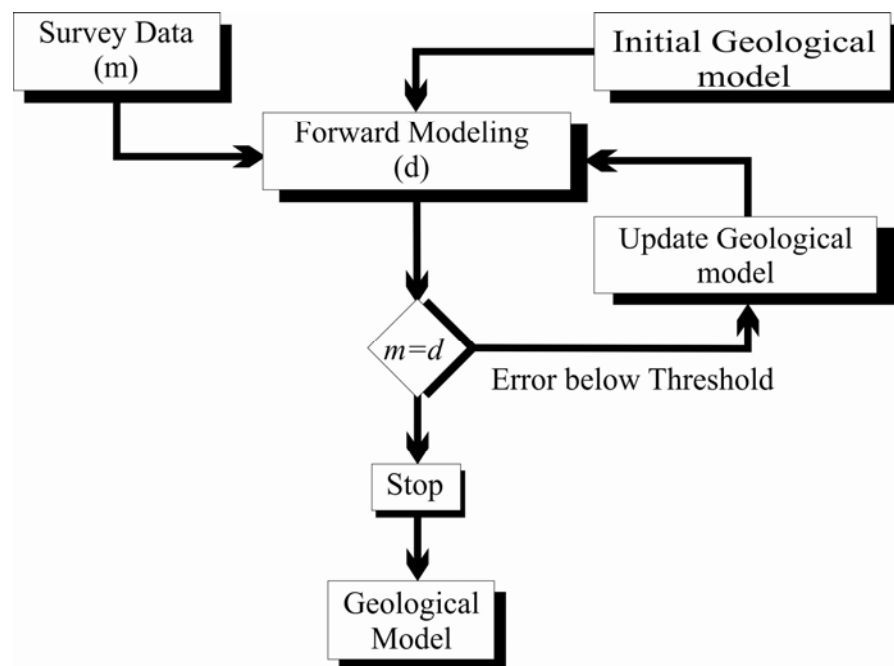


Figure 1.1 - The flow diagram for a conventional approach for Inversion flow to construct geological model

Figure 1.1 shows the flow diagram of the conventional approach for inversion. It shows the forward modeling is performed on a given geological model of known medium properties to produce theoretical data (d). The already existing surveys data

(m) will be compared with theoretical data (d). If survey data (m) is not same as theoretical data (d) then the existing model will be modified repeatedly until the artificial data (d) match the theoretical data (m).

1.4 Marine Controlled Source Electromagnetic Method

Most of the oil and gas reserves from continent shelf and immediate shallow water are already explored. Over the past few decades, the search for oil and gas reserves is extended from continent and shallow water areas to deeper waters. However, in deep water exploration, interpretation of seismic data is difficult [3]. On the other hand, the significant improvement in theory, methodology and instrumentation has helped to push for the development of a new technique called marine controlled source electromagnetic (CSEM) method. In year 2000, first marine CSEM experiment was carried out for the exploration of oil and gas reserves in deeper water [2]. After many years the marine CSEM techniques has been considered as the most successful technique for remote detection of petroleum reserves. Although marine CSEM technique is proven successfully for exploration of oil and gas reserve, there are still numerous aspects that must be improved for the purpose of minerals exploration such as survey geometry and modeling techniques (virtual simulation).

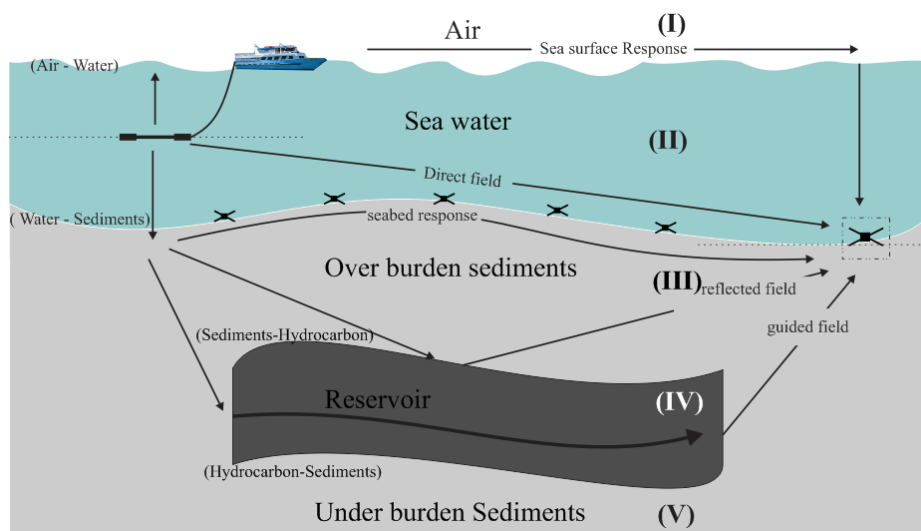


Figure 1.2 - Basic marine CSEM and SBL layout. The HED (source) is towed with water vessel and receivers are placed on seafloor.

In marine EM surveys, there are four different types of controlled sources, namely Vertical Electric Dipole (VED), Vertical Magnetic Dipole (VMD), Horizontal Magnetic Dipole (HMD) and Horizontal Electric Dipole (HED) [2]. The VED and

VMD induce only transverse magnetic and transverse electric modes respectively, while on the other hand HED and HMD can induce both modes. The HMD system is less sensitive to thin resistive media; as a result HED system has been proposed because it is more flexible for the application of seabed logging (SBL) [3]. In real time survey the typical source frequency is varied from 0.1 Hz to 10 Hz and it radiates EM energy to the surrounding media.

The schematic of marine CSEM survey is shown in Figure 1.2, where the geological model has been divided into five regions, air (region I), sea water (region II), over burden sediments (region III), buried hydrocarbon (region IV) and under-burden sediments (region V). This model also provides four different interfaces i.e. air to seawater (*air-water*), seawater to overburden sediments (*water-sediments*), overburden sediments to hydrocarbon (*sediments-hydrocarbon*) and hydrocarbon to under burden sediments (*hydrocarbon-sediments*). The sea water is more conductive than overburden and under-burden sediments. Similarly sediments are more conductive than hydrocarbon saturated reservoir resistive layer (region IV).

Overall response of signal propagation includes response from sea-surface, direct field, sea bed, reflected field and guided field. Figure 1.2 also shows that at short source-receiver separation distance, field received at the receiver is dominated by the direct field. On the other hand, at long separation distance, the reflected, sea-surface and guided signal dominate the direct field signal. The change in phase amplitude of guided and reflected signals carries the information about the reservoir.

In a marine CSEM experiment, the frequency of the source dipole is within the given band of 0.1 Hz to 10 Hz. Arrays of receivers are placed on the sea floor and the separation distance between seafloor receivers varies from 1 km to several kilometers. The mobile dipole source is moved by towing it with transportable water vessel and it is powered by surface generator through an underwater unit [2]. In typical survey the normal length of the dipole is 100 m (or more). If the source is placed very close to the seafloor, it is able to transmit more energy through the sedimentary rocks.

In marine CSEM survey, the proper orientation and position of source receiver is known as survey geometry. This can be divided in two different transects. These

transects are defined by the axis of the source and a straight line that joins receivers. If the axis of the source has 0° azimuth with the line, it is called *inline survey geometry*, if the azimuth is 90° , it is called *broad side survey geometry* [6]. The survey geometry is most critical factor in marine CSEM experiments as improper source-receiver orientation and/or position causes irregularities in survey data. To reduce the positioning irregularities, HED is steered by a navigation system to keep track of the source position.

In a typical EM survey, MT survey data is also collected in addition to active EM data (CSEM) to enable the exploration of hidden properties up to hundreds of kilometers deep. The MT data is collected when the marine CSEM source becomes inactive. Data obtained through this survey can be used as a back ground profile. However the good lateral resolution and high quality data can only be achieved by an active geophysical method.

Over the last few decades the energy sector has changed drastically. The increasing demand of petroleum energy and corresponding growing consumption pose various challenges. To fulfill the increasing demand it is necessary to explore more energy reservoirs especially in deep sea. In deeper water, marine CSEM is a useful method to explore energy reservoir but it requires improvements in survey techniques as well as modeling techniques. The above challenges can be improved by carrying the forward modeling for different background resistivity models.

The immediate objective of this research work is to investigate behavior of EM field as it propagates through earth layers with different conductivity and to investigate the effects of survey geometry onto the survey data. With the help of forward modeling solution, better selection of survey geometry can be used in designing viable survey geometry for real time survey. The mathematical theory of EM fields provides the essentials tools for forward problem solution and the basic description of EM field can be extracted from macro-electrodynamics theory.

Approximation of EM field in given discretized geological model is obtained through numerical solution for field governing equations. The numerical method used for this research is Finite Difference (FD) method with *staggered-grid* scheme [13]. The resultant equations of *staggered-grid* scheme are used for solving one-

dimensional (1D) and two-dimensional (2D) geological models. The algorithms are implemented in MATLAB for each geological model.

The irregularities caused by improper source orientation are also studied using similar approach on 2D geological models. Also forward modeling in spatial temporal domain known as *forward time center space* (FTCS) is used to find an optimal speed for mobile source in marine CSEM/SBL.

1.5 Problem Statement

The most crucial factor of marine CSEM method is its survey geometry [6]. In real time surveys, the field measurements are very sensitive to the source-receiver position and orientation. One end of HED source is towed with a mobile water vessel and other is allowed to move freely. The position of the HED in marine CSEM survey is steered by a navigation system. However, the movement of HED free end along the vertical plane and horizontal plane will have effect on its orientation. In addition, there is the need to calculate the optimal speed of the mobile dipole source.

The irregularities in survey data due to source position is normalized using the navigation system to find the exact location of dipole source [1]. Furthermore, the anomalies due to improper orientation of mobile dipole source are normalized using different techniques called *short baseline* and *long base line*. However these techniques provide limited accuracy in normalizing the marine CSEM survey data. Although, the positions and orientation can be modeled using near field EM radiation pattern it still requires a human interpreter to guide the interpretation process.

To improve the interpretation process there is a need to have qualitative understanding of how physical earth structure can interact with EM field and how survey geometry can affect the real time survey data.

1.6 Research Objective and Contribution

Objective of the research is to study the EM field behavior for different geological scenarios and anomalies caused by survey geometry i.e. source position, orientation and speed. The major research contributions are as follows,

- 1D forward modeling to determine the optimal frequencies for various target depths.
- 2D forward modeling to investigate EM field behavior for single interface model, multi interface model and dipping effect of dipole source.
- Analysis of dipole source speed effects on marine CSEM survey using *forward time central space* (FTCS) scheme.

1.7 Thesis Organization

The main emphasis of this research is electromagnetic sounding in stratified media, to assess the hydrocarbon saturated reservoir and to find the irregularities caused by improper survey geometry. The forward modeling solution is used to understand the behaviour of EM signal for stratified geological models. The solution is obtained by first designing a geological model with specified electrical properties and then by applying numerical formulation to create artificial geophysical data. The artificial data asserts the spatial distributive property of physical earth. The irregularities in real time survey due to improper survey geometry generate errors in inversion. The forward modeling can provide the basis for detecting abnormalities due to improper survey geometry, thus providing a feasible alternate to real time surveys.

Careful mathematical formulation is required for understanding EM principles that are defined by macro-electrodynamics theory. The description of low frequency EM induction is presented in **Chapter 2**. This chapter involves the discussion of basic electromagnetic propagation for conductive and nonconductive mediums. Maxwell's equations are solved in frequency domain for general wave equation that describes the behaviour of EM field in any medium. The general wave equation is solved in complex permittivity medium for the equations of skin depth, wavelength and wave velocity. *Quasi-static* equations are solved for the description of low frequency EM induction and used to calculate the field governing equation for layered media. The Snell's law description is used to calculate the equations for reflected and refracted EM field. The auxiliary potential function and Maxwell's equations are considered to study the propagation of EM fields from an infinitesimal dipole.

1D forward modeling formulation and algorithm are implemented for finding the optimal survey design and frequency. **Chapter 3** presents 1D forward modeling of

marine CSEM survey for seabed logging. In this chapter *staggered-grid* scheme is used with field governing equations to provide 1D numerical solution. The 1D simulation is accomplished for both isotropic and anisotropic geological models using two different frequencies. The algorithm for 1D geological model is implemented in MATLAB. The numerical results for 1D forward modeling show very good agreement with previously published work [1], [2]. This also shows the behaviour of EM field travelling through stratified geological model.

The real geological structure of the marine environment consists of horizontally stratified media. **Chapter 4** presents mapping of hydrocarbon with marine EM method using 2D modeling. In this chapter, the 2D forward modeling is performed for single-interface and multi-interface geological models. The algorithm for 2D models is also implemented in MATLAB. The obtained results of single interface geological model showed a very good agreement with real time survey published by K. A. Weitemeyer [15]. The forward modeling for layered media is performed and obtained results are consistent with previous work [10]. It also demonstrated that well-defined layered media and survey geometry can be used to study the effects of source-receiver orientation and position.

Chapter 5 presents modeling of infinitesimal dipole in spatial and temporal domain. Forward modeling is done for propagation of low time-varying signal into 2D single interface geological model. Only transmitted energy is considered to measure the abnormalities in survey data caused by improper orientation of source. The obtained results are the consistent with K. A. Weitemeyer publication on hydrates [15]. The modeling for optimal speed of source is done by calculating the propagated energy in spatiotemporal domain. The basic idea is taken from the work of G. W. Recktenwald on heat equation and is implemented for *quasi-static* EM equation in this study [16]. The obtained results are consistent with the work on EM induction in conductive medium. The final chapter provides the conclusion and discussion of this research.

CHAPTER 2

EM FIELD INDUCTION IN GEOPHYSICS

2.1 History

Traditional EM geophysical surveys have been used for a long time to delineate the electrical properties of the earth. The foremost objective of marine CSEM induction survey is to map the spatial distribution of electrical properties in sedimentary rocks. A simple EM method was the direct current resistivity method developed by the Schlumberger brothers in 1926 [3]. Similarly, one of the earliest attempts of EM sounding was the Sundberg horizontal loop method in 1923 [18]. This technique was useful for mineral exploration. The main intention of EM sounding was to detect and assess the presence of ore-body. In 1933, a controlled source EM technique was conducted for the study of layered earth by Blau [7]. This technique proved to be cost-effective for the petroleum industry in exploring oil reserves. Advancement in controlled source EM technique was relatively slow because of inadequate instrumentation and effective interpretation methods [17]. The dc (direct current) technique was used, with specified configuration of electrodes (Wenner array) for applications of resistivity sounding in shallow water. A related method was proposed by Wynn (1988) for mineral exploration [3]. In recent years a vertical dipole source was used for off-shore applications known as Magneto-metric Off-Shore Electrical Sounding (MOSES) [3]. The MOSES technique used seafloor receivers that measured two component of magnetic field as a function of source receiver separation distance and frequency [19].

The first experiment of marine CSEM/SBL survey was conducted by Statoil, Scripps Institution of Oceanography, and the Southampton Oceanography on an area of previously proven hydrocarbon reserves [1]. This survey was conducted in the same manner as described by Cox and Young [2]. In this experiment, a towed mobile

HED was positioned 40-50 m (or more) above from seafloor and steered by a navigation system. The field recorders (seafloor receivers) were placed on the seafloor. The survey was carried out two times with different frequencies of 0.25 Hz and 1.00 Hz. The results obtained showed very good agreement with predicted results by forward modeling [1]. However the survey had some limitations which are sensitive to survey geometry and bathymetry effects.

Exploration of hydrocarbon in deep water is a challenging and expensive job. The geological features and bathymetry effects in deep water needs significant improvement in the design of survey geometry. The important features of survey geometry can be studied through forward problem solution rather than real time survey. In forward modeling for different geological models, second order partial differential equations are solved using numerical methods such as the finite difference technique. The solution obtained gives EM field readings at node points in the geological model region. The detailed descriptions of the EM field governing equations for geological model are given in the next section.

2.2 Basic Principles of EM Induction

In marine CSEM techniques, EM source utilize an extremely low time-varying signal. Consequently the geophysical survey requires the study of the essential principles for low frequency electric and magnetic field that provided by macro-electrodynamics theory. The Maxwell's equations are the most concise and easy way to describe the behavior of electric and magnetic field for EM sounding.

2.2.1 Field Governing Equations

The basic behavior of EM field can be described either in terms of magnetic field intensity vector \mathcal{H} (A/m) and electric field intensity vector \mathbf{E} (V/m) or magnetic field density vector \mathbf{B} (C/m²) and electric field density vector \mathbf{D} (W/m²) [20]. Faraday's and Ampere's law defines the coupling of magnetic field intensity with electric field intensity. The coupling of field intensities defines the circulation of each field (\mathbf{E} and \mathcal{H}) that generates a time varying component of the other field.

The typical relations defined by Maxwell's equations are given by [21],

$$\nabla \times \mathbf{H} = \mathbf{J}_t + \frac{\partial \mathbf{D}}{\partial t} \quad (2.1)$$

Similarly, Maxwell's equation from Faraday Law of Induction can be given as,

$$\nabla \times \mathbf{E} = -\frac{\partial \mathbf{B}}{\partial t}. \quad (2.2)$$

Equation 2.1 shows that the magnetic field intensity can also be induced by external source \mathbf{J}_t which is the total current density. The EM geophysical surveys works in the very low frequency band, in the range of 0.1 Hz to 10 Hz. In Equation 2.1, magnetic fields generated by the displacement current $\partial \mathbf{D} / \partial t$ are negligible [22]. Equation 2.2, shows the time-varying magnetic field density, $\partial \mathbf{B} / \partial t$ generates an electric field (Faraday law of electromagnetic induction). Gauss law states that the patterns of generated magnetic field by positive and negative charges are inseparable; consequently the net magnetic flux is zero as describe by,

$$\nabla \cdot \mathbf{B} = 0. \quad (2.3)$$

The earth's geological structures have finite conductivity(σ), permeability (μ) and permittivity (ϵ). The conductivity of the media is defined as a measure of ability to conduct electric charges and its unit is Siemens per meter (S/m). Similarly, permittivity of the medium defines the resistance encountered in the medium to form an electric field and it is measured in Farad per meter (F/m). Furthermore, permeability is defined as the ability of the medium to support the formation of magnetic field and is measured in Newton per meter (N/m). This type of the media is known as a conductive medium. Equation 2.4 indicates *divergence* of electric field vector in a closed surface is equal to free volume charge density as,

$$\nabla \cdot \mathbf{D} = \rho_v, \quad (2.4)$$

where ρ_v is the sum of spatial free charge density and charge density of external active sources as,

$$\rho_v = q_f + q_s, \quad (2.5)$$

where q_f and q_s are spatial free electric charges and external source charges. In equation 2.1, total current density is the sum of as conduction current density \mathbf{J}_c and current density of active source \mathbf{J}_s as

$$\mathbf{J}_t = \mathbf{J}_c + \mathbf{J}_s \quad (2.6)$$

The strength of electric field is linearly dependent on the electrical properties of the medium according to Ohm's Law,

$$\mathbf{J}_c = \sigma \mathbf{E}. \quad (2.7)$$

The microscopic imbalance of charge distribution in medium describes the effects of constitutive relation given as,

$$\mathcal{D} = \epsilon \mathbf{E}, \quad (2.8)$$

$$\mathcal{B} = \mu \mathcal{H}. \quad (2.9)$$

A medium is referred to as uniform if the properties are linear (\mathcal{D} is proportional to \mathbf{E} , and \mathcal{B} is proportional to \mathcal{H}), homogeneous and isotropic [23]. In isotropic medium, the values of ϵ and μ are independent of direction and in homogeneous medium the EM properties (σ, ϵ, μ) is constant throughout the medium. Maxwell's equations and constitutive relation requires vector identities for the study of EM fields as given below,

$$\nabla \times \nabla \times \psi = \nabla (\nabla \cdot \psi) - \nabla^2 \psi, \quad (2.10)$$

$$\nabla \times [-\nabla \cdot \mathcal{G}] = 0. \quad (2.11)$$

In forward modeling, a second order partial differential equations (PDE) is calculated from Maxwell's equation for layered media. Equations 2.1 and 2.2 can be further simplified for second order PDE by using Equations 2.6, 2.7, 2.8 and taking the curl operator at both sides as;

$$\nabla \times \nabla \times \mathcal{H} = \sigma (\nabla \times \mathbf{E}) + \nabla \times \mathbf{J}_s + \epsilon \frac{\partial (\nabla \times \mathbf{E})}{\partial t}, \quad (2.12)$$

$$\nabla \times \nabla \times \mathbf{E} = -\mu \frac{\partial (\nabla \times \mathcal{H})}{\partial t}. \quad (2.13)$$

Using vector identities of 2.10, the above equations can be written as,

$$\nabla(\nabla \cdot \mathcal{H}) - \nabla^2 \mathcal{H} = -\sigma\mu \frac{\partial \mathcal{H}}{\partial t} - \epsilon\mu \frac{\partial^2 \mathcal{H}}{\partial t^2} + \nabla \times \mathbf{J}_s, \quad (2.14)$$

$$\nabla(\nabla \cdot \mathbf{E}) - \nabla^2 \mathbf{E} = \mu \frac{\partial \mathbf{J}_s}{\partial t} + \sigma\mu \frac{\partial \mathbf{E}}{\partial t} + \epsilon\mu \frac{\partial^2 \mathbf{E}}{\partial t^2}, \quad (2.15)$$

where divergence of a vector field is defined as the tendency of EM field to flee or diverge from any single point in the medium. A medium is known as source-free medium if the external source term \mathbf{J}_s is zero.

In the absence of external source and divergence of vector field ($\nabla \cdot \psi = 0$), the above equation can be written as [22]

$$\nabla^2 \mathcal{H} - \sigma\mu \frac{\partial \mathcal{H}}{\partial t} - \epsilon\mu \frac{\partial^2 \mathcal{H}}{\partial t^2} = 0, \quad (2.16)$$

$$\nabla^2 \mathbf{E} - \sigma\mu \frac{\partial \mathbf{E}}{\partial t} - \epsilon\mu \frac{\partial^2 \mathbf{E}}{\partial t^2} = 0. \quad (2.17)$$

Equations 2.14 and 2.15 are the general wave equations of diffused electromagnetic field in a uniform and source free medium. The first order terms in above equations are showing the factor of field decay in a medium. In perfect dielectric medium the signal attenuation is less. The general wave equation can also be written in frequency domain as

$$\nabla^2 \mathcal{H} - (i\sigma\mu\omega - \epsilon\mu\omega^2) \mathcal{H} = 0, \quad (2.18)$$

$$\nabla^2 \mathbf{E} - (i\sigma\mu\omega - \epsilon\mu\omega^2) \mathbf{E} = 0. \quad (2.19)$$

The above equations will be solved further to obtain the expression for *skin depth*, *wave length* and *phase velocity* in conductive medium.

2.2.2 Quasi-static Equations

The source in marine CSEM geophysical surveys produces a low time-varying signal. In Equation 2.1, the generated magnetic field due to temporal displacement current $\partial \mathcal{D} / \partial t$ can be ignored. This type of equation is known as *quasi-static* equations [12].

In frequency domain the equation of Faraday's law and Ampere's law can be written as

$$\nabla \times \mathcal{H} = \mathbf{J}_s + \sigma \mathbf{E}, \quad (2.20)$$

$$\nabla \times \mathbf{E} = i\mu\omega\mathcal{H}. \quad (2.21)$$

Employing the divergence operator on Equation 2.20, the equation takes the form of,

$$\nabla \cdot \nabla \times \mathcal{H} = \nabla \cdot \mathbf{J}_s + \nabla \cdot (\sigma \mathbf{E}). \quad (2.22)$$

Using product rule ($\nabla \cdot (\sigma \mathbf{E}) = \nabla \sigma \cdot \mathbf{E} + \sigma \nabla \cdot \mathbf{E}$), the Equation 2.22 can be rewrite as,

$$\nabla \cdot \mathbf{E} = -(\nabla \cdot \mathbf{J}_s + \mathbf{E} \cdot \nabla \sigma) / \sigma, \quad (2.23)$$

Where ($\nabla \cdot \nabla \times \mathcal{H} = 0$). Using Equations 2.20 and 2.21 the curl operator, the can be solved to obtain the *telegraph* equations [21] given as,

$$\nabla (\nabla \cdot \mathcal{H}) - \nabla^2 \mathcal{H} - i\sigma\mu\omega\mathcal{H} = \nabla \times \mathbf{J}_s, \quad (2.24)$$

$$\nabla (\nabla \cdot \mathbf{E}) - \nabla^2 \mathbf{E} + i\mu\sigma\omega\mathbf{E} = -i\mu\omega\mathbf{J}_s. \quad (2.25)$$

Telegraph equations are differential equations and is used to describe the phenomena of voltage and current in transmission medium. By substituting Equation 2.7 into Equations 2.24 and 2.25 as [8],

$$\nabla^2 \mathcal{H} + i\sigma\mu\omega\mathcal{H} = -\nabla \times \mathbf{J}_s, \quad (2.26)$$

$$\nabla^2 \mathbf{E} + i\mu\sigma\omega\mathbf{E} = -i\mu\omega\mathbf{J}_s. \quad (2.27)$$

Equation 2.26 and 2.27 are valid for calculating the electric and magnetic field in geological mediums in which the source uses a low frequency signal. Equation 2.26 will be used for forward modeling to calculate the electric field in 1D and 2D geological models.

2.3 Skin depth, Wavelength and Phase Velocity

2.3.1 Skin Depth

The generated EM field is time dependent and has two vector components (\mathbf{E} and \mathcal{H}) simultaneously. *Skin depth* is defined as a covered distance of \mathbf{E} or \mathcal{H} field in

a medium where its magnitude drops to $1/e$ of its initial value [17]. The skin depth equation can be simplified from the complex coefficient of Equation 2.18 or 2.19 and phasor diagram as shown in Figure 2.1

The complex coefficient is also known as propagation constant γ_c and can be written as,

$$\gamma_c^2 = i\sigma\mu\omega - \epsilon\mu\omega^2, \quad (2.28)$$

$$\gamma_c^2 = -\omega^2\mu\left(\epsilon\left(1-i\frac{\sigma}{\omega\epsilon}\right)\right), \quad (2.29)$$

$$\gamma_c^2 = -\omega\sqrt{\mu\hat{\epsilon}}. \quad (2.30)$$

In Equation 2.30 $\hat{\epsilon}$ is the complex permittivity of the conductive medium which can be simplified using the phasor diagram.

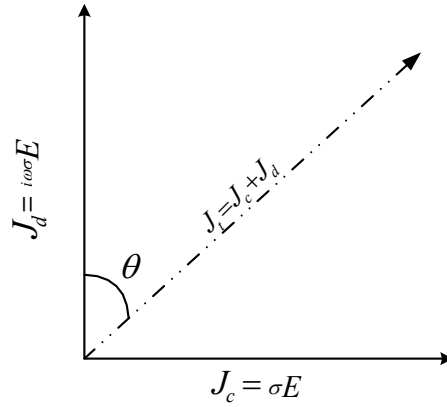


Figure 2.1 – Phasor diagram of displacement current and conduction current

In conduction medium, the total current density, \mathbf{J}_t is the sum of conduction current and displacement current ($\mathbf{J}_c + \mathbf{J}_s$). It is clearly revealed from the diagram as,

$$\tan \theta = \left(\frac{\sigma}{\omega\epsilon}\right), \quad (2.31)$$

where θ is loss tangent angle. The propagation constant can be further solved as,

$$\gamma_c = i\omega\sqrt{\mu\epsilon\left(1-i\left(\frac{\sigma}{\omega\epsilon}\right)\right)} = i\omega\sqrt{\mu\epsilon(1-i\tan\theta)}, \quad (2.32)$$

$$\gamma_c = i\omega\sqrt{\mu\epsilon\left(1-i\left(\frac{\sin\theta}{\cos\theta}\right)\right)}, \quad (2.33)$$

As a result, the propagation constant can be written as

$$\gamma_c = i\omega\sqrt{\mu\epsilon(\sec\theta(\cos\theta - i\sin\theta))}. \quad (2.34)$$

In above equation, the propagation constant is a complex quantity. The real part of the *propagation constant* α represents attenuation constant and measured in Neper per meter (Np/m). However, imaginary part of the propagation constant represents *phase constant* β and measured in radian per meter [24]. The *propagation constant* can be further solved as,

$$\alpha = \omega\sqrt{\frac{\mu\epsilon}{2}(\sec\theta(1 - \cos\theta))} = \omega\sqrt{\frac{\mu\epsilon}{2}\sqrt{(\tan^2\theta + 1)} - 1}, \quad (2.35)$$

$$\alpha = \omega\sqrt{\frac{\mu\epsilon}{2}\sqrt{\left(\frac{\sigma}{\omega\epsilon}\right)^2 + 1} - 1}. \quad (2.36)$$

Equation 2.36 shows $\sigma \gg \omega\epsilon$ and permittivity can be ignored because a CSEM survey utilizes a very low frequency [25]. As a result propagation constant can be written as,

$$\alpha = \sqrt{\mu\pi\sigma f}, \quad (2.37)$$

and the equation for *skin depth* can be obtained from previous equation as,

$$\delta = \frac{1}{\alpha} = \frac{1}{\sqrt{\mu\pi\sigma f}} \approx \frac{503.3}{\sqrt{\sigma f}}. \quad (2.38)$$

Equation 2.38 shows the skin depth δ is inversely proportional to the electrical conductivity of the medium and source frequency. Skin depth equation also shows that the high frequency signal is not able to penetrate deep in earth. In marine environment, skin depth in sea water is shorter than in sedimentary rocks and buried reservoir. The skin depth provides the information of optimal frequency for given target depth. In marine CSEM survey the magnitude of magnetic permeability is considered to be same as in vacuum ($4\pi \times 10^{-7} \text{N/A}^2$). Skin depth also shows that the magnitude of EM field drops to less than one percent of its total value after covering distance equal to 5δ [24].

Figure 2.2 shows the skin depth at various frequencies with different conductivities of the medium. It shows, the five different frequencies (1.0 Hz, 2.0 Hz, 3.0 Hz, 4.0 Hz and 5.0 Hz) are considered for finding *skin depth* in various conductive medium. The conductivity of five various mediums are 0.25 S/m, 0.50 S/m, 1.00 S/m, 2.00 S/m and 4.00 S/m. In marine CSEM survey, the source height from seafloor is set at a value less than the *skin depth* in seawater.

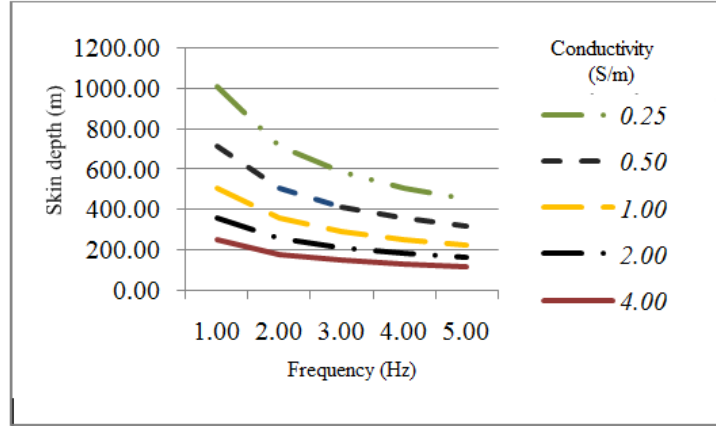


Figure 2.2 –Skin depth at different conductive layers with varying frequencies.

2.3.2 Wavelength

In marine CSEM survey, source and receivers both are immersed in conductive medium. As a result, the equation for calculating the wavelength of a wave in conductive medium is different that used in vacuum. In conductive medium the equation for wavelength wave can be simplified by using the equation of phase constant β as [24],

$$\lambda = \frac{2\pi}{\beta}, \quad (2.39)$$

where equation for phase constant can be rewritten as,

$$\beta = \omega \sqrt{\mu \epsilon \sec \theta} \left(\cos \left(\frac{\theta}{2} \right) \right). \quad (2.40)$$

Equation 2.40 can be more simplified by using trigonometric functions as,

$$\beta = \omega \sqrt{\frac{\mu \epsilon}{2} (\sec \theta (1 + \cos \theta))} = \omega \sqrt{\frac{\mu \epsilon}{2} (\sqrt{(\tan^2 \theta + 1)} + 1)} \quad (2.41)$$

Finally, equation for phase constant signal in conductive medium is as,

$$\beta = \omega \sqrt{\frac{\mu\epsilon}{2} \sqrt{\left(\frac{\sigma}{\omega\epsilon}\right)^2 + 1} + 1}. \quad (2.42)$$

The term $\sigma/\omega\epsilon$ in equation 2.42 can be more simplified by considering that $\sigma \gg \omega\epsilon$ and it can be rewritten as,

$$\lambda \approx 3162 / (\sqrt{\sigma f}). \quad (2.43)$$

Equation 2.43 shows that the wave length is inversely proportional to the conductivity of the media and frequency. Table 2.1 shows the wavelength of the wave at different frequencies and conductivity.

Table 2.1- Wavelength of signal that utilize for EM sounding in conductive media

$f(\text{Hz})$	Conductivity (S/ m)				
	0.25	0.50	1.00 m	2.00 m	4.00
1	6324 m	4472 m	3162 m	2236 m	1581 m
2	4471 m	3162 m	2236 m	1581 m	1118 m
3	3651 m	2582 m	1826 m	1291 m	913 m
4	3162 m	2236 m	1581 m	1118 m	791 m
5	2828 m	2000 m	1414 m	1000 m	707 m

2.3.3 Phase Velocity

Phase velocity of EM wave in conductive medium is dependent on signal frequency and electrical properties of the medium. The phase velocity of the wave in conductive medium can be expressed as [11],

$$C_p = \frac{\omega}{\beta} = \frac{2\pi f}{\sqrt{\mu\pi\sigma f}} = 3162 \sqrt{\frac{f}{\sigma}}. \quad (2.44)$$

Equation 2.44 shows that, the phase velocity C_p is less in resistive medium than the conductive one. Similarly, higher frequency signal can penetrate at higher speed than low frequency signal. Figure 2.3 shows, the phase velocity of wave at three different mediums of conductivity: 0.25 S/m, 1.00 S/m and 3.3 S/m and the wave frequency is varied from 0.25 Hz to 5.0 Hz. It shows that the phase velocity increases if the medium conductivity decreases.

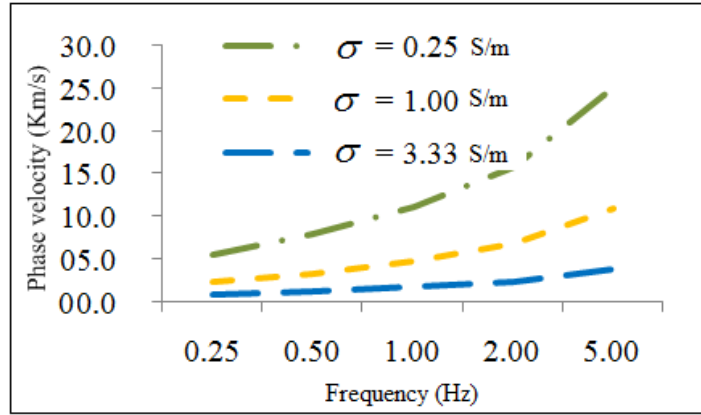


Figure 2.3 - Phase velocity of the wave at different frequencies in conductive media.

2.4 Horizontal Electric Dipole

Controlled source EM sounding has gained acceptance for the exploration of petroleum reserves in deeper water because it can provide high quality data for the use in geological mapping. As a result, marine CSEM survey is considered as an effective technique for hydrocarbon exploration. The theoretical principle of marine CSEM survey is to utilize a dipole as an EM source which radiates energy both towards the overlying water column and towards subsurface rocks. The controlled source method provides highly precise data as compared to data obtained through MT techniques [8].

Typical length (l) of dipole for marine CSEM survey is 100m (or more) where the source frequency ranges from 0.01 Hz to 10 Hz. The dipole antenna with $l \leq \frac{\lambda}{50}$ is known as *infinitesimal dipole* because the length is much smaller than the wavelength. The radiation pattern of an infinitesimal dipole is shown by a graphical presentation of spatial distribution of EM radiation from the source. Usually radiation pattern is determined for the far field region (region $\geq \sqrt{l^3/\lambda}$ from source) using radiation properties that include radiation power density, directivity and polarization. The *radiation power density* describes the power associated in the medium due to EM field. The Instantaneous *Poynting vector* is used to calculate radiation power density that is associated by EM field in medium [26],

$$\mathcal{W} = \mathbf{E} \times \mathcal{H}. \quad (2.45)$$

In Equation 2.45 \mathcal{W} is instantaneous Poynting vector measured in Watt per meter square (W/m^2). Similarly, \mathbf{E} and \mathcal{H} are the instantaneous electric and magnetic field

respectively. Directivity of the antenna describes the ratio of radiation intensity in a given direction to the average radiation intensity in all direction. The polarization of dipole antenna affects the radiation of electric and magnetic fields into surrounding mediums.

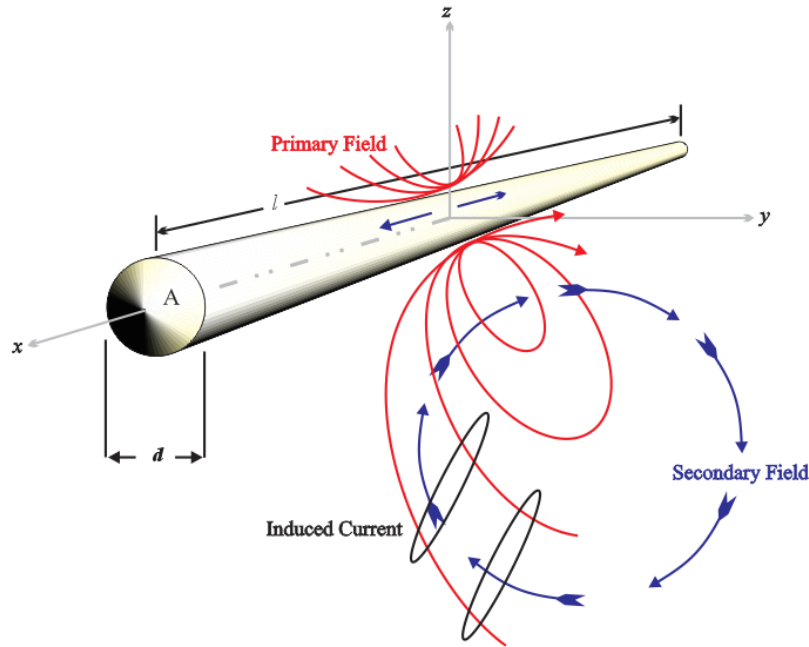


Figure 2.4- Dipole antenna with uniformly distributed charges in dipole and resulting radiated field in dispersive medium

Figure 2.4 illustrates the fields induced when a dipole antenna radiating EM waves in a dispersive medium. The current flow in the dipole generates electric charges that induce a primary field into the surrounding media. Similarly the secondary field generated by primary field induces eddy currents in the surrounding medium. The induced eddy current changes its behavior in terms of phase and magnitude depending on the electrical properties of media. The EM receivers receive the sum of primary and secondary field which contains the information of surrounding media [3].

Proper mathematical modeling can be used to determine the components of electric and magnetic fields component for radiation pattern. The most common way for calculating \mathbf{E} and \mathbf{H} fields component on given current source densities (electric source \mathbf{J}_s^e , magnetic source \mathbf{J}_s^m) is by using auxiliary potential function.

2.4.1 Auxiliary Potential Functions

Analysis of EM field (produced by infinitesimal dipole) is done by placing the source position in rectangular coordinate system and then determines the radiated field. The variables of electromagnetic fields (\mathbf{E} and \mathbf{H}) can be calculated directly from physical sources and in this case, the electric current source \mathbf{J}_s^e . On the other hand, a conventional approach is used by introducing auxiliary potential functions given by

$$\mathbf{B} = \nabla \times \mathbf{\Pi}_e, \quad (2.46)$$

from which the EM fields are derived [26]-[27]. Here $\mathbf{\Pi}_e$ is an auxiliary potential vector for magnetic field. The curl of magnetic potential is equal to magnetic field intensity. Radiated EM field in homogeneous medium is caused by an electric current source. Using the auxiliary potential function of magnetic field in Equation 2.2 in the frequency domain, it can be resolved as,

$$\nabla \times \mathbf{E} = -i\omega\mu\mathbf{H} = -i\omega(\nabla \times \mathbf{\Pi}_e). \quad (2.47)$$

Taking the curl operator of both terms in above equation to the left side it can be rewritten as,

$$\nabla \times [\mathbf{E} + i\omega\mathbf{\Pi}_e] = 0. \quad (2.48)$$

In the view of Equation 2.11, then above equation can be simplified as,

$$\mathbf{E} = -[i\omega\mathbf{\Pi}_e + \nabla \mathcal{G}_e], \quad (2.49)$$

where \mathcal{G}_e is arbitrary electric scalar potential. If the external source carries only electric current density then Equation 2.1 can be rewritten in frequency domain as,

$$\nabla \times \nabla \times \mathbf{\Pi}_e = \mu\mathbf{J}_s^e + i\epsilon\mu\omega\mathbf{E}. \quad (2.50)$$

Substituting Equation 2.49 into above equation gives,

$$\nabla \times \nabla \times \mathbf{\Pi}_e = \mu\mathbf{J}_s^e - i\mu\epsilon\omega(i\omega\mathbf{\Pi}_e + \nabla \mathcal{G}_e). \quad (2.51)$$

By using vector identity of Equation 2.10 for the solution of the above equation it becomes,

$$\nabla(\nabla \cdot \mathbf{\Pi}_e) - \nabla^2 \mathbf{\Pi}_e = \mu\mathbf{J}_s^e + \mathbf{\Pi}_e - i\omega\mu\epsilon\nabla \mathcal{G}_e, \quad (2.52)$$

and can be simplified as,

$$\nabla^2 \mathbf{\Pi}_e + \mu\epsilon\omega^2 \mathbf{\Pi}_e = -\mu \mathbf{J}_s^e + \nabla(i\omega\mu\epsilon\vartheta_e + \nabla \cdot \mathbf{\Pi}_e), \quad (2.53)$$

where according to Lorentz condition $\nabla \cdot \mathbf{\Pi}_e = -i\mu\epsilon\omega\vartheta_e$ and above equation can be rewritten as,

$$\nabla^2 \mathbf{\Pi}_e + k^2 \mathbf{\Pi}_e = -\mu \mathbf{J}_s^e, \quad (2.54)$$

where $k^2 = \mu\epsilon\omega^2$ and above equation is known as *Helmholtz* equation.

Similarly, the magnetic potential vector will be used when source carries only magnetic current density (\mathbf{J}_s^m). The auxiliary potential function for electric field density can be defined as,

$$\mathcal{D} = -\nabla \times \mathbf{\Pi}_h, \quad (2.55)$$

where $\mathbf{\Pi}_h$ is potential vector of electric field. Substituting the above expression into Equation 2.1 in frequency domain gives,

$$\nabla \times \mathcal{H} = i\omega(-\nabla \times \mathbf{\Pi}_h). \quad (2.56)$$

Taking both curl operator of above equation to the left side gives,

$$\nabla \times [\mathcal{H} + i\omega \mathbf{\Pi}_h] = 0. \quad (2.57)$$

Above expression can be further simplified by comparing it with equation 2.11 and given as,

$$\mathcal{H} = -[\nabla \vartheta_m + i\omega \mathbf{\Pi}_h]. \quad (2.58)$$

where ϑ_m is an arbitrary magnetic scalar potential. The EM field is considered to be generated by \mathbf{J}_s^m source, so equation 2.2 in frequency domain can be written as,

$$\nabla \times \mathbf{E} = \mathbf{J}_s^m - i\omega \mathcal{B}. \quad (2.59)$$

By using Equation 2.56 and constitutive relation, so the above equation becomes,

$$\nabla \times \nabla \times \mathbf{\Pi}_h = \epsilon \mathbf{J}_s^m - i\mu\epsilon\omega \mathcal{H}. \quad (2.60)$$

Using Equations 2.10 and 2.58 into the above equation, can be written as,

$$\nabla(\nabla \cdot \mathbf{\Pi}_h) - \nabla^2 \mathbf{\Pi}_h = -\epsilon \mathbf{J}_s^m - i\mu\epsilon\omega [\nabla \vartheta_m + i\omega \mathbf{\Pi}_h], \quad (2.61)$$

and

$$\nabla^2 \mathbf{\Pi}_h + \mu\epsilon\omega^2 \mathbf{\Pi}_h = -\epsilon \mathbf{J}_s^m + \nabla (i\mu\epsilon\omega \mathcal{G}_m + \nabla \cdot \mathbf{\Pi}_h), \quad (2.62)$$

where according to Lorentz condition $\nabla \cdot \mathbf{\Pi}_h = -i\mu\epsilon\omega \mathcal{G}_m$ and above equation can be simplified as [23],

$$\nabla^2 \mathbf{\Pi}_h + k^2 \mathbf{\Pi}_h = -\epsilon \mathbf{J}_s^m. \quad (2.63)$$

Equation 2.54 and 2.63 can use to find radiation pattern of a dipole source. In fact, the procedure requires the auxiliary potential functions (Π_h, Π_e) are found first for the solution of Equations 2.54 and 2.63. The equations for the electric and magnetic potential are given as,

$$\Pi_e = \frac{\mu}{4\pi} \iiint_v (\mathbf{J}_{s(v)}^e) \frac{e^{-kr}}{r} dv', \quad (2.64)$$

$$\Pi_h = \frac{\epsilon}{4\pi} \iiint_v (\mathbf{J}_{s(v)}^m) \frac{e^{-kr}}{r} dv', \quad (2.65)$$

where $\mathbf{J}_{s(v)}^e$ and $\mathbf{J}_{s(v)}^m$ are the volume current density of electric current source and magnetic current source respectively; r is the distance from any point on the source to observation point. In marine CSEM survey, the source dipole consists of an ideal conductor wire terminal by which current resides on the surface of the wire. As a result, volume charge density change into surface charge density and above equation can be simplified as,

$$\Pi_e = \frac{\mu}{4\pi} \iint_s (\mathbf{J}_{s(s)}^e) \frac{e^{-kr}}{r} ds, \quad (2.66)$$

$$\Pi_h = \frac{\epsilon}{4\pi} \iint_s (\mathbf{J}_{s(s)}^m) \frac{e^{-kr}}{r} ds, \quad (2.67)$$

In Equations 2.66 and 2.67, terms $\mathbf{J}_{s(s)}^e$ and $\mathbf{J}_{s(s)}^m$ are surface current density of electric and magnetic source respectively. The cross sectional area A of dipole terminal (Figure 2.3) is very small ($l \gg A$).

Resultant surface integral change into line integral and Equations 2.71 and 2.72 can be rewritten as,

$$\Pi_e = \frac{\mu}{4\pi} \int (\mathbf{I}_s^e) \frac{e^{-kr}}{r} dl \quad (2.68)$$

$$\Pi_h = \frac{\epsilon}{4\pi} \int (\mathbf{I}_s^m) \frac{e^{-kr}}{r} dl, \quad (2.69)$$

where \mathbf{I}_s^e and \mathbf{I}_s^m are current of electric and magnetic source respectively. In marine CSEM survey, the source dipole carries only electronic current \mathbf{I}_s^e . Furthermore magnetic current \mathbf{I}_s^m and potential functions Π_h are zero. The above expressions are valid to calculate the component of \mathbf{E} and \mathcal{H} fields at any distance from the source except on source itself.

2.4.2 Infinitesimal Dipole

In marine CSEM survey, the source dipole is much smaller than the wavelength of the signal (*infinitesimal dipole*) and immersed in seawater. The EM field from infinitesimal electric dipole source is calculated by solving Maxwell's equation in terms of potential. Figure 2.4 shows an infinitesimal dipole located at the origin along x -axis in rectangular coordinate system such that the directivity of the radiated EM energy is towards z -axis. A typical point of observation ' r ' from the any point on the source can be calculated by,

$$r = \sqrt{(x-x')^2 + (y-y')^2 + (z-z')^2} = \sqrt{x^2 + y^2 + z^2}, \quad (2.70)$$

where (x', y', z') is a point located at origin of rectangular coordinate system and (x, y, z) is a point of observation located at distance ' r ' from origin.

The survey is conducted by utilizing very low frequency signal with spatial variation in \mathbf{I}_e is assumed to be constant given as,

$$\mathbf{I}_e(x', y', z') = \hat{a}_x I_0, \quad (2.71)$$

where \hat{a}_x is unit vector.

Equation 2.71 can be used to solve auxiliary magnetic potential vector given by,

$$\Pi_e(x, y, z) = \frac{\mu}{4\pi} \int_{-l/2}^{+l/2} \mathbf{I}_e(x', y', z') \frac{e^{-ikr}}{r} dl = \hat{a}_x \frac{\mu I_0 l e^{-ikr}}{4\pi r}, \quad (2.72)$$

where the upper and lower limit refers the physical dimension of *infinitesimal* dipole with orientation along the x -axis.

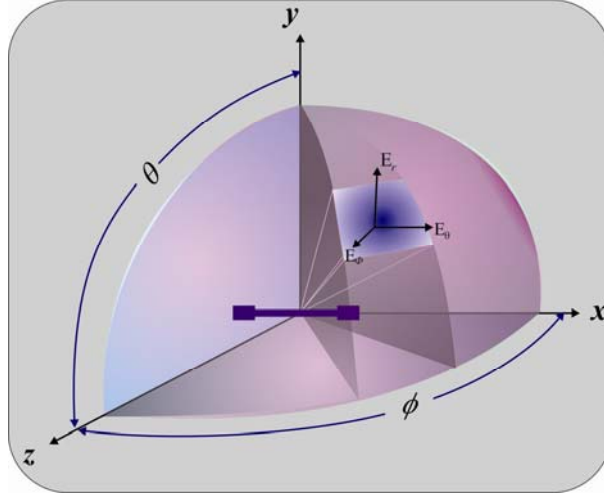


Figure 2.5 - Geometrical arrangement of infinitesimal dipole with electric field components. on spherical surface.

Figure 2.5 also shows the spherical coordinate system (r, θ, ϕ) for the electrical field, where ' r ' is the distance from dipole to point of orientation; θ and ϕ are angle of elevation and azimuth respectively. The corresponding auxiliary potential vectors in spherical coordinate system can be calculated by using the transformation between rectangular to spherical coordinate system and Equation 2.72 as,

$$\Pi_{e(r)} = \left(\frac{\mu I_0 l e^{-ikr}}{4\pi r} \right) \sin(\theta) \cos(\phi), \quad (2.73)$$

$$\Pi_{e(\theta)} = \left(\frac{\mu I_0 l e^{-ikr}}{4\pi r} \right) \sin(\theta) \cos(\phi), \quad (2.74)$$

$$\Pi_{e(\phi)} = \left(\frac{\mu I_0 l e^{-ikr}}{4\pi r} \right) \sin(\theta) \cos(\phi), \quad (2.75)$$

where $\Pi_{e(r)}$, $\Pi_{e(\theta)}$ and $\Pi_{e(\phi)}$ are the auxiliary magnetic potential vectors in spherical coordinate system.

By using the Equation 2.46 and symmetry of the problem the magnetic field density

vector can be calculated as,

$$\mathcal{B} = \frac{1}{r^2 \sin \theta} \left(r \sin \theta \left(\frac{\partial r \Pi_{e(\theta)}}{\partial r} + \frac{\partial \Pi_{e(r)}}{\partial \theta} \right) \right). \quad (2.76)$$

Substitution of Equations 2.73 and 2.74 into 2.76 to gives magnetic field intensity vector as,

$$\mathcal{H}_\phi = -\hat{a}_\phi \frac{ikI_0 l \sin \theta}{4\pi r} \left(1 + \frac{1}{ikr} \right) e^{-ikr}, \quad (2.77)$$

Furthermore, two components of the electric field can be calculated by using equation 2.77 with Maxwell's equation given as [25],

$$\mathbf{E} = \frac{1}{i\omega\epsilon} \nabla \times \mathcal{H}. \quad (2.78)$$

By substituting 2.73 and 2.75 into 2.78, the other two components of spherical coordinate system can be calculates as,

$$E_r = -\eta \frac{I_0 l \cos \theta}{2\pi r^2} \left(1 + \frac{1}{ikr} \right) e^{-ikr}, \quad (2.79)$$

$$E_\theta = \eta \frac{I_0 l \sin \theta}{4\pi r} \left(1 + \frac{1}{ikr} - \frac{1}{(kr)^2} \right) e^{-ikr}, \quad (2.80)$$

where $\eta = \sqrt{\mu/\epsilon}$ is the intrinsic impedance.

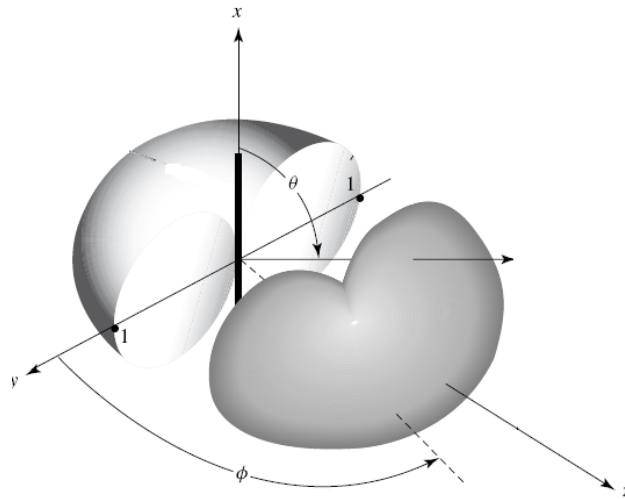


Figure 2.6 - Radiation pattern of infinitesimal dipole [27].

The given component of magnetic field and electric field are given in spherical coordinate system. These components are valid everywhere for calculating EM field except on the dipole itself. The radiation pattern of infinitesimal dipole is similar to the omni-directional antenna as shown in Figure 2.6.

2.5 Reflection and Refraction

Figure 2.6 shows the interface between two different uniform mediums with electrical properties $\sigma_1, \mu_1, \epsilon_1$ for medium-1 (M-1) and $\sigma_2, \mu_2, \epsilon_2$ for medium-2 (M-2) respectively. The normal and tangential component of the electric field at an interface becomes [28],

$$a_n \cdot (\mathcal{D}_1 - \mathcal{D}_2) = \rho_s, \quad (2.81)$$

$$a_n \times (\mathbf{E}_1 - \mathbf{E}_2) = 0 \quad (2.82)$$

where subscripts with field vectors assert to medium, wherever subscripts 1 and 2 correspond to quantity related to medium 1 and 2 respectively and unit vector a_n is normal to the interface as shown in Figure 2.6.

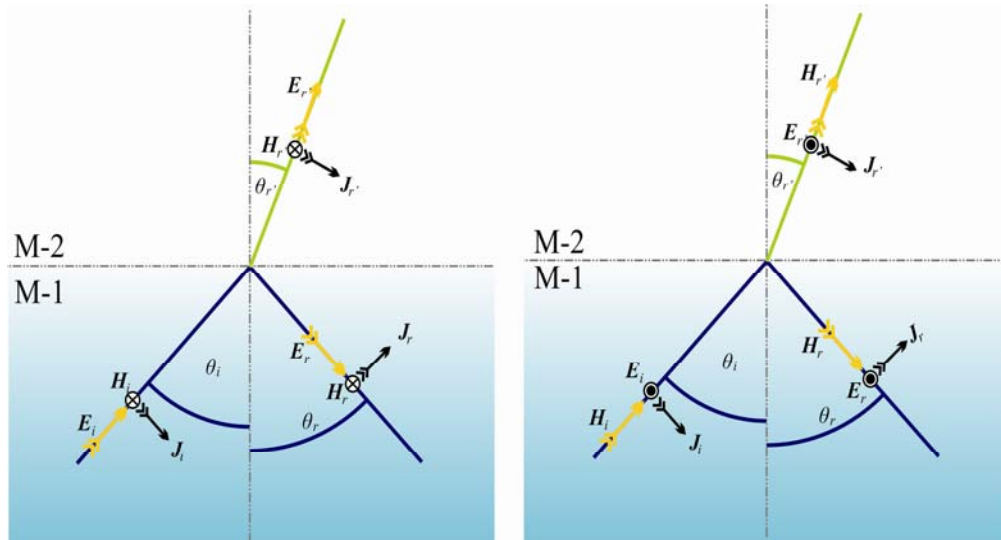


Figure 2.7- Incident, reflection and refraction of plane waves described by rays theory at plane interface of different medium.

Similarly the normal and tangential component of magnetic field at interface are given as,

$$a_n \cdot (\mathcal{B}_1 - \mathcal{B}_2) = 0, \quad (2.83)$$

and

$$a_n \times (\mathcal{H}_1 - \mathcal{H}_2) = \mathbf{J}_s. \quad (2.84)$$

Equations 2.83 shows the normal components of magnetic flux density are equal at the boundaries. In Equation 2.84 \mathbf{J}_s is the surface charge density which shows that the tangential components of magnetic field intensities are discontinuous at the boundaries.

Maxwell's equations characterize EM behavior at any point in the medium. In marine environment, EM field is generated by infinitesimal electric dipole source and in far-field region radiated field is treated as plane wave. In EM field propagation, the field components are normal to the direction of propagation as shown in above figure. It shows, the incident electric and magnetic waves \mathbf{E}_i and \mathcal{H}_i are meet at medium interface with an angle of incidence θ_i . Upon impinging in the interface, some part of the incident wave got reflected back indicated as \mathbf{E}_r and \mathcal{H}_r . According to Snell's law, the angle of reflection θ_r would be same as angle of incident θ_i . However at mediums interface, some part of incident field, determined by electrical properties of *medium-2*, radiate forward into and indicated by \mathbf{E}_r , and \mathcal{H}_r . The angle of reflection can be determined by Snell's law [28],

$$\sin \theta_i = \sin \theta_r, \quad (2.85)$$

$$k_1 \sin \theta_i = k_2 \sin \theta_r. \quad (2.86)$$

where angle of refraction θ_r , is the function of electrical properties of M-1, M-2 and θ_i is the angle of incident.

The tangential component of electric and magnetic field can be written in terms of the incident, reflected and refracted given as,

$$a_n \times (\mathbf{E}_i + \mathbf{E}_r) = a_n \times \mathbf{E}_r, \quad (2.87)$$

$$a_n \times (\mathcal{H}_i + \mathcal{H}_r) = a_n \times \mathcal{H}_r. \quad (2.88)$$

Equation 2.87 can be further simplified by substituting the condition of *Snell's law* ($\theta_i = \theta_r$). to obtain,

$$\mu_2 k_1 \cos \theta_1 \mathbf{E}_i - \mu_2 k_1 \cos \theta_1 \mathbf{E}_r = \mu_1 k_2 \cos \theta_{r'} \mathbf{E}_{r'}, \quad (2.89)$$

$$\mu_2 k_1 \cos \theta_1 \mathbf{E}_i - \mu_2 k_1 \cos \theta_1 \mathbf{E}_r = \mu_1 k_2 \cos \theta_{r'} (\mathbf{E}_i + \mathbf{E}_r). \quad (2.90)$$

The reflected electric field from above equation can be given as [28]

$$\mathbf{E}_r = \left(\frac{\mu_2 k_1 \cos \theta_1 - \mu_1 k_2 \cos \theta_{r'}}{\mu_2 k_1 \cos \theta_1 + \mu_1 k_2 \cos \theta_{r'}} \right) \mathbf{E}_i. \quad (2.91)$$

Equation 2.91 is used to find the reflected field where angle of incident would be calculated by using the definition of grazing angle. Similarly the expressions for refracted field from an interface can be calculated by simplifying the Equation 2.89 as,

$$\mathbf{E}_r \mu_2 k_1 \cos \theta_1 = \mathbf{E}_i \mu_2 k_1 \cos \theta_1 - \mathbf{E}_{r'} \mu_1 k_2 \cos \theta_{r'}, \quad (2.92)$$

$$(\mathbf{E}_{r'} - \mathbf{E}_i) \mu_2 k_1 \cos \theta_1 = \mathbf{E}_i \mu_2 k_1 \cos \theta_1 - \mathbf{E}_{r'} \mu_1 k_2 \cos \theta_{r'}, \quad (2.93)$$

The reflected electric field from above equation can be given as [28],

$$\mathbf{E}_{r'} = \left(\frac{2\mu_2 k_1 \cos \theta_1}{\mu_1 k_2 \cos \theta_{r'} + \mu_2 k_1 \cos \theta_1} \right) \mathbf{E}_i \quad (2.94)$$

Equations 2.94 allowed us to calculate the transmitted field to find transmitted field from an interface. The stratified geological model is normally consists on multi-interfaces. Equations 2.91 and 2.94 will be used to find the component of electric field at both sides of each interface.

2.6 Forward Modeling

Figure 2.8 shows the flow diagram of forward modeling used to obtain results for a defined field problem. Numerical results are obtained by constructing different geological models to apply field governing equations through numerical model. Maxwell's equations essentially provide the basis for a concise way to describe the relationship between \mathbf{E} field and \mathbf{H} field. EM geophysical surveys utilize very low frequency signal for delineating the physical properties of earth. Due to the use of low

frequency signal the displacement current density can be ignored in Maxwell's equations. The resulting equations are known as *quasi-static* equations that could be used to calculate the general wave equation. The general wave equations are also known as field governing equations that describe the behavior of EM field in conductive medium.

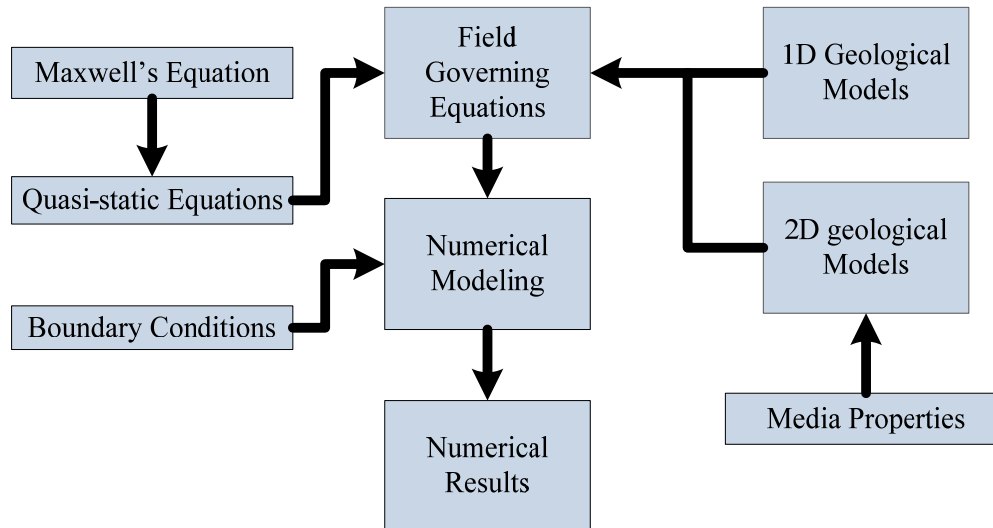


Figure 2.8 – Flow diagram of forward modeling.

In geophysical surveys the forward modeling consists of constructing different geological models to create artificial data for the study of EM behavior and survey geometry. Geometry and dimensions of geological model are defined using EM parameters related to the field problem. Furthermore, there are several ways to obtain discrete analogous of Maxwell's equation (field governing equations) for specified geological model. To implement numerical formulation, the model region is discretized into small elements. Then EM field is calculated at each node of discretized region by using numerical technique with boundary conditions. The result can be obtained by implementing algorithm for proposed numerical method in MATLAB programming.

2.7 Summary

Geophysical surveys are non-intrusive techniques and used for delineating the spatial distribution of earth's physical properties. In case of EM geophysical surveys, the most pertinent physical property is the electrical conductivity of subsurface rocks,

which is sensed by a physical time-varying EM field propagated through interior of buried rocks. The procedure of converting the real time survey data into physical properties of the earth is known as inversion. In a conventional approach for survey data analysis, geological models are constructed to obtain theoretical data. The theoretical data is compared with real-time survey data to approximate real geological structure. This conventional approach is known as forward modeling. Forward modeling is a convenient approach to study the behaviour EM field for specific geological models and source-receivers survey geometry. The most crucial feature for EM modeling is the mathematical theory of EM field used to calculate the field's governing equations.

In this chapter we derived the expressions of calculating EM field in dispersive medium from Maxwell's equations. The derived equations of EM field involve the well known mathematical description for EM propagation in stratified geological structure. In the next chapter, we focus on understanding the effects of mediums inhomogeneity on EM field. The modeling used an omni-directional source transmitting at low frequency. We will use equation 2.27 in 1D forward modeling to study the behavior of EM field in isotropic and anisotropic mediums.

CHAPTER 3

ONE DIMENSIONAL FORWARD MODELING

3.1 Introduction

In EM modeling, differential equations are normally used to describe the relations between radiated fields and their rates of change with respect to space and time. Some forms of mathematical techniques are required to calculate these relations, which can be classified as either analytical method or numerical methods. Analytical method provides an exact solution to the field problem. However it is difficult to find an exact solution because the solution region is inhomogeneous, anisotropic and time-dependent boundary condition [29]. Thus, a numerical solution is preferred for calculating the EM potentials in solution region.

There are many techniques to find numerical solution of field problem. However, the most well known numerical techniques are finite different (FD), finite element (FE), and integral equation (IE) methods. In EM field problems, IE provides accurate and fast numerical solution where FD and FE methods are preferred for complex structured media with large scale variation in electrical properties [30]. The marine environment consists on air, seawater, subsea sediments and buried hydrocarbons that give large scale variation in electrical properties of the media. For the proposed problem, study of marine CSEM survey geometry and understanding of EM field behavior, FD numerical method will be used because it is based on rectangular grid and requires relatively less computational time.

In mathematical modeling the dimensions of mediums are defined as the minimum number of coordinates needed to describe direction of variation. In a real time survey, the EM energy is propagated through the interior of a three dimensional earth with respect to time. However, the defined problem can be studied through 1D and 2D

numerical modeling. In this scenario, solution to 1D forward modeling is first performed in order to obtain optimal frequency and target depths for 2D forward modeling. In this chapter, the solution of 1D forward problem will be implemented with different combination of frequency and target depths.

3.2 Finite Difference Scheme for 1D Model

FD numerical method is used for approximating the solution of differential equations and extensively used for the application of heat diffusion and EM problems. This method gives estimated solution to EM fields using Taylor's series expansion. In EM field problem, the 1D geological model is characterized by varying EM parameters only in one direction and assumed to be constant along other all directions. A rectangular coordinate system will be considered for 1D model as: the specific direction of varying parameters lies along z -axis and constant along x -axis and y -axis.

FD method is obtained by replacing the solution of differential equations with respective derivatives [30]. In EM field problem the solution region is obtained by calculating the discrete values of magnetic and electric field using Maxwell's expression as given in Equations 2.26 and 2.27 respectively. The discrete values are calculated using optimal gridding scheme to discretize the solution regions into small elements as shown in Figure 3.1. In FD method, the most effective and optimal gridding scheme is *staggered-grid* scheme [31].

In the rectangular coordinate system, the 1D geological model can be presented by a single line as shown in Figure 3.1. This shows the single layered media (single line) is discretized into number of elements along z -axis, where indices on σ represents the element number. The EM parameters for the 1D model are defined as; electric permittivity of the medium which is ignored because of very low frequency; magnetic permeability of the medium is equal as in vacuum and electrical conductivity is define by σ_i with respective indices.

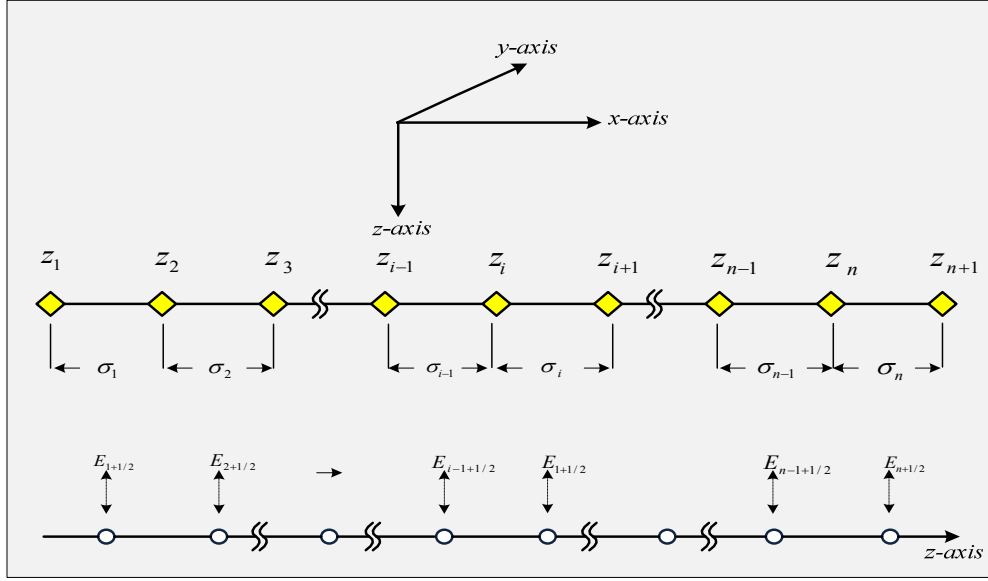


Figure 3.1 – 1D model region is discretized into number of finite elements. The indices i is used to number the nodes in z direction.

In FD method, the numerical approximation for electric field is obtained by solving Maxwell's Equation 2.27 for each element. The elementary procedure requires the mediums to be discretized along z -axis as $[z_1, z_2 \cdots z_{i-1}, z, z_{i+1} \cdots z_n]$. However the approximation of electric field is done in the mid point of each element as $[E_{(1+1/2)}, E_{(2+1/2)} \cdots E_{(i-1/2)}, E_{(i+1/2)}, E_{(i+3/2)} \cdots E_{(n-1/2)}]$. Only three types of differential approximation are considered as forward difference, backward difference and central difference formula. The expression for this formulation can be obtained by taking three consecutive nodes from Figure 3.1 as $E_{(i-1+1/2)}$, $E_{(i+1/2)}$ and $E_{(i+3/2)}$. The expressions for forward difference, backward difference and central difference are given as respectively,

$$\frac{1}{\Delta h} (E_{(i+3/2)} - E_{(i-1+1/2)}), \quad (3.1)$$

$$\frac{1}{\Delta h} (E_{(i+1/2)} - E_{(i-1+1/2)}), \quad (3.2)$$

$$\frac{1}{\Delta h^2} (E_{(i-1+1/2)} - 2E_{(i+1/2)} + E_{(i+3/2)}), \quad (3.3)$$

where Δh is the step size.

The computation of electric field in uniform medium is done using computational modeling as a mathematical tool. This involves the discretization of the solution region into several finite elements for \mathbf{E} field as shown in Figure 3.1. The finite

approximation is essentially prepared by estimating second order derivatives for the solution of Laplace's operator in Equation 2.27. A more general approach to estimate the second order derivative is done by Taylor's series and according to its expansion given as,

$$E(z_i + \Delta h_z) = E(z_i) + E'(z_i)(\Delta h_z) + \frac{1}{2!}E''(z_i)(\Delta h_z)^2 + \dots, \quad (3.4)$$

Similarly, backward finite difference expansion is given as,

$$E(z_i - \Delta h_z) = E(z_i) - E'(z_i)(\Delta h_z) + \frac{1}{2!}E''(z_i)(\Delta h_z)^2 - \dots, \quad (3.5)$$

where Δh_z is the step size from origin z_i . The sum of Equations 3.4 and 3.5 are used to obtain the second order difference formulas and can be written as;

$$E(z_i + \Delta h_z) + E(z_i - \Delta h_z) = 2E(z_i) + E''(z_i)(\Delta h_z)^2 + O(\Delta h_z^4) + \dots \quad (3.6)$$

The $O(\Delta h_z^4)$ is a truncation error of order (Δh_z^4) , which is introduced by constructing finite approximation. The truncation error is considered to be negligible and above equation can be written as,

$$E''(z_i) = \frac{1}{(\Delta h_z)^2} [E(z_i + \Delta h_z) - 2E(z_i) + E(z_i - \Delta h_z)]. \quad (3.7)$$

The above equation is obtained by ignoring the truncation error in Equation 3.6. FD method can be used to provide exact solution (*analytical*) by using the higher order differential equations from the expansion of Taylor's series [29]. However, to simplify the method, the infinite series has to be truncated before the fourth order differential term in central difference formula. Equation 3.4 can be used to calculate the solution of Equation 2.27 for a 1D discretized model. This essentially involves the calculation of forward and backward difference formula for $(i + \frac{1}{2})^{th}$ node from figure 3.1 as,

$$\Delta E_z|_{s(i+1/2)}^{+z} = \frac{1}{\Delta h_z} (E_{(i+3/2)} - E_{(i+1/2)}), \quad (3.8)$$

$$\Delta E_z|_{s(i-1/2)}^{-z} = \frac{1}{\Delta h_z} (E_{(i+1/2)} - E_{(i-1/2)}). \quad (3.9)$$

where $\Delta E_z|_{s(i+1/2)}^{+z}$ and $\Delta E_z|_{s(i-1/2)}^{-z}$ are the first order spatial derivative to calculate forward and backward difference formula. Both forward and backward difference formulas are used to obtain the second order equation for determining electric field. From Figure 3.1, it can be obtained by taking the finite difference from node $(i + \frac{1}{2})$ with respect to $(i + \frac{3}{2})$ and $(i - \frac{1}{2})$ respectively.

Equation 3.8 and 3.9 also can be used to calculate the second order differential form as,

$$\Delta^2 E_z|_{(i+\frac{1}{2})} = \frac{1}{\Delta h_z} \left(\Delta E_z|_{s(i+1/2)}^{+z} - \Delta E_z|_{s(i-1/2)}^{-z} \right) \quad (3.10)$$

where $\Delta^2 E_z|_{(i+\frac{1}{2})}$ is evaluated by taking the derivative of forward and difference formula in spatial domain. By substituting above expression into equation 2.27, the equation can be written as,

$$\frac{1}{\Delta h_z} \left(\Delta E_z|_{s(i+1/2)}^{+z} - \Delta E_z|_{s(i-1/2)}^{-z} \right) + i\omega\sigma_i\mu_0 E_{(i+\frac{1}{2})} = -i\omega\mu_0 J_s, \quad (3.11)$$

$$\frac{1}{\Delta h_z^2} \left(E_{(i-1/2)} - E_{(i+1/2)} (2 + i\omega\sigma_i\mu_0) + E_{(i+\frac{3}{2})} \right) = -i\omega\mu_0 J_s \quad (3.12)$$

The above equation will be used to calculate the electric field for any node except at boundaries. The resulting system of linear algebraic equations and associated boundary conditions can be expressed in the matrix form as,

$$M\tilde{\mathbf{e}} = i\omega\mu_0(\sigma\tilde{\mathbf{e}}^a + \mathbf{b}), \quad (3.13)$$

Where

$$M = \begin{pmatrix} D_1 & d_{1,1} & 0 & \dots & \dots & 0 \\ d_{2,1} & D_2 & d_{1,2} & \ddots & & \vdots \\ 0 & d_{2,2} & D_3 & d_{1,3} & \ddots & \vdots \\ \vdots & \ddots & \ddots & \ddots & \ddots & 0 \\ \vdots & & \ddots & \ddots & \ddots & d_{1,n-1} \\ 0 & \dots & \dots & 0 & d_{2,n-1} & D_n \end{pmatrix}$$

Similarly, $\tilde{\mathbf{e}}$ and $\tilde{\mathbf{e}}^a$ are column matrix of unknown and known electric field respectively; σ is the conductivity of media; M is $n \times n$ matrix of coefficient for the

system. The elements $\vartheta_{1,k}$, $\vartheta_{2,k}$ and ξ_k of matrix \mathbf{M} can be defined as;

$$D_k = -\left(\frac{2}{\Delta h_z^2} + i\omega\mu_0\sigma\right) \quad 2 \leq k \leq n-1, \quad (3.14)$$

$$d_{1,k} = \frac{1}{(\Delta h_z)^2} \quad 2 \leq k \leq n-1, \quad (3.15)$$

$$d_{2,k} = \frac{1}{(\Delta h_z)^2} \quad 1 \leq k \leq n-2. \quad (3.16)$$

In Equation 3.13, \mathbf{b} is the boundary values, where elements $\xi_1, \xi_n, \vartheta_{1,1}$ and $\vartheta_{2,n-1}$ of matrix \mathbf{M} involves the boundaries of 1D model. The vector $\tilde{\mathbf{e}}$ has a structure

$$\tilde{\mathbf{e}} = \left[E_{(1/2)}, E_{(1+1/2)}, \dots, E_{(j-1/2)}, E_{(1+1/2)}, \dots, E_{(n-1/2)} \right]^T \quad (3.17)$$

The given form of the system in equation 3.13 is readily solved by using the numerical methods of linear algebra.

In EM boundary value problem, the behavior of radiated EM field is dependent upon medium's electrical properties, type of source excitation and boundary conditions. In selected 1D forward problem, the electrical parameters are varying along z -axis, while they are constant along x -axis and y -axis. The dimension of z -axis is larger than 5δ . Consequently, we assumed the field at z_n as

$$E_{\left(n-\frac{1}{2}\right)} = 0 \quad (3.18)$$

Similarly, the boundary at z_1 can be calculated using Maxwell's equation as

$$\nabla \times E_z = \frac{\partial E_z}{\partial z} = \frac{1}{\Delta h_z} \left(E_{1+\frac{1}{2}} + E_{1-\frac{1}{2}} \right) = -i\omega\mu H_y \quad (3.19)$$

In Equation (3.19), the magnetic field vector is non zero. Its magnitude is assumed to be equal to one and we can rewrite it as,

$$\frac{1}{\Delta h_z} \left(E_{1+\frac{1}{2}} + E_{1-\frac{1}{2}} \right) = -i\omega\mu \quad (3.20)$$

Equations (3.18) and (3.19) are used to solve 1D isotropic and anisotropic geological models.

3.3 Stability and Accuracy of FD method

The most important factor of numerical method is accuracy and stability. The accuracy of numerical method is to find how well it agrees with analytical solution. In FD method the accuracy can be improved by considering higher order terms of Taylor's series in solution of differential equations.

In numerical modeling there are three types of errors namely discretization error, modeling error and computational error [29]. Modeling error caused by considering the continuous function by discretized functions. Discretization error involves the error due to truncation and ignoring higher order terms of Taylor expansion. The computational error is caused by determining one component of field (magnetic field) directly from other component (electric field) that is calculated by discretization. In the given FD method the truncation error rate is negligible by taking the central difference formula and fine meshing.

3.4 1D Forward Modeling

The procedure of converting real time survey data into physical property distribution is called inversion or backward modeling; whereas the forward modeling is done by constructing different geological structure of defined physical properties to create artificial data. In this section the numerical modeling readily implemented on two different types of 1D geological model. The main intention of 1D numerical modeling is to understand the mechanisms behind the EM field propagation and to calculate optimal frequency for desired target depth. Modeling essentially requires constructing of 1D geological model with defined electrical properties and then applying numerical techniques.

In conductive medium the relative strength of electric field is a function of frequency, electrical parameter of the medium and source-receiver separation distance. Prior to implement the selected numerical scheme for 1D forward modeling is verified by implementing it onto previously existing model. The results obtained are compared as shown in Figure 3.2 and it validates to selected numerical method. The 1D forward modeling is prepared in the next section to study the effects on

electric field caused by varying frequency, conductivity and source-receiver separation distance.

The 1D forward modeling is implemented for test problem to verify results and methodology using two different frequencies of 0.25 Hz and 1.0 Hz. The results obtain for magnitudes verses offset are shown in Figure 3.2 and it verifies the magnitude of diffused field attenuate rapidly if medium is more conductive and for higher frequency.

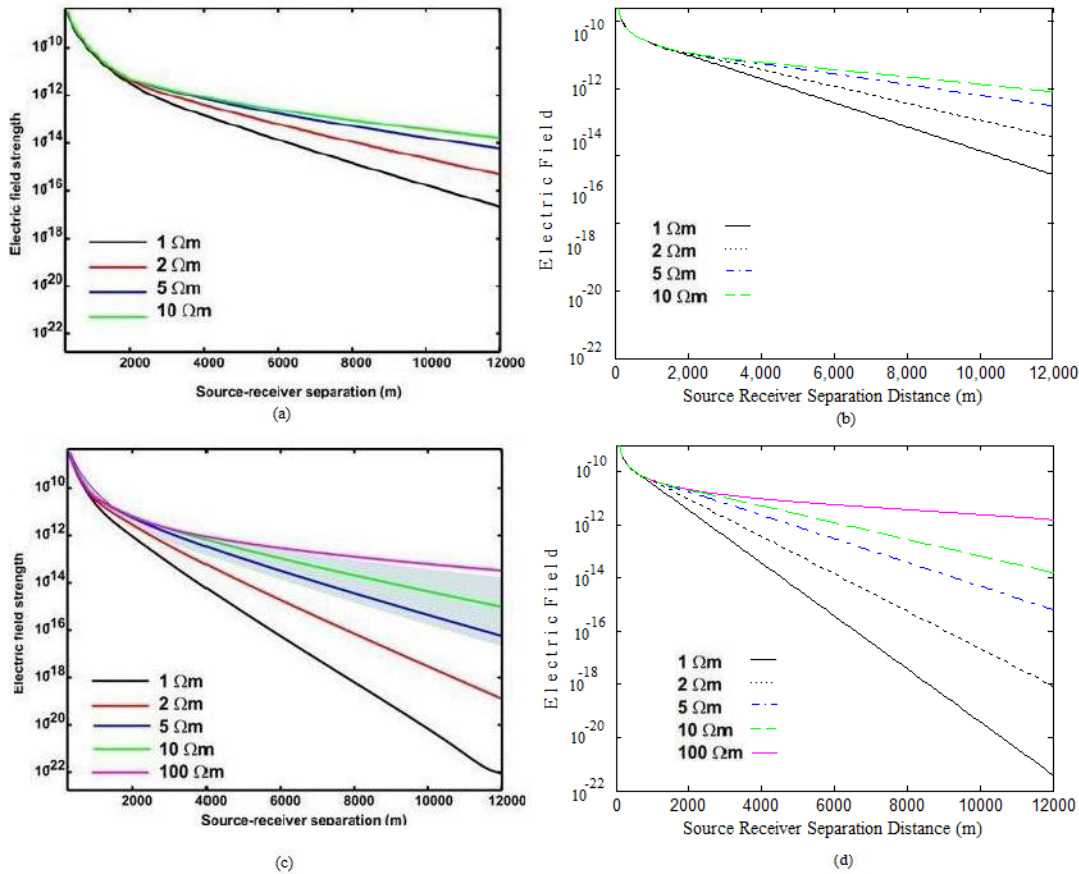


Figure 3.2 – In figure (a) and (c) shows the previously existing results at frequency of 0.2 Hz and 1.0 Hz, however the results obtained for validation are showing in figure (b) and (d) at frequency 0.2 Hz and 1.0 Hz.

3.4.1 1D Isotropic Geological Model

Isotropic geological structure is chosen to study the effects of frequency, electrical conductivity on diffused signal. Selected model contains three isotropic layers (I, II and III) of different conductivity as shown in Figure 3.3. The layer length is 10 km along z-axis and constant along other all directions. The electrical properties for given isotropic model are chosen according to the real earth model. Usually the conductivity

of earth materials is greater than 1×10^{-4} S/m, where electrical permittivity is less than 1×10^{-11} F/m. Consequently, the value of permittivity is negligible due to the use of low frequency signal (0.01 Hz to 10 Hz). The magnetic permeability is assumed to be the same value as in vacuum ($4\pi \times 10^{-7}$ N/m²).

In isotropic model the electrical conductivity of selected layers I, II and III are 0.01 S/m, 0.02 S/m and 0.04 S/m respectively. A stationary point source is considered to radiate energy with frequency of 0.25 Hz and 1.0 Hz. The discretized layer of isotropic model is divided into 100 equal elements with step size (Δh_z) of 100 m. Each layer contains 102 nodes with same electrical property at each element. Equation 3.13 is solved for each node with zero source (J_s) term except for first node.

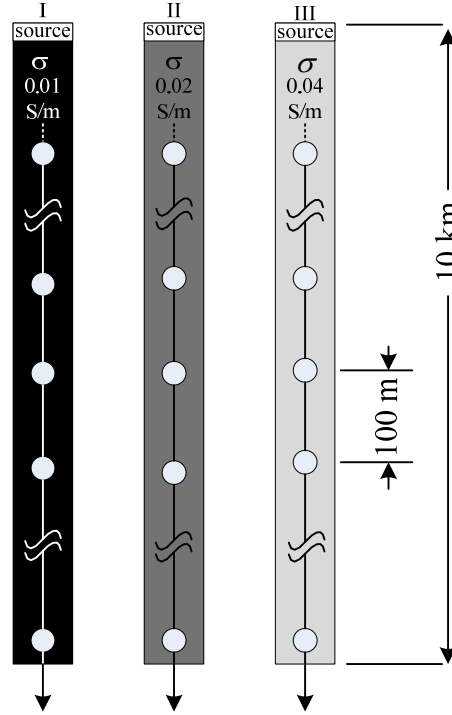


Figure 3.3- Isotropic geophysical model of three different layers I, II and III.

3.4.2 Numerical Results of Isotropic geological Model

Algorithm for field expressions of 1D forward modeling were implemented in MATLAB and given in **APPENDIX-A**. The plots in Figure 3.3 shows the real and imaginary part of electric field in logarithmic scale verses source-receiver separation distance. The response of electric field is calculated for each layer of isotropic model

with two different frequencies. The electrical conductivity and frequency for each plot of Figure 3.4, 3.5 and 3.6 are given in Table 3.1

Table 3.1 - Electrical conductivity and frequency for each plot of Figure 3.3

Figure 3.3	Conductivity (S/m)		Frequency (Hz)
(a)	Layer – I	0.01	0.25
(b)		0.01	1.00
(c)	Layer - II	0.02	0.25
(d)		0.02	1.00
(e)	Layer - III	0.04	0.25
(f)		0.04	1.00

The magnitude of electric field at frequency 0.25 Hz and 1.0 Hz for each layer of isotropic model is presented in Figure 3.3. The figure shows the magnitude of electric field for Layer-I at two different frequencies in logarithmic scale. It shows that the medium is resistive to high frequency than low frequency signal. Similarly Figures 3.5 and 3.6 shows, the response of electric field for Layer-II and Layer-III at both frequencies of 0.25 Hz and 1.0 Hz. Phase response at frequency of 0.25 Hz for isotropic geological model is shown in Figure 3.7(a), where for frequency of 1.0 Hz is in Figure 3.7(b). It shows the phase response of Layer-III is dominating to Layer-I and Layer-II, which conclude that there is more phase delay when medium becomes more conductive.

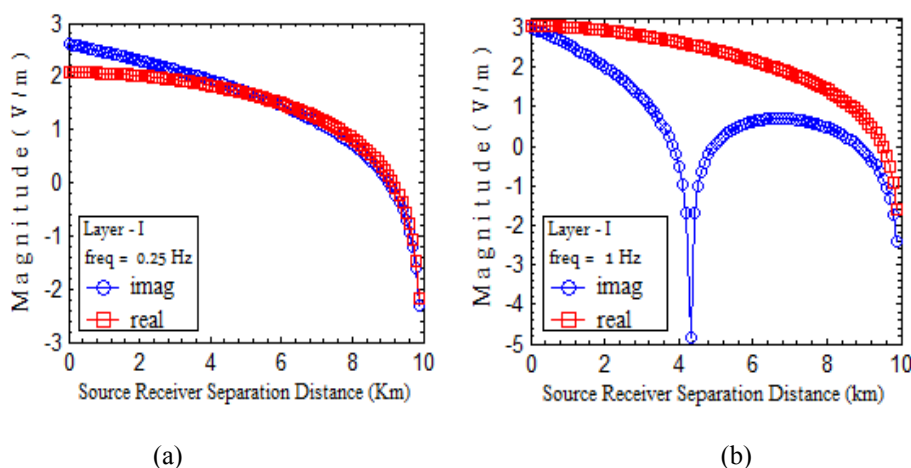


Figure 3.4 – Magnitude response of isotropic geological model for layer-I at (a) frequency of 0.25 Hz and (b) frequency of 1Hz

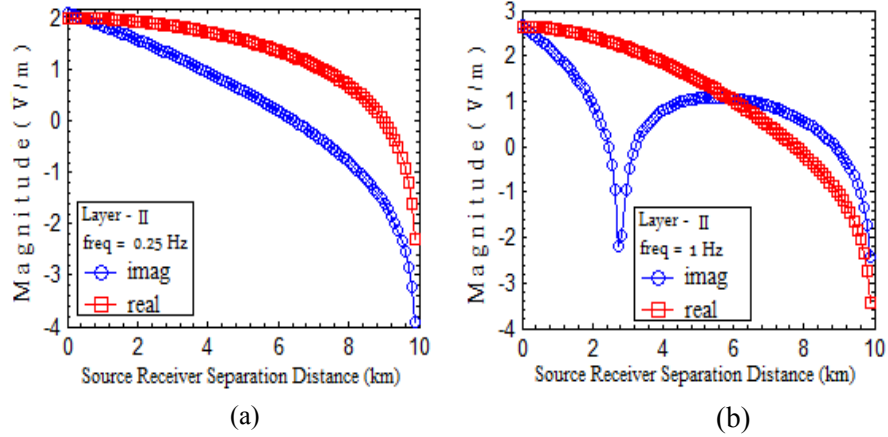


Figure 3.5 - Magnitude response of isotropic geological model for layer-II at (a) frequency of 0.25 Hz and (b) frequency of 1Hz

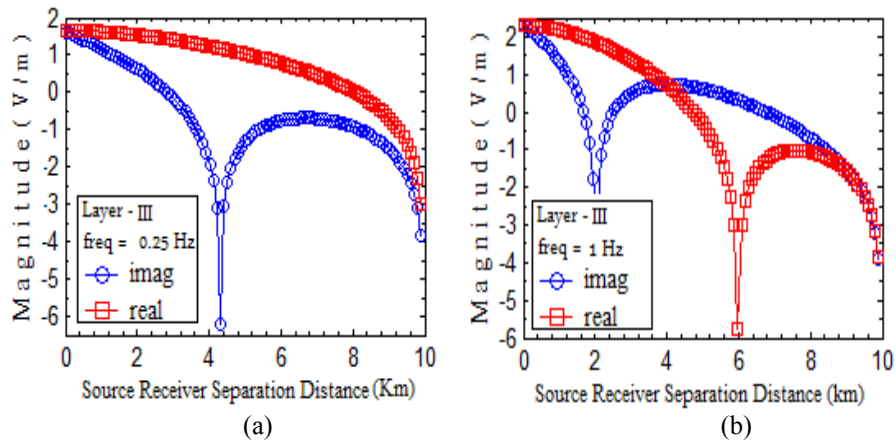


Figure 3.6 - Magnitude response of isotropic geological model for layer-III at (a) frequency of 0.25 Hz and (b) frequency of 1Hz

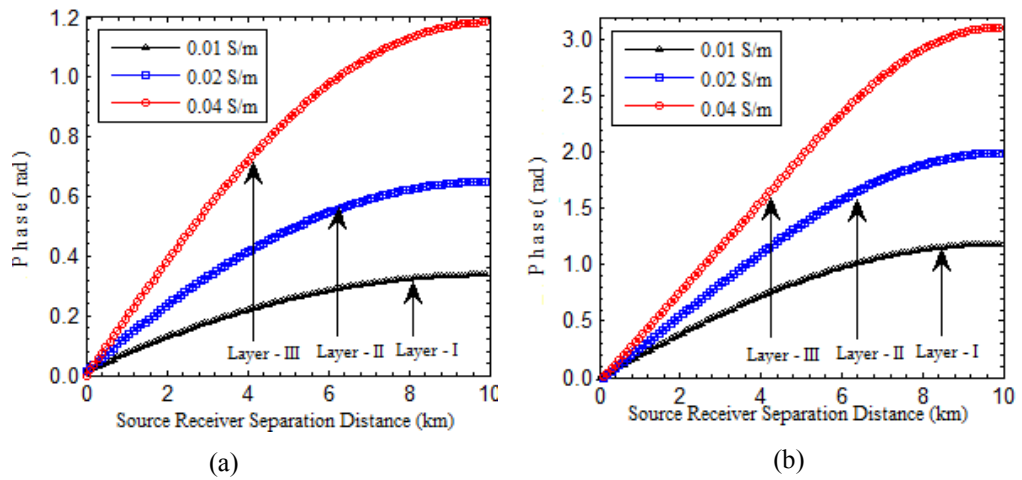


Figure 3.7- Phase response of isotropic geological model for layer-III at (a) frequency of 0.25 Hz and (b) frequency of 1Hz

It is evident that the relative strength of electric field is dependent on media properties and frequency. The diffused fields are more attenuated if the medium is more conductive. Furthermore if the source frequency increases, the penetration depth decreases. Up to this point, it is clear the obtained results for electric at frequency 0.25 Hz are less attenuated and also have less phase delay. So for the next, the numerical forward modeling will be prepared by using frequency 0.25 Hz.

3.4.3 1D Anisotropic Geological Model

To study the field behavior for irregularities in medium, an anisotropic geological model is considered. This model is also consisted on three selected layers I, II and III having different electrical conductivity as shown in Figure 3.8.

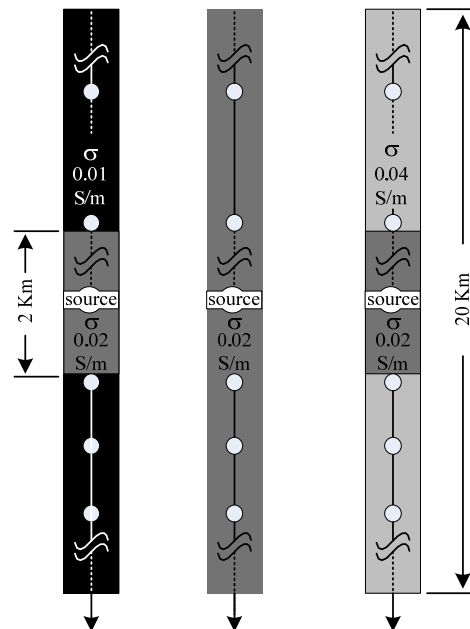


Figure 3.8- Anisotropic geophysical model of three different layers.

The length of each layer in anisotropic geological model is 20 km along z-axis and constant along other all directions. Layers I and II shows anisotropy because of different electrical conductivity as shown in Table 3.2. The solution region is discretized same as isotropic model where source is considered at middle for each layer. Remaining parameters are same as in isotropic model.

Table 3.2 - Electrical conductivity of layers I, II and III for anisotropic media

Layer-I			Layer-II	Layer-III		
9 km	2 km	9 km	20 km	9 km	2 km	9 km
0.01 S/m	0.02 S/m	0.01 S/m	0.02 S/m	0.04 S/m	0.02 S/m	0.04 S/m

3.4.4 Numerical Results of Anisotropic geological Model

The essentials of 1D forward modeling are to understand the effects of inhomogeneous medium on EM signal. The spatial variation in medium electrical properties affects on diffused electric fields by two ways. Firstly the electric field distorted by the deposit charge at interface due to change in electrical properties and secondly the direct electric field is distorted by indirect electric field that's created by time varying magnetic field of eddy current [8]. Numerical modeling uses a procedure by which we calculate the radial component of electric field created by a point source.

Simulation result for field response of electric field of anisotropic geological model is shown in Figure 3.9. It shows that the electric field response for three different layers of anisotropic geological model. In model, the distance after 1.0 km from the middle of the layer I and III, the electrical conductivity is change. Resultant the response of electric field changes its behavior after covering distance 1.0 Km. The field response of less conductive medium, dominate to the response of high conductive medium.

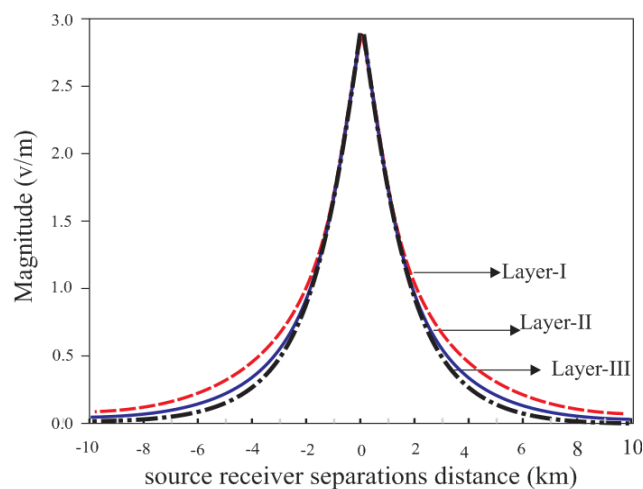


Figure 3.9 – Magnitude of electric field for anisotropic geological model at Frequency 0.25 Hz

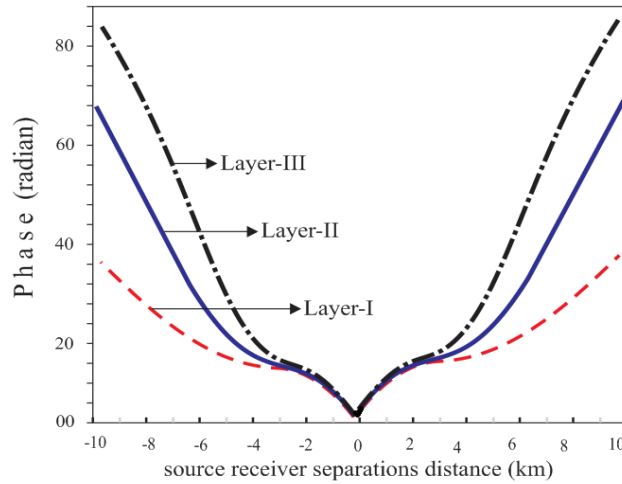


Figure 3.10 – Phase response of electric field for anisotropic geological model at Frequency 0.25 Hz

In Figure 3.10, the cumulative sum of phase delay for electric field of anisotropic geological model is shown. This shows there is more phase delay while the medium is conductive in comparison to the less conductive medium. Obtained results shows the pattern of induced field is not fixed and change caused by frequency of the signal and electrical properties of the medium. The E-field and phase profile for the 1D anisotropic geophysical model is in consistent with the one published by [32]-[33].

3.5 Summary

1D forward modeling allows us to generate EM response for different frequencies and geological models which is useful for survey operators in designing of an optimal survey set-up for seabed logging. Although it has been known for a long time that the EM field can radiate from conductive medium to resistive medium, its appreciation its use for determining the petroleum reserves remotely is only introduced only few years ago. Relative slow developments in controlled source EM sounding was caused by lack of understanding with uncertainty in field response for thin resistive buried layers. Thus, laboratory experiments and numerical modeling improve the procedure by which we can understand the physical response of the signal to discriminate between physical earth properties. Here we present 1D forward modeling with consistent results that shows the EM energy is more attenuated in less resistive media. In the next chapter, we will study the EM behavior for reservoir that is saturated with resistive hydrocarbon or conductive saline fluids in layered media.

CHAPTER 4

TWO DIMENSIONAL FORWARD MODELING USING FINITE DIFFERENCE METHOD

4.1 Introduction

In layered earth media, the conductive sea water is situated between two resistive mediums, namely air half-space and subsea sedimentary rocks. In this form, the marine environment acts as a low pass filter because it allows only low frequency signal to pass through it [2]. In marine CSEM/SBL, mobile dipole source is oriented at a height from seafloor that is not more than the skin depth of EM wave in host medium. The dipole source radiates the EM energy both towards the overlying water column and the subsea surface. This physical field is propagated through the interior of conductive seawater; air half space and subsea sedimentary rocks. The seawater height from seafloor should be 300 m or more to minimize the interference from air half space [34]. The radiated EM fields will reflect back towards seafloor where it is received by the seafloor based receivers. The received signal contains the information of the spatial distribution of earth physical properties.

The forward modeling will be done in order to understand the physical behavior of EM field while it passes through the layered earth media. Previously most of the work was done by using 2D numerical modeling because EM field can be separated into two different classes as TE and TM mode. In 2D layered media, the dimension of the medium and field excited by the source is larger in comparison with the skin depth in host medium. In such cases the excited field terminates along strike directions and only the reflected field carries the information contains about earth physical properties.

The surrounding medium that carries EM energy is known as the field region. The field region of EM source can be classified into near field-region and far field region. The inner boundary of near field region starts immediately from surrounding area of the antenna and its outer boundary is taken at a distance of $R < 0.62\sqrt{D^3/\lambda}$ [16]. On the other hand, the far-field region starts from the outer boundary of near-field region and extended to infinity. In this chapter, 2D forward modeling is carried out to understand the signal behavior in far field region. The numerical results from 2D numerical modeling are also discussed in great detail.

4.2 EM Field Equation.

For geophysical surveys, the marine environment is different from a continental environment. In marine environment the sea floor is filled with conductive water with conductivity varies from 3.2 S/m to 5.2 S/m [2]. The variation in conductivity is a function of seawater salinity, temperature and pressure [35]. The seawater is situated in between two resistive medium of air half space and sedimentary rocks as shows in figure 4.1. The electrical conductivity of air half space 0.295×10^{-14} S/m [36], the electrical conductivity of sediment is 1.0 S/m and the electrical conductivity hydrocarbon saturated reservoir and saline water reservoir is 0.5 S/m and 5.2 S/m respectively.

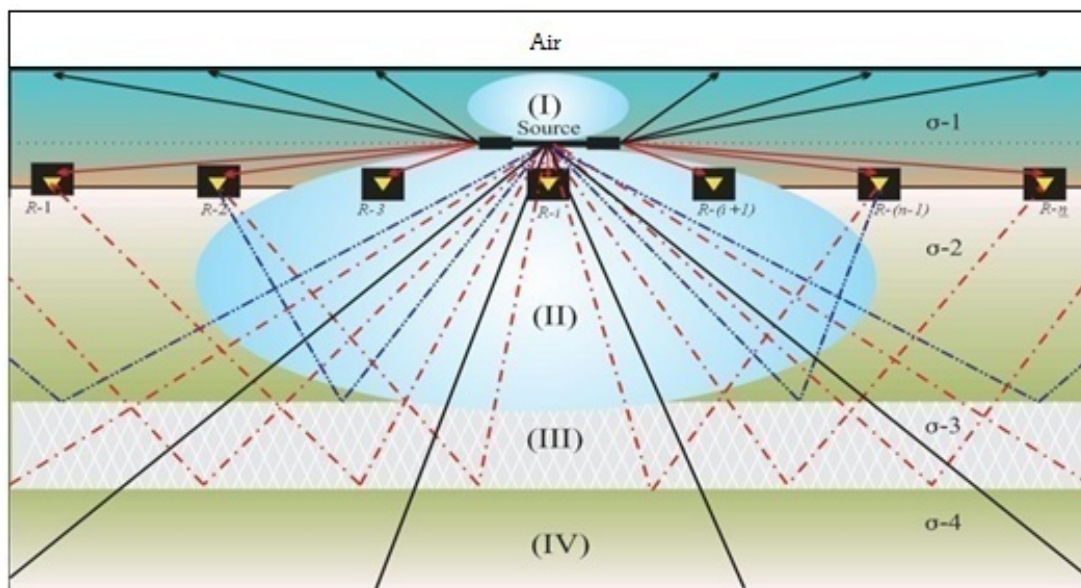


Figure 4.1- The typical layout of propagated signal in a 2D geophysical model.

The direct measureable components of the EM field are \mathbf{E} and \mathbf{H} , where both are functions of time and space. The Maxwell's equations in frequency domain can be written as [5]

$$\nabla \times \mathbf{H} = \sigma \mathbf{E} - i\omega \mathbf{D} + \mathbf{J}_s, \quad (4.1)$$

$$\nabla \times \mathbf{E} = -i\omega \mu \mathbf{H}. \quad (4.2)$$

Similarly, the divergence of magnetic field density and electric field density can be written as,

$$\nabla \cdot \mathbf{B} = 0, \quad (4.3)$$

$$\nabla \cdot \mathbf{D} = q + q^s. \quad (4.4)$$

In previous equations, the four vectors quantities \mathbf{E} , \mathbf{D} , \mathbf{B} and \mathbf{H} are considered to be continuous and finite in the entire domain. Similarly, the constitutive relation shows $\mathbf{B} = \mu \mathbf{H}$ and $\mathbf{D} = \epsilon \mathbf{E}$ for a linear, homogeneous and isotropic medium, which is also known as uniform medium. The 2D forward modeling is performed by considering a piecewise linear medium.

The 2D forward modeling is attractive because the Maxwell's equations can be used rigorously to separate EM field into TE and TM modes. The characteristics of 2D geological model are defined by considering that the electrical properties of the earth vary only along the vertical plane. In rectangular coordinate system, it is assumed that the electrical conductivities of layered medium are varying along two dimensions (along x -axis and z -axis) and constant along third dimension (along y -axis). The field equations for the considered geological area can be obtained by solving Equations 4.1 and 4.2 as,

$$\begin{vmatrix} a_i & a_j & a_k \\ \frac{\partial}{\partial x} & \frac{\partial}{\partial y} & \frac{\partial}{\partial z} \\ \mathcal{H}_x & \mathcal{H}_y & \mathcal{H}_z \end{vmatrix} = \sigma \mathbf{E} + \mathbf{J}_{s(x,z)}, \quad (4.5)$$

$$\begin{vmatrix} a_i & a_j & a_k \\ \frac{\partial}{\partial x} & \frac{\partial}{\partial y} & \frac{\partial}{\partial z} \\ E_x & E_y & E_z \end{vmatrix} = i\omega \mu \mathbf{H}. \quad (4.6)$$

In Equation 4.1 the magnitude of $i\omega\mathbf{D}$ is negligible due to low frequency signal. Furthermore, the Equations 4.5 and 4.6 can be used to obtain the expression for TM and TE modes can be written as,

$$-\frac{\partial \mathcal{H}_y}{\partial z} = \sigma E_x + J_{s,x}, \quad (4.7a)$$

$$\frac{\partial E_z}{\partial x} - \frac{\partial E_x}{\partial z} = i\omega\mu\mathcal{H}_y, \quad (4.7b)$$

$$\frac{\partial \mathcal{H}_y}{\partial x} = \sigma E_z + J_{s,z}, \quad (4.7c)$$

Similarly Equation 4.6 can be written as,

$$-\frac{\partial E_y}{\partial z} = i\omega\mu\mathcal{H}_x, \quad (4.8a)$$

$$\frac{\partial \mathcal{H}_x}{\partial z} - \frac{\partial \mathcal{H}_z}{\partial x} = \sigma E_y + J_{s,y}, \quad (4.8b)$$

$$\frac{\partial E_y}{\partial x} = i\omega\mu\mathcal{H}_z. \quad (4.8c)$$

From Equation 4.7a through 4.8c, indices \mathbf{s} and $(\mathbf{x}, \mathbf{y}, \mathbf{z})$ with source terms refers to external source and rectangular coordinates respectively. Equations 4.7a, 4.7b and 4.7c contains the component \mathbf{E}_x , \mathcal{H}_y and \mathbf{E}_z for TM *polarization* mode. Similarly the components \mathcal{H}_x , \mathbf{E}_y and \mathcal{H}_z in equations 4.8a, 4.8b and 4.8c are for TE *polarization* mode. This separation of TM and TE mode provides the solution to EM equation into two scalar variables and each satisfy complete independent equations [5]. These two independent equations can be solved by substituting Equations 4.7a and 4.7c into Equation 4.7b as,

$$\left[\left(\frac{\partial^2 \mathcal{H}_y}{\partial x^2} \right) + \left(\frac{\partial (J_{s,z})}{\partial x} \right) + \left(\frac{\partial^2 \mathcal{H}_y}{\partial z^2} \right) + \left(\frac{\partial (J_{s,x})}{\partial z} \right) \right] = -i\omega\sigma\mu\mathcal{H}_y, \quad (4.9)$$

and

$$\frac{\partial^2 \mathcal{H}_y}{\partial x^2} + \frac{\partial^2 \mathcal{H}_y}{\partial z^2} + i\omega\sigma\mu\mathcal{H}_y = - \left(\frac{\partial (J_{s,z})}{\partial x} + \frac{\partial (J_{s,x})}{\partial z} \right), \quad (4.10)$$

Similarly the equations of TE polarization can be solved by substituting Equations 4.8a and 4.8c into Equation 4.8b as,

$$\frac{\partial^2 E_y}{\partial x^2} + \frac{\partial^2 E_y}{\partial z^2} + i\omega\mu\sigma E_y = -i\omega\mu J_{s,y}. \quad (4.11)$$

In the next section, a 2D layered medium will be considered in which the region of interest is located in far field region. The region of interest will be studied by calculating E-polarized field that originates from an external source \mathbf{J}_s .

4.3 Signal Propagation in 2D Model

Marine CSEM survey is used to discriminate between the resistive hydrocarbon reservoir and conductive saline fluid reservoir. To understand the field behavior of EM, it is necessary to consider a well defined layered medium. The general view of 2D geological layered media is in Figure 4.1.

In reference to Figure 4.1, the layered model consists on air half space (half space is assumed to approximate the medium in mathematical model), seawater layer (I), overburden sediments (II), saturated reservoir (III) and under burden sediments (IV). To quantify the transmitted field in 2D media we need to consider the possible direction of signal propagation. In a selected media, the electrical properties of each layer need to be defined. At interface the transmitted field will divide into reflect field and refracted field pattern. The chosen geological model has four different interfaces as air half-space to seawater layer, seawater layer to overburden sediments layer, overburden sediments layer to saturated reservoir layer and saturate reservoir layer to under burden sediment layer. Furthermore, receivers are placed on seafloor and EM source is oriented 50 m above from seafloor. The signal propagation for the geological media of hydrocarbon containing reservoir is indicated in Figure 4.1. More detail of propagated signal is given in section 1.4.

In marine CSEM, the target area occurs in far field region. In such case, the radiated field travels to the region of interest from a distant mobile source through conductive sediments and seawater. The reduction in far field strength is a function of the source-receiver separation distance. To enable profiling of target depth, the source- receiver separation distance should be larger as compared to the distance of

target from the source [3]. Due to this, in selected 2D geological model the strike length of EM radiated field is larger than both the skin depth of the field and physical dimension of model. In such a case the radiated field terminates along the strike direction (direction of propagation) and only the reflected field contains the information of subsea layered media. In numerical modeling only the reflected field will be considered to understand the behavior of the EM field for selected geological models.

4.4 FD Scheme for 2D Geological model

FD numerical techniques can be used to evaluate the EM field in 2D layered geological models. The most elementary step of implementing numerical method is to assume layered media of an arbitrary shape with defined EM parameters. To implement the numerical method the selected medium is first discretized into several elements. Maxwell's equations are solved for each element using an optimal grid scheme.

The most common technique for discretization of solution region is the *staggered-grid* scheme. This technique has the advantage where \mathbf{E} and \mathbf{H} field component are continuous at the edges and face of each elements [31]. The solution region is discretized into number of elements as shown in Figure 4.2.

The *staggered-grid* scheme uses central difference formula to quantify \mathbf{E} field for each element of discretized media [31]. The differential form of Equation 4.11 can be calculated for any node (i, j) using centered difference formula. The differential form is taken by substituting simple derivative terms with respect to space by using Figure 4.2. To calculate the differential operator of Equation 4.11 in 2D spatial domain for any test point (i, j) it requires four adjacent nodes (a, b, c, d) except at boundaries points i.e. test point (i, j) and its four adjacent nodes $[(i - 1/2, j), (i + 1/2, j), (i, j - 1/2), (i, j + 1/2)]$ as shown in Figure 4.2.

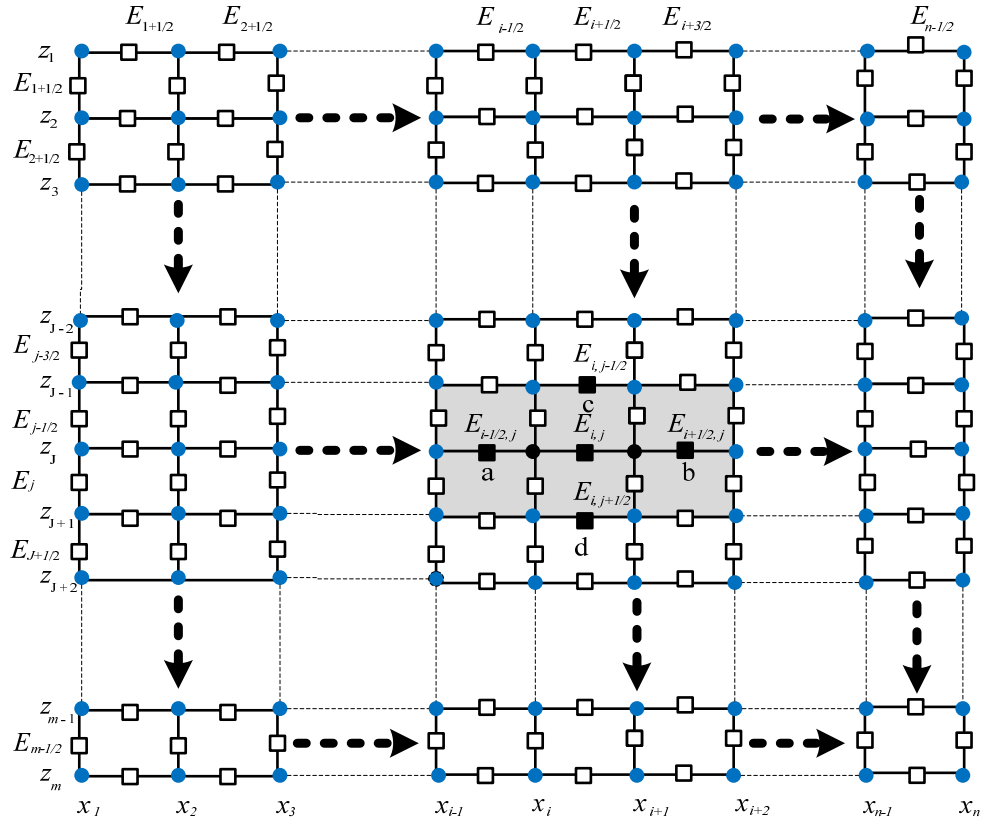


Figure 4.2 - 2D stratified geological model that is discretized into a number of rectangular grids.

The differential form can be obtained for a point (i, j) with respect to its four adjacent nodes as,

$$\Delta E_x \big|_{S(i,j)}^{+x} = \frac{1}{\Delta h_x} \left(E_{(i+1/2, j)} - E_{(i, j)} \right), \quad (4.12)$$

$$\Delta E_x \big|_{S(i,j)}^{-x} = \frac{1}{\Delta h_x} \left(E_{(i, j)} - E_{(i-1/2, j)} \right), \quad (4.13)$$

$$\Delta E_z \big|_{S(i,j)}^{+z} = \frac{1}{\Delta h_z} \left(E_{(i, j+1/2)} - E_{(i, j)} \right), \quad (4.14)$$

$$\Delta E_z \big|_{S(i,j)}^{-z} = \frac{1}{\Delta h_z} \left(E_{(i, j)} - E_{(i, j-1/2)} \right). \quad (4.15)$$

The ΔE is obtained by taking the finite differences as from above equation $S_{(i,j)}^{+x}$ is forward difference; $S_{(i,j)}^{-x}$ is backward difference; $S_{(i,j)}^{+z}$ is upward difference and $S_{(i,j)}^{-z}$ is the

downward difference. Equations 4.12, 4.13, 4.14 and 4.15 can be used to calculate second order differential form as follows,

$$\Delta^2 E_x \Big|_{S(i,j)}^x = \frac{1}{(\Delta h_x)^2} \left(\Delta E_x \Big|_{S(i,j)}^{+x} - \Delta E_x \Big|_{S(i,j)}^{-x} \right), \quad (4.16)$$

$$\Delta^2 E_z \Big|_{S(i,j)}^z = \frac{1}{(\Delta h_z)^2} \left(\Delta E_z \Big|_{S(i,j)}^{+z} - \Delta E_z \Big|_{S(i,j)}^{-z} \right). \quad (4.17)$$

Equations 4.16 and 4.17 can be used for obtaining the solution of the second order differential operator of Equation 4.11. The resulting form can be written as,

$$\nabla^2 \mathbf{E} = \frac{\partial^2 E_y}{\partial x^2} + \frac{\partial^2 E_x}{\partial z^2} = \Delta^2 E_x \Big|_{S(i,j)}^x + \Delta^2 E_z \Big|_{S(i,j)}^z, \quad (4.18)$$

where ∇^2 is Laplace operator and in 2D modeling it can be defined as $\left(\frac{\partial^2}{\partial x^2} + \frac{\partial^2}{\partial z^2} \right)$ for a given 2D layered medium. The above equation can be rewritten in a more generalized form as,

$$\nabla^2 \mathbf{E} = \frac{1}{(\Delta h_x)^2} \left(\Delta E_x \Big|_{S(i,j)}^{+x} - \Delta E_x \Big|_{S(i,j)}^{-x} \right) + \frac{1}{(\Delta h_z)^2} \left(\Delta E_z \Big|_{S(i,j)}^{+z} - \Delta E_z \Big|_{S(i,j)}^{-z} \right). \quad (4.19)$$

The resulting system of linear algebraic equation can be written in matrix form and its can be expressed as,

$$(M) \tilde{e} = i\omega\mu_0 (\sigma \tilde{e}^a + \mathbf{b}), \quad (4.20)$$

where \tilde{e} and \tilde{e}^a are vectors for known and unknown electric field in region of interest, σ is the electrical conductivity of media, M is a $N \times N$ matrix of coefficient and known as system matrix, however $N = m \times n$ where m and n are the numbers of rows and columns. The magnitude of each element $[D_k, d_{1,k}, d_{2,k}, k_{1,k}, k_{2,k}]$ in matrix M except the boundaries are given as,

$$D_n = - \left(\frac{2}{\Delta h_x^2} + \frac{2}{\Delta h_z^2} + i\omega\mu_0\sigma \right), \quad (4.21)$$

$$d_{1,k} = d_{2,k} = \frac{1}{(\Delta h_x)^2}, \quad (4.22)$$

$$K_{1,k} = K_{2,k} = \frac{1}{(\Delta h_z)^2}. \quad (4.23)$$

In matrix m is the number of nodes in one row along x -axis. Furthermore in Equation 4.20 the \mathbf{b} is the boundary values variable. The vector $\tilde{\mathbf{e}}$ has a structure of

$$\tilde{\mathbf{e}} = \begin{bmatrix} E_{(1,1)} & \cdots & E_{(1,i)} & E_{(2,1)} & \cdots & E_{(2,i)} & E_{(3,1)} & \cdots & E_{(i,j)} \end{bmatrix}^t, \quad (4.24)$$

$$M = \begin{pmatrix} D_1 & d_{1,1} & 0 & \cdots & 0 & k_{1,1} & 0 & \cdots & 0 \\ d_{2,1} & D_2 & d_{1,2} & \ddots & & \ddots & \ddots & \ddots & \vdots \\ 0 & d_{2,2} & D_3 & d_{1,3} & \ddots & & \ddots & \ddots & 0 \\ \vdots & \ddots & d_{2,3} & D_4 & d_{1,4} & \ddots & & \ddots & k_{1,m} \\ 0 & & \ddots & d_{2,4} & D_5 & d_{2,4} & \ddots & & 0 \\ k_{2,1} & \ddots & & \ddots & d_{2,5} & D_6 & d_{1,6} & \ddots & \ddots \\ 0 & \ddots & \ddots & & \ddots & \ddots & \ddots & \ddots & 0 \\ \vdots & \ddots & \ddots & \ddots & & \ddots & \ddots & \ddots & d_{1,n-1} \\ 0 & \cdots & & k_{2,m} & 0 & \cdots & 0 & d_{2,n-1} & D_n \end{pmatrix}$$

In second order Maxwell's equation the electric component of EM field is calculated separately, however the magnetic field component can be computed using Equation 4.2. The second order differential equation of Maxwell's equation becomes with supplementary equations of boundary conditions. The solution region of 2D geological model is unbounded. Such domains are impractical and it is necessary to limit the solution region by creating artificial boundary conditions. At boundary $d\Omega_a$ the magnetic field vector is non zero and its value is same as given in Equation 3.20. Similarly at boundary $d\Omega_b$, $d\Omega_c$ and $d\Omega_d$ create perfectly matched layers and at boundaries staggered grid scheme provides the normal derivative of form as,

$$\frac{\partial E}{\partial n} = f(x, z) \quad (4.25)$$

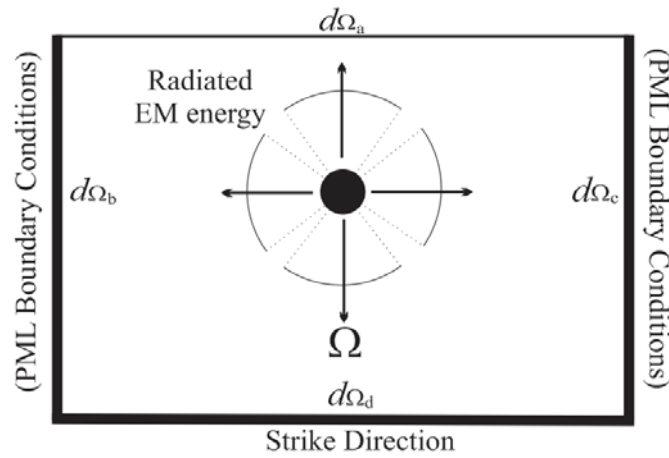


Figure 4.3 – 2D solution region with artificial boundary conditions.

4.5 Far Field Region and 2D Modeling

The source signal in CSEM survey is provided by HED with length, dl varied from 100 m to 500 m (or more). The dipole source utilizes frequency in the range of 0.1 Hz to 10 Hz. At this frequency range, the wavelength of EM wave is much larger than the dimension of source antenna. For the given conditions the source is also known as infinitesimal dipole.

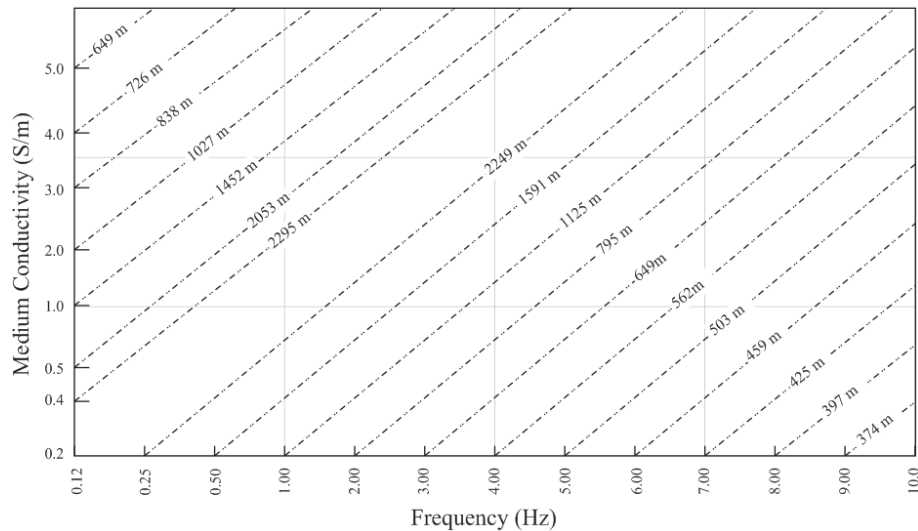


Figure 4.4 - Skin depth (δ) of radiated EM signal at different combinations of conductivity and frequencies

The radiation pattern of infinitesimal dipoles is similar to the omni-directional radiator [37]. In a given medium the source is oriented along x -axis where the strike direction of EM field is along z -axis. The region of interest to be profiled in the selected geological model is situated in the far field region. As such an omni-directional radiator will be considered for the study EM file behavior in selected geological models. The electric and magnetic field in the medium is a function of frequency, medium properties and source-receiver separation distance. Similarly the medium properties and frequency of source signal defines the skin depth.

In the selected medium, the strike length of propagated EM field is relatively large in comparison with the skin depth of the field in host medium as shown in Figure 4.4 and 4.5. Figure 4.4 shows the skin depth as the function of earth conductivity and frequency. Figure 4.5 illustrates the effective penetration depth which is defined to be 5δ at different combinations of medium conductivity and signal frequency [24].

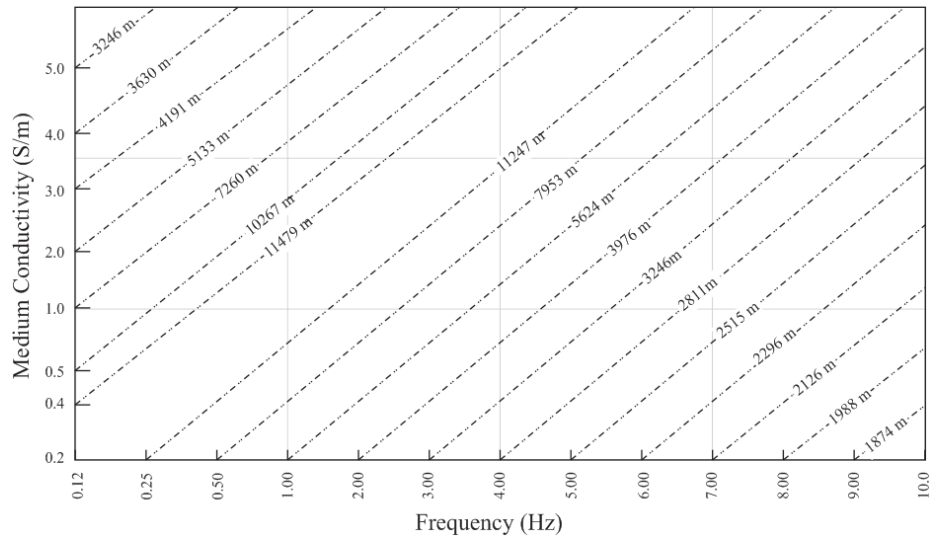


Figure 4.5 - Effective Penetration depth (5δ) of radiated EM signal at different combinations of conductivity and frequencies

4.6 Single Interface Geological Model

The aforementioned numerical approach is validated by implementing it onto multi-interface model which is selected from previously published work of L. Loseth. The reference work is done by using semi analytical approach which shows slightly difference in obtained results as shown in Figure 4.6.

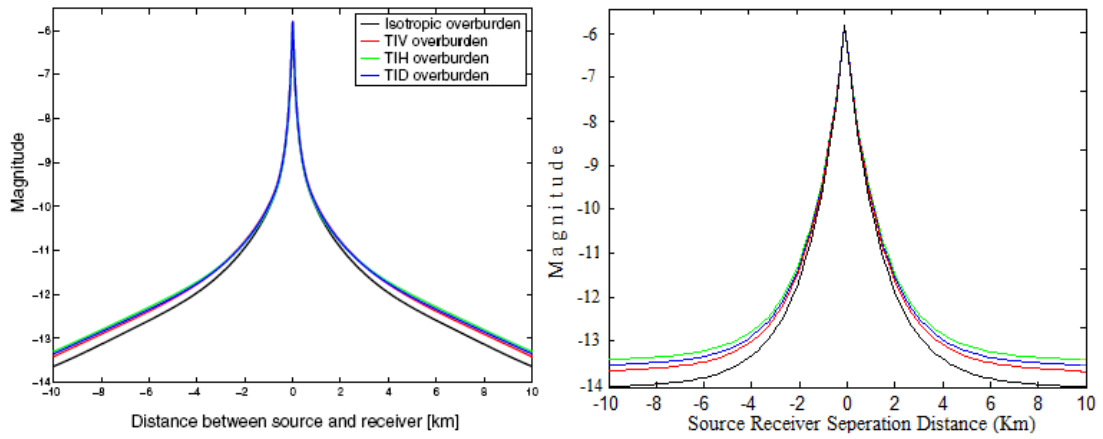


Figure 4.6 - figure (a) shows the previously existing results of multi interface geological model, however the produced results from selected model is shown in (b).

A single interface geological structure is selected in order to quantify EM field behavior at the interface of two different mediums. This model gives concept to understand EM field behavior at any interface of layered media. It was used before to obtain explicit spatial expression for reflected field [25]. However, in this modeling,

the expression will be obtained for refracted field for three different environments. This modeling will give insight of EM field behavior that travels from high conductive medium to less conductive mediums and less conductive medium to high conductive medium.

Figure 4.7 shows single interface layered medium that contains an interface between *medium-I* and *medium-II*. The mobile signal source is oriented in *medium-I* to radiate energy in a single interface model and a receiver is located in *medium-II* to measure refracted field. In numerical modeling, the mobile source is assumed to be moved from left to right of the single interface geological model as indicated by dotted line in Figure 4.7.

The layout of propagated signals path are illustrated in Figure 4.7 in which it can be subdivided into incident field, reflected field and refracted field at interface. The radiated field from source in strike direction meets at interface with an angle θ_i and known as incident angle. On the other hand at the layer boundary the incident field is separated into reflected and refracted fields. The direction of reflected field is back to the host medium with an angle θ_r where the refracted field enters into medium-II by making an angle θ_t . The strength of separated component from incident field is dependent on medium properties and position of source receiver.

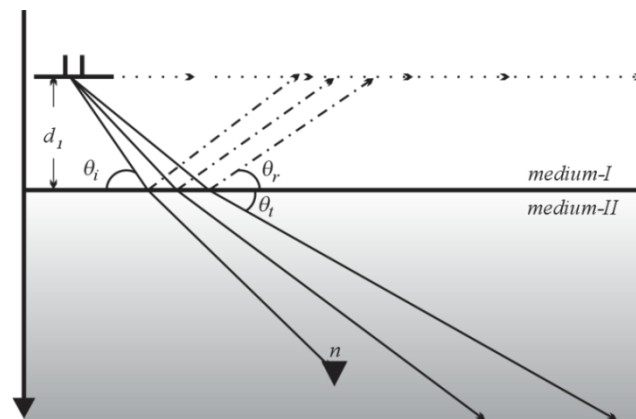


Figure 4.7 – Single interface geological model

The selected model will be used for three different interfaces by changing the electrical properties of *medium-I* and *medium-II*. Table 4.1 summarizes the electrical conductivity σ_0 and σ_1 for the interfaces between seawater-sediments (SW-SM), sediments to hydrocarbon (SD-HC) and hydrocarbon to sediments (HC-SM)

respectively. The magnetic permeability for all cases is considered to be same as in vacuum, the frequency of source signal is set to be at 0.25 Hz and the electrical permittivity is assumed to be negligible.

Table 4.1- Electrical Conductivity for three interface of single layered model

Interfaces		σ_0	σ_1
Seawater-Sediments	SW-SM	3.2 S/m	1.0 S/m
Sediments – Hydrocarbon	SM-HC	1.0 S/m	0.5 S/m
Hydrocarbon-Sediments	HC-SM	0.5 S/m	1.0 S/m

4.7 Numerical Results for Single Interface Model

In single interface model, the electric field for region of interest is obtained by solving the TE polarization by using Equation 4.11 for each interface. The results are obtained for each selected interface by using forward modeling technique. The Magnitude vs. Offset (MVO) for the electric field response of each condition in single interface model is shown Figure 4.8.

The result obtained for MVO shows the response of diffused **E**-field and that is dependent on the characteristic of medium properties. The MVO of HC-SM (Hydrocarbon to Sediments interface) shows the strength of electric field is more attenuated. This is caused by the source host medium is less conductive than the conductivity if *medium-II*. On the other end, MVO for SM-HC (Sediments to Hydrocarbon interface) is dominating because signal wave is radiating from conductive medium and *medium-II* is resistive medium.

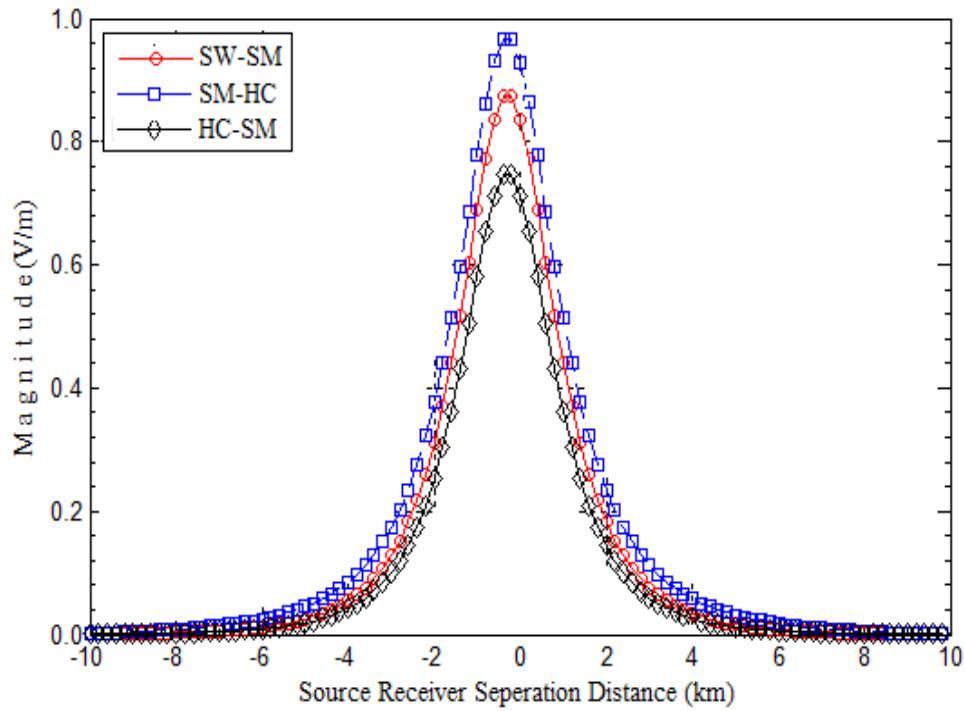


Figure 4.8 - Magnitude response of single interface geological model by using mobile source with frequency of 0.25 Hz

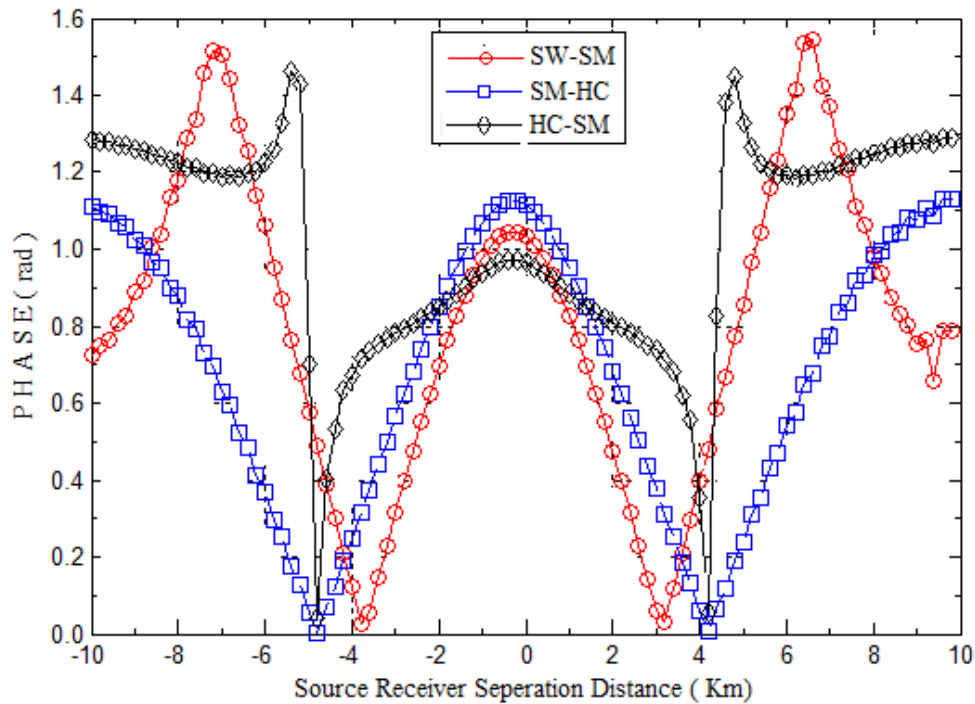


Figure 4.9 - Phase response of single interface geological model by using mobile source with frequency of 0.25 Hz

The phase response of diffused field is function of medium properties and frequency. Figure 4.9 shows the Phase vs. Offset (PVO) for single interface model. It shows that the phase response dominates while *medium-I* and *medium-II* are seawater

and sediments respectively. It is because of more conductive mediums. Similarly, the fields that pass through the interface of less conductive mediums would assert small delay. The model is prepared by writing the algorithm to implement the field equations using FD numerical method in MATLAB. The algorithm for single interface geological model is given in **APPENDIX-B**

4.8 Multi-interface Geological Model

The actual marine environment consists on air half space, seawater, overburden sediments, reservoir and under-burden sediments. In the same way, there are four different interfaces as air-half space to seawater, seawater to overburden sediments, overburden sediments to saturated reservoir and saturated reservoir to sediments. However the reservoir might be filled with resistive hydrocarbon or saturated saline fluids. The layered structure of 2D geological model is similar to real earth. The forward modeling was earlier carried out by Lars O. Loseth for 2D layered media of hydrocarbon containing reservoirs [37]. However in this case, forward modeling will be used to study the EM field pattern for both hydrocarbon saturated reservoir and saline fluids saturated reservoir.

Forward modeling of layered geophysical model allows us to investigate the EM field behavior which can assist us in interpretation of real time survey data. Figure 4.10 shows two stratified geological models of different dimensions. In this, the model (a) and the model (b) are known as thin and thick hydrocarbon saturated reservoir geological model. In real situation, most of the saturated reservoirs are buried inside the sediments as shown in Figure 4.10 (c), (d), (e) and (f). In this model, the lengths of hydrocarbon containing reservoirs are shorter than previous models of (a) and (b). In Figure 4.10, the models (c) and model (d) contains thin and thick reservoir that are filled with resistive hydrocarbon. Similarly, model (e) and model (f) is filled with conductive saline fluids to study EM behavior for water saturated reservoirs.

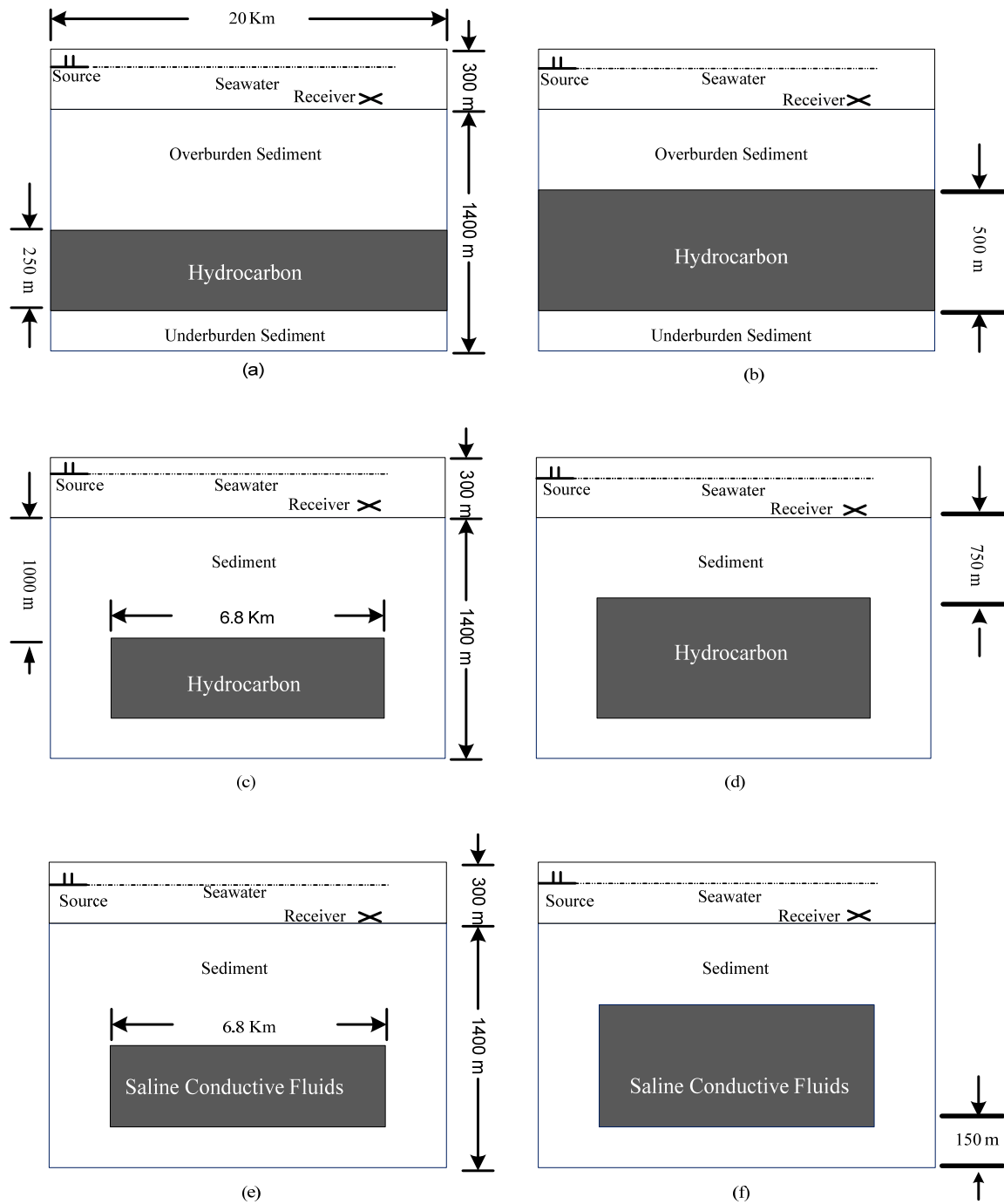


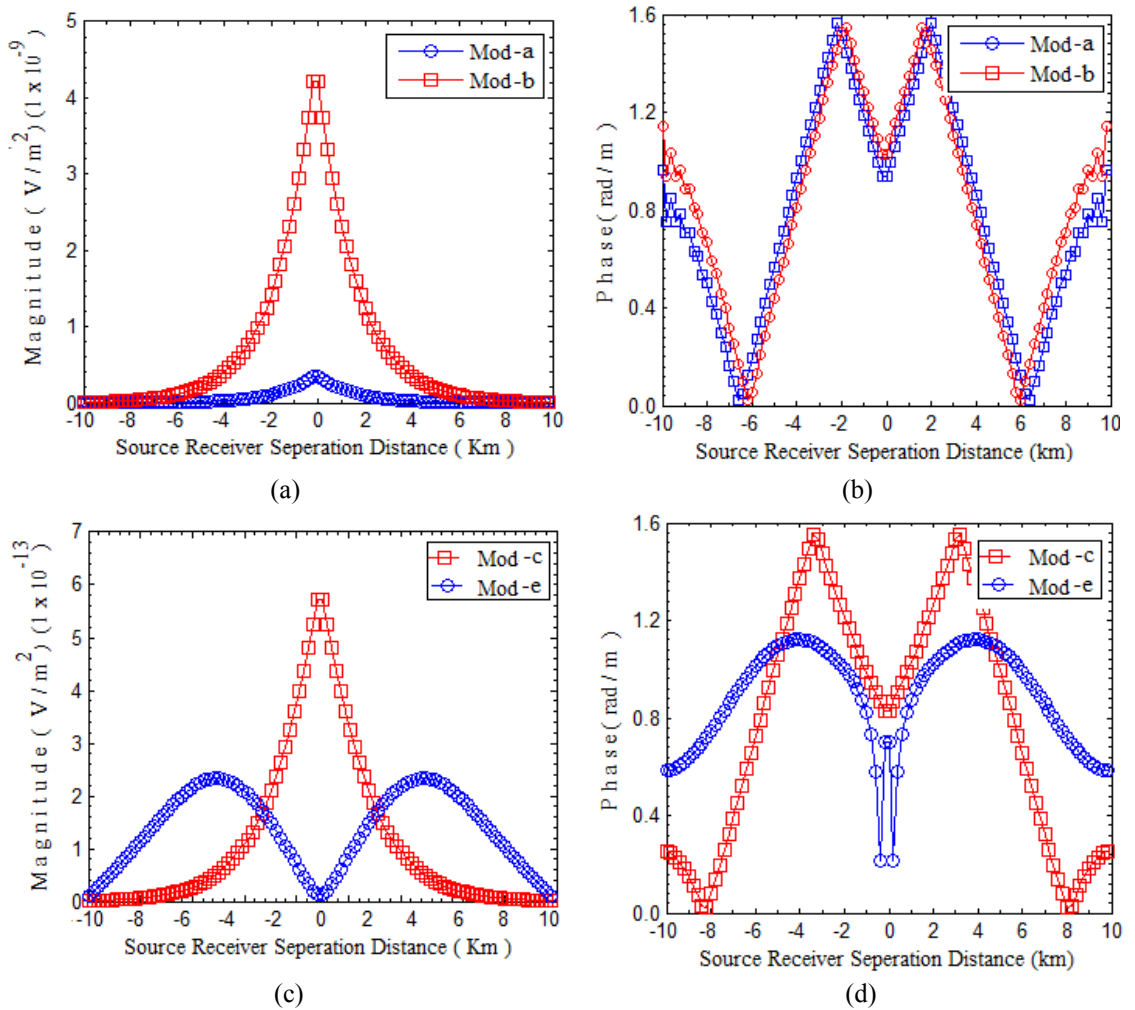
Figure 4.10 - 2D anisotropy layered geological model for idealized marine CSEM/SBL survey

In selected multi-interface model, the electrical property of seawater is assumed to be 3.2 S/m; for overburden and under-burden sediments is assumed to be 1.0 S/m; for resistive hydrocarbons and conductive saline fluids are 0.5 S/m and 5.2 S/m respectively. The mobile source is positioned 50 m above from seafloor and EM field receiver is placed at seafloor. The frequency of mobile source signal wave is set at

0.25 Hz. The remaining EM parameters for seawater, sediments and hydrocarbon are assumed to be same as in previous models.

4.9 Numerical Results for Multi-Interface Model

The numerical modeling is accomplished for each selected multi-interface model of Figure 4.10. The forward modeling technique is used to obtain the results of electric field for selected models. The magnitudes vs. offset (MVO) of electric field for layered media of Figure 4.10 (a) and (b) are shown in Figure 4.11 (a). It shows the strength of electric field dominates while model contain thin hydrocarbon reservoir. However the magnitude of electric field is attenuated if the resistive hydrocarbon is thicker. It asserts, the most of the diffused energy is trapped inside the resistive layer of hydrocarbon and over all response of electric field is less than the response of thin hydrocarbon containing reservoir.



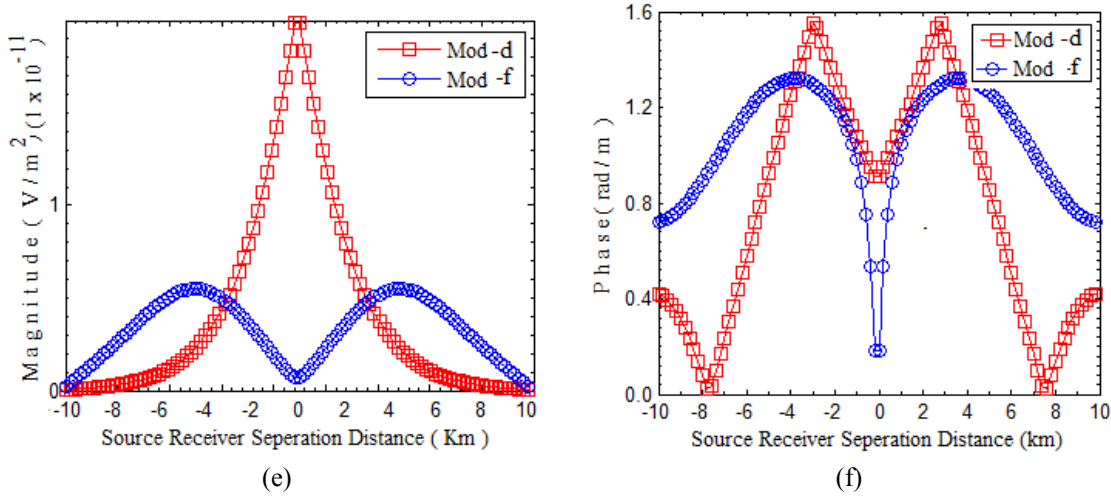


Figure 4.11 – Numerical results of electric field for idealized CSEM/SBL scenarios of models Figure 4.8.

In layered media the phase delay is the function of electrical conductivity. There is more phase delay if the medium is conductive. The obtained results of Figure 4.11 (b) show the phase response for geological model of Figure 4.10 (a) and (b). It shows there is more phase delay for the model of thin hydrocarbon reservoir. It asserts in real marine CSEM environment the diffused field is sensitive to electrical properties of the medium.

In layered earth media the primary field of the mobile source produced electric charges at each interface. The excess in produced electric charges create secondary electric field in layered media [39]. To simplify, in selected 2D layered media, the secondary field can be generated at four different interfaces. In given case, the primary field will be generated by mobile source in seawater and at interface of seawater to sediments the charges create a secondary field. The produced secondary electric fields will be added vectorially because the sediments are less conductive than seawater. This effect is also known as depolarization. On the other hand, if inhomogeneity is more conductive than the host medium, the produced secondary will tends to cancel the primary field of host medium.

The obtained results shows the strong agreement with previously published work of Lars O. Loseth and G. R. Jiracek, however the geological models and dipole source are different. 3D dipole source were used in publications and 2D dipoles used in this thesis. The obtained results can easily differentiate between resistive hydrocarbon

reservoir and conductive saline fluid reservoir. The model is prepared by writing the algorithm to implement the field equations using FD numerical method in MATLAB. The algorithm of single interface geological model is given in **APPENDIX-C**.

4.10 Summary

This chapter involves the forward modeling on 2D geological models for calculating electric field in layered medium. The formulation for electromagnetic field can be obtained by solving Maxwell's equation for 2D models. The obtained expressions for EM field in stratified media are used for implementing the forward modeling. Two geological models were considered here namely single-interface and multi-interface model. The Maxwell's equations of electric field are solved for each discretized model by using FD numerical method with *staggered-grid* scheme. The resulting grid stencil of electric field for at any test point has five points and solving the PDE for each node. The system of equations is expressed in a matrix form with boundary conditions. The obtained results show that total electric field will decrease over the body for a reservoir filled with saline conductive fluids and increase if the reservoir is filled with resistive hydrocarbons.

CHAPTER 5

SOURCE DIPOLE DIPPING AND OPTIMAL MOVING SPEED

5.1 Introduction

The most commonly used EM source for prospecting earth hidden properties in marine CSEM survey is infinitesimal dipole. The source dipole, used in marine environment for the exploration of petroleum reserves, would typically be 100m long (or more). In real time survey of marine CSEM, one end of the mobile dipole source is towed using water vessel to move it horizontally just above the seafloor. Due to its close positioning to the seafloor it is also classified as seafloor-based transmitter. This transmitter is powered by a surface power generator through an underwater unit. It radiates energy both toward overlying water column and beneath the seafloor sediments. The field measurements are conducted by using seafloor receivers. The survey data is collected at several different source-receivers positions. In real time survey, the position and orientation of source receivers in conductive seawater is known as source-receivers survey geometry. The irregularity in source-receiver position and orientation may cause anomalies in the survey data.

To reduce the irregularity in survey data of marine CSEM method, a navigation system is used to find the exact position of mobile source receivers [2]. However, this method still needs improvements to reduce the effects of source-receiver orientation. The irregularities in survey data due to the inaccurate orientation of source will be studied and discussed in this chapter. This study involves 2D forward modeling to study the effect on survey data caused by inaccurate orientation of source. Furthermore, the numerical modeling is also required in order to obtain the optimal velocity to be used for the mobile dipole source.

5.2 Controlled Source Orientation.

In marine CSEM survey, the height of mobile source from sea floor is not more than the skin depth of a signal wave used in the host medium [3]. Figure 5.1 shows a towed dipole which is oriented horizontally above the seafloor through an underwater unit. One end of infinitesimal dipole is towed by a surface vehicle and other end is allowed to move freely. As a reference for discussion, the mobile dipole source orientation is assumed to be along the x -axis in rectangular coordinate system. The movement of the free end of the source in reference to the z -axis is called dipping and its angle (zenith angle) of movement is denoted by φ . Similarly the movement of the free end of the source in reference to the y -axis is called rotation and notation for its angle (azimuth angle) is denoted by θ . Due to the nonlinearities in vessel speed and seawater tides, it is very difficult to overcome the effects of dipole dipping and rotation. The effect of both dipping and rotation will only be studied using 3D modeling. In this chapter a 2D numerical modeling will be used to study the effects of dipping on the survey data.

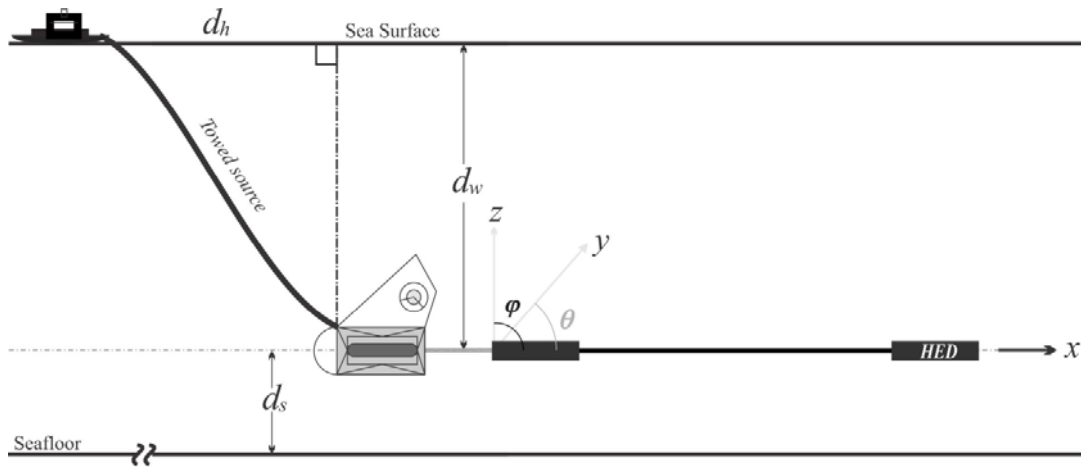


Figure 5.1- A dipole source orientation along x -axis in rectangular coordinate system

Referring to Figure 5.1 the vertical distance of the buoy dipole source from sea surface, height of seafloor-based transmitter from seafloor and separation distance between water vessel and source position are denoted by d_w , d_s and d_h respectively. The small variation in d_w , d_s and d_h creates anomalies in source orientation in terms of irregularities in survey data. In real time survey, the mobile dipole source is assumed to follow the path of the moving water vessel. However, the dipping and

rotation of the mobile dipole source are not well constrained. As a result, the quality of the marine CSEM survey data is dependent on accurate navigation data. Some conventional approaches have been used to find navigational information including short baseline acoustic navigation system and large base line acoustic navigation system. However these techniques are not as accurate as expected or could only provide limited accuracy [39].

The survey geometry for marine CSEM method and geological conditions of the earth are extremely varied. It is rarely possible to feasibly turn real time survey data directly into a reliable picture of earth structure using the application of an automatic process. Thus a human interpreter is needed to guide this automated interpretation process. Consequently, there is a need for the human to have a good qualitative understanding of how dipping and rotation will effect on diffused EM field.

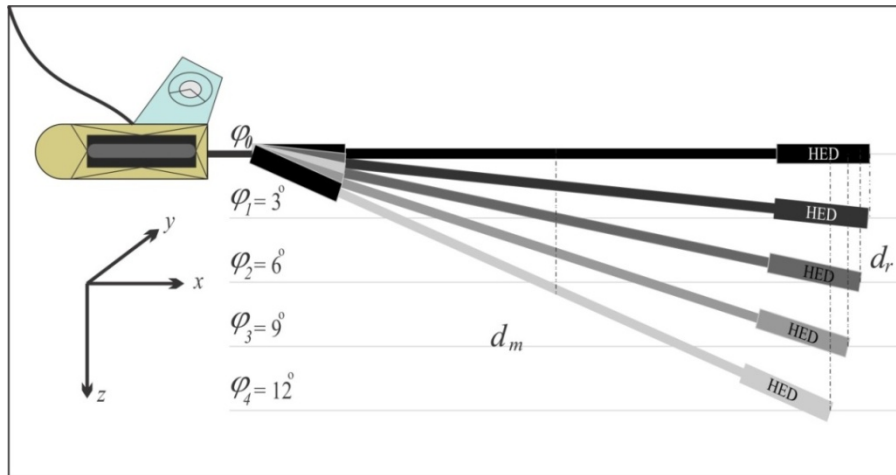


Figure 5.2 – Inaccurate orientation of mobile source dipole in terms of dipping

The dipping effects of a mobile dipole source are a function of variation in zenith angle φ . To understand the effects of dipping, the EM field response will be studied using forward modeling method. In numerical modeling the dipping effects will be recreated by changing the position of dipole free end in reference to z -axis as shown in Figure 5.2. In this figure, the variable d_r is the vertical distance of dipole free end from x -axis. The vertical distance from the center of mobile is the originating point of antenna radiation pattern and indicated by d_m of antenna radiation pattern exists in the center of infinitesimal dipole. The forward modeling is obtained with various zenith

angles by using five different lengths of dipoles labeled as HED-I, HED-II, HED-III, HED-IV and HED-V.

Figure 5.2 illustrate that the mobile dipole source is oriented along x -axis in rectangular coordinate system with $\varphi_0 = 0^\circ$. The dipping effects are formed by changing the azimuth angle i.e. the variables of zenith angles $\varphi_1, \varphi_2, \varphi_3$ and φ_4 with values $3^\circ, 6^\circ, 9^\circ$ and 12° respectively. Furthermore in selected case of this study, different lengths of dipole will be considered to study the dipping effects when the source length is large.

5.3 Numerical Modeling for Dipping Dipole Source

To study the dipping effects, two different 2D layered media are considered namely geological model of dipping-I (GMD-I) and geological model of dipping-II (GMD-II). In the case of GMD-I the dipping effect will be created by using different zenith angles as $0^\circ, 3^\circ, 6^\circ, 9^\circ$ and 12° for the entire domain. However in GMD-II the dipping will be created with the same angles for a selected range from the entire domain. In GMD-II model, it provides the study of dipping effects at particular instant. The numerical modeling for each respective geological model will be accomplished and discussed section wise.

5.3.1 Numerical modeling for GMD-I

The 2D model of GMD-I is illustrated in Figure 5.3. This layered media consists of two different layers of seawater and sediments. The length of each layer is assumed to be 20 km long. The thickness of the overlying seawater layer is assumed to be 300 m. Similarly the thickness of subsea water sediments is supposed to be 800m. The electrical properties for seawater and sediments are assumed to 3.2 S/m and 1.0 S/m. The electrical permittivity of the medium is assumed to be negligible due to very low frequency of the signal typically at 0.25 Hz. The magnetic permeability of media is assumed to be same as in vacuum. The mobile dipole source is positioned at 60 m above from seafloor with different orientations. The length of mobile dipole source is chosen to be 200 m long and receiving point of radiated EM field is located at point 'A' as shown in Figure 5.3. In model of GMD-I, the electric field with

dipped mobile dipole source is obtained by solving the TE polarization using Equation 4.11.

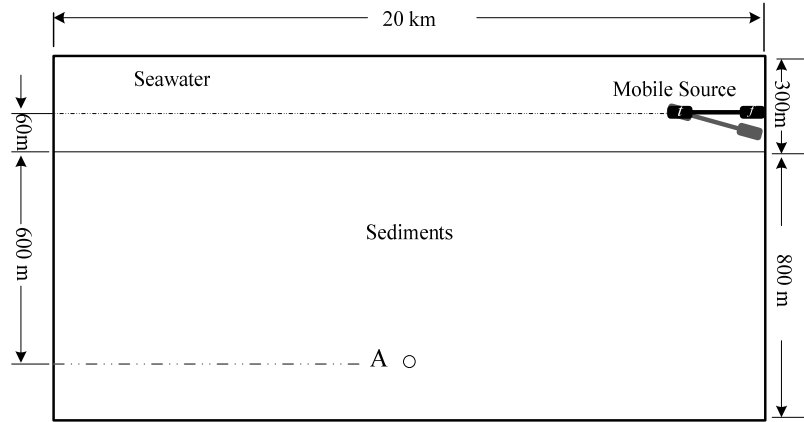


Figure 5.3 – Sketch of 2D geological model of GMD-I in which mobile dipole source is dipped along entire length of domain.

5.3.2 Numerical Results for GMD-I

The results obtained for GMD-I geological model for the electric field response is shown in Figure 5.4. These results are obtained by writing the algorithm of *forward modeling* in MATLAB. The algorithm for selected single interface model is given in **APPENDIX-E**.

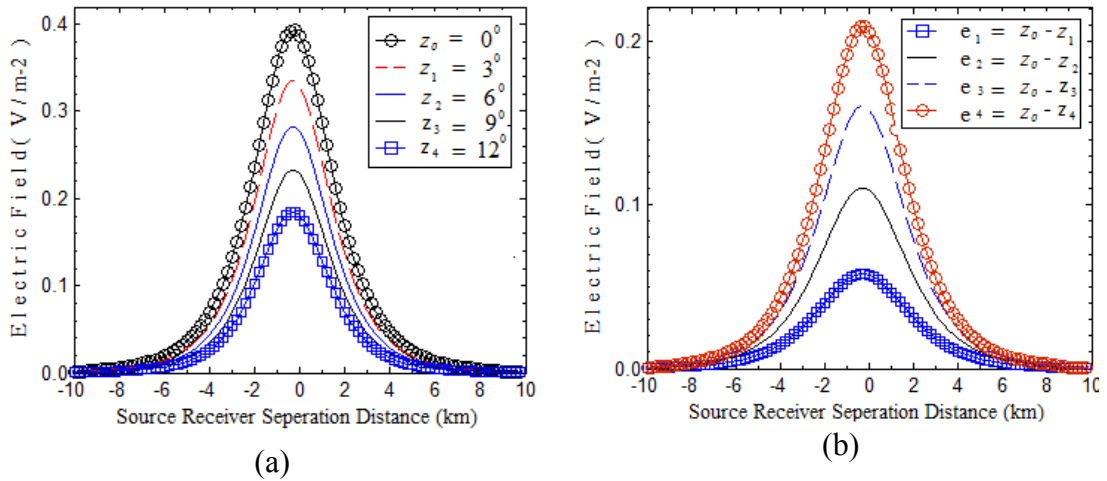


Figure 5.4 – Numerical results of electric field response for model of GMD-I. In figure (a) and (b) shows the results of electric field response with dipped source and dipping error

The results obtained show the electric field response when mobile dipole source is moving on seafloor from left of the selected model to right side. The response of the

electric field illustrates a small change in source orientation will change the response of the diffused electric field. However, as Figure 5.4(b) shows, the error rate in the response of the diffused field will increase with increasing degree of order change in the orientation of mobile dipole source. The model is prepared by writing the algorithm to implement the field equations using FD numerical method in MATLAB.

5.3.3 Numerical Modeling for GMD-II

The 2D layered media for numerical modeling of GMD-II is shown in Figure 5.5. This layered media also consists of two different layers of seawater and sediments. The electrical properties and physical dimensions for this model are assumed to be same as of GMD-I. However, in this model the mobile dipole source is dipped for some part of the region as shown in figure, labeled as D-region. From the numerical modeling of GMD-I, if the mobile dipole source or dipped with fixed angle on entire domain, the data can be easily normalized. However in real marine environment for CSEM survey, the variable dipping effects of a mobile dipole source occur randomly. As a result, it is necessary to study the dipping effects at certain points and compare the results obtained with normalized data

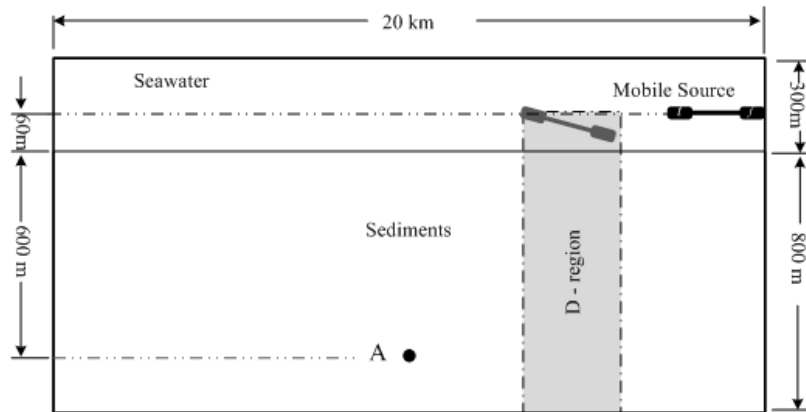


Figure 5.5 – Sketch of 2D geological model of GMD-II in which mobile dipole source is dipped at partial region.

The selected geological model of GMD-II contains a partial region (D-region) for dipping. In this media it is assumed to be the mobile dipole source is oriented with different dipping angles as 0° , 3° , 6° , 9° and 12° in D-region. However outside this region, dipole is oriented with 0° angle. Furthermore in this model, five different

lengths of the mobile dipole source will be used to also understand the effects of dipping when dipole length is short or long. In reference to Figure 5.2 the distance of dipole free d_r end in reference to x -axis are given in Table 5.1. The originating point for EM field radiation pattern of mobile dipole sources can be calculated by taking the half of distance d_r .

Table 5.1 - Distance of dipole free end because of dipping effects

Source	Length	d_r				
		$\varphi_0 = 0^\circ$	$\varphi_1 = 3^\circ$	$\varphi_2 = 6^\circ$	$\varphi_3 = 9^\circ$	$\varphi_4 = 12^\circ$
HED-I	120 m	0.0 m	6.28 m	12.62 m	19.00 m	25.50 m
HED-II	140 m	0.0 m	7.34 m	14.72 m	22.16 m	29.76 m
HED-III	160 m	0.0 m	8.38 m	16.82 m	25.32 m	34.00 m
HED-IV	180 m	0.0 m	4.72 m	18.92 m	28.50 m	38.26 m
HED-V	200 m	0.0 m	10.48 m	21.02 m	31.66 m	42.50 m

In Table 5.1, the originating point of EM field in radiation pattern is ($d_m = d_r/2$) and its value is a function of the zenith angle and dipole length. The dimensions of HED's with zenith angle are given in Table 5.1. It shows there are five different lengths of dipole that are labeled HED-I, HED-II, HED-III, HED-VI and HED-V with lengths of 120m, 140m, 160m, 180 and 200m long respectively.

The entire domain of 2D layered media of Figure 5.5 is discretized into several elements. To quantify the electric field for each element is obtained to solve Equation 4.1 of TE mode using *staggered grid* scheme. The system of linear algebraic equation is obtained by using finite difference numerical schemes as discussed in chapter 4. The resulting form of linear algebraic equations for discretized region becomes in matrix form as given in Equation 4.20.

5.3.4 Numerical Results for GMD-II

For the exploration of hydrocarbon reservoirs by using marine CSEM techniques, the zone of interest exists in the far field region. In this case the structure of geological model and source field is larger than the skin depth of the signal wave in host medium. In such cases, the dipping effects can be studied by calculating electric field in strike direction through forward modeling. In marine CSEM survey, the

moving source and static receivers are located on parallel traverse lines. In such a configuration, the moving source produces anomalies caused by improper orientation as shown in Figure 5.4. In Figure 5.4(a) the magnitude of electric field response shows the pattern of electric field. In Figure 5.4(b) the error curve is obtained by taking the differences of electric field, when source is oriented at 0° and 3° zenith angle.

The simulation results for geological model of Figure 5.3 are obtained by using different length of dipole source and are shown in Figures 5.6 to 5.10. The shape of electric field strength is the function of source relative position and orientation. Similarly, the shape of anomalies obtained by changing free end of source dipole and compare to it with the response at zero zenith angle. The results for the electric field strength for each positions of the source with different length of sources are shown in Figures 5.6 to 5.10.

The obtained results of MVO shows, if HED length is large (200 m in selected model) the anomalies will be greater in the survey data compared with a shorter length of dipole at same zenith angle. In the selected models, the profile of electric field strength varies as a change occurs in orientation of the dipole. It shows that the real time survey data of EM field is difficult to interpret because of complex source receiver survey geometry and multifaceted conductive environment.

In the moving source method, the ideal mobile source position is at a single traverse line. But this is impractical in real environment due to irregularities in orientation and position of mobile source. This uncertainty also creates irregularities in the phase of the diffused field as shown in Figures from 5.4 to 5.8. These results shows the irregularities in survey data caused by dipping will be more if the HED length is larger.

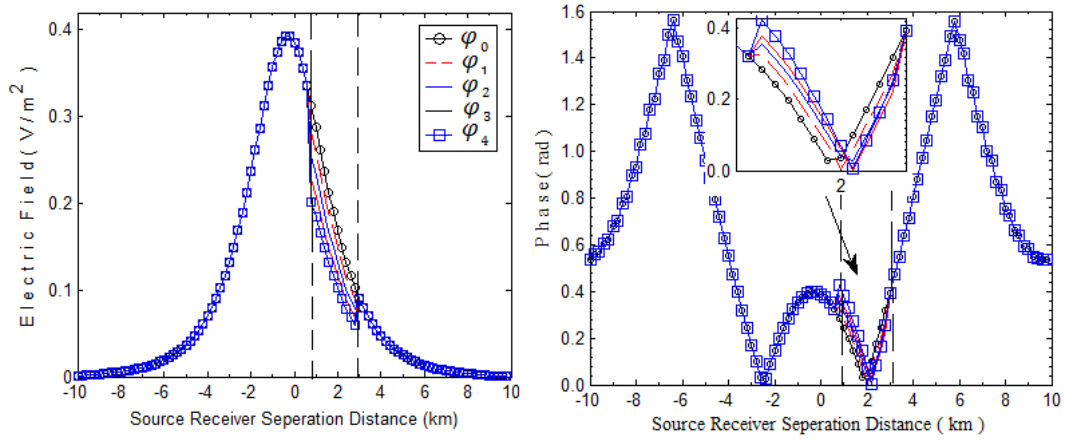


Figure 5.6 - Modeling results for geological model of dipping HED-I as given in Table 5.1

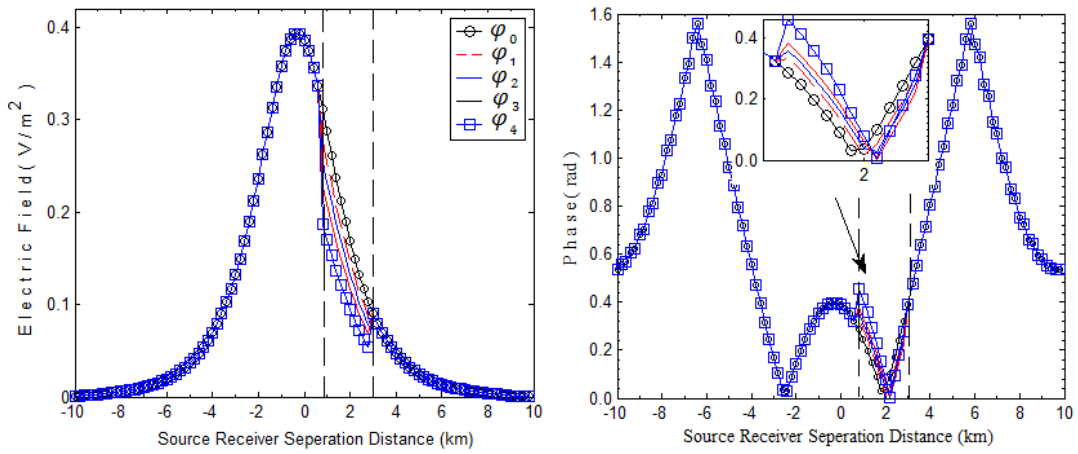


Figure 5.7 - Modeling results for geological model of dipping HED-II as given in Table 5.1.

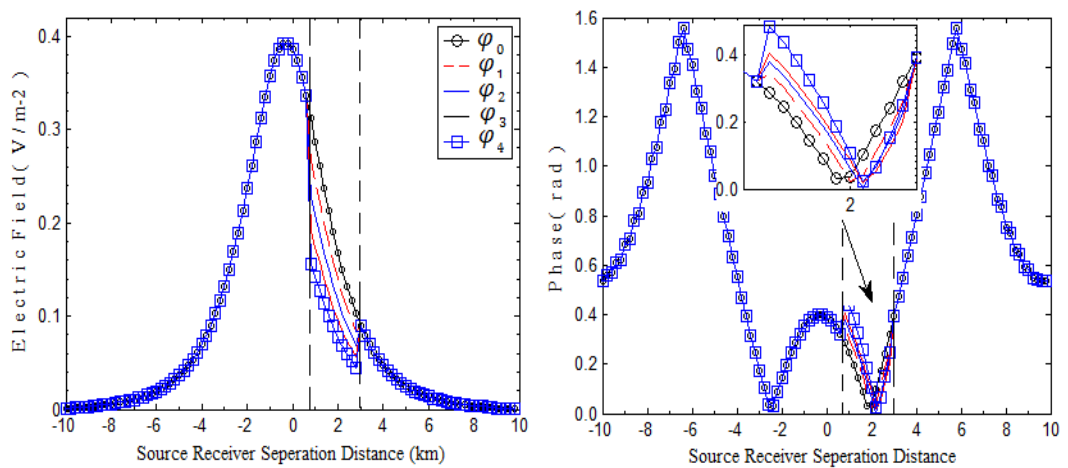


Figure 5.8 - Modeling results for geological model of dipping HED-III as given in Table 5.1.

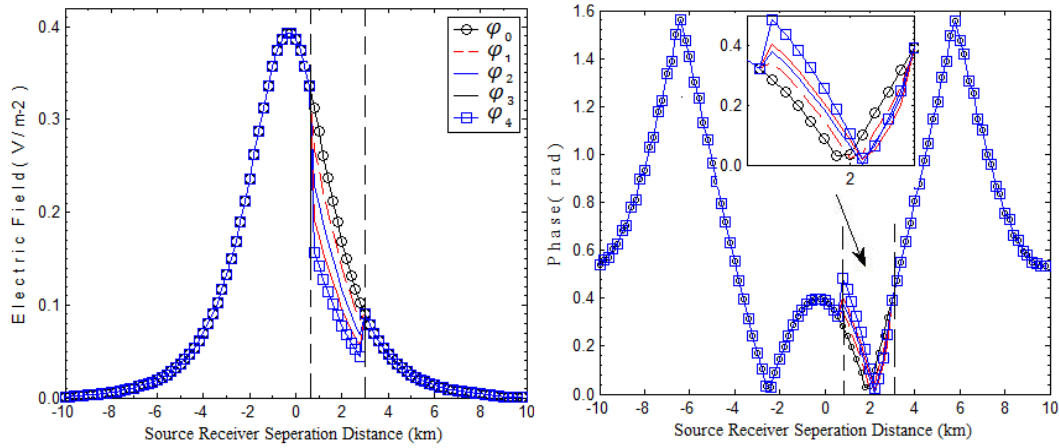


Figure 5.9 - Modeling results for geological model of dipping HED-IV as given in Table 5.1.

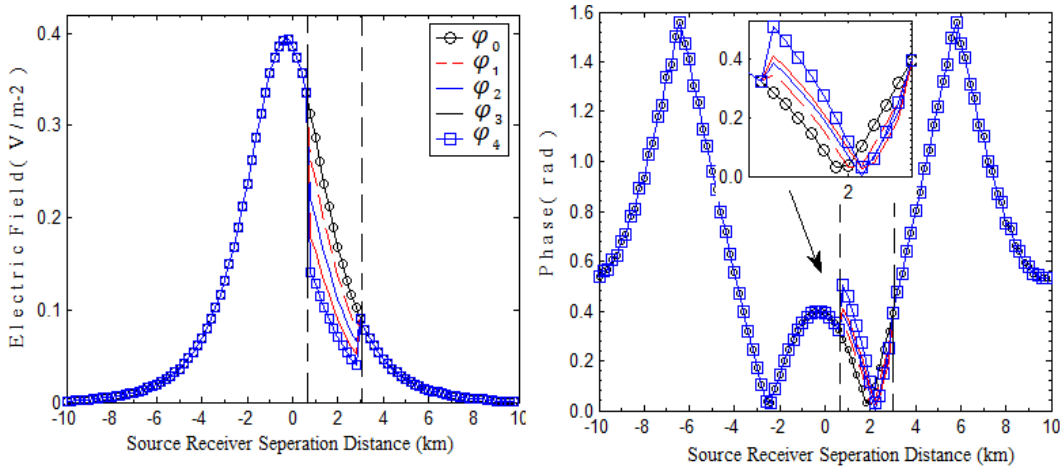


Figure 5.10 - Modeling results for geological model of dipping HED-V as given in Table 5.1.

This numerical modeling study the dipping effects on the EM data and the results shows agreement with K. A. Weitmeyer work on “Marine Electromagnetic Methods for Gas Hydrates Characterization” [39]. At this stage of the problem the results obtained shows that the received signal at seafloor receivers are the functions of earth physical properties, frequency of signal and source receiver survey geometry. To understand the actual spatial distribution of earth physical properties requires improved technologies for finding proper orientation and position of mobile source. The algorithm for selected a single interface model is given in **APPENDIX-E**.

5.4 Phase Velocity in Conductive Medium

In real time survey of marine CSEM, the mobile dipole source is towed with a moving water vessel along a certain traverse line (Traverse Line - I). The field receivers are located at a different and parallel traverse line (Traverse Line - II) as shown in Figure 5.11. The field measurements are taken at several source receivers' positions by moving the mobile dipole source with a water vessel. This dipole is moved at a specified speed along the traverse line while receivers continue to record the measurement of EM field. The measurement of EM field is dependent on the geological conditions as well as the position of dipole source. In real time survey, to estimate the spatial distribution of earth physical properties at particular depth, the source receiver separation distance should be larger than the depth of the target area. Subsequently the reflected EM field would be more dominant than the direct field. Furthermore the target depth is a function of the signal frequency and the source receiver position. Referring to Figure 5.11, the field receivers are shown as to be placed at different positions, while the seafloor based transmitter is moved just above the seafloor. Suppose when this mobile dipole source reaches at point p_1 and it radiated EM energy in surrounding media at time t_0 . This radiated energy will pass through the interior of earth materials and reflect back towards seafloor, where it is received by receivers at time t_1 . The time t_1 can be defined as

$$t_1 = t_0 + t_d, \quad (5.1)$$

where t_d is time delay and its magnitude is dependent on the electrical properties of the media and frequency of signal used by the dipole source.

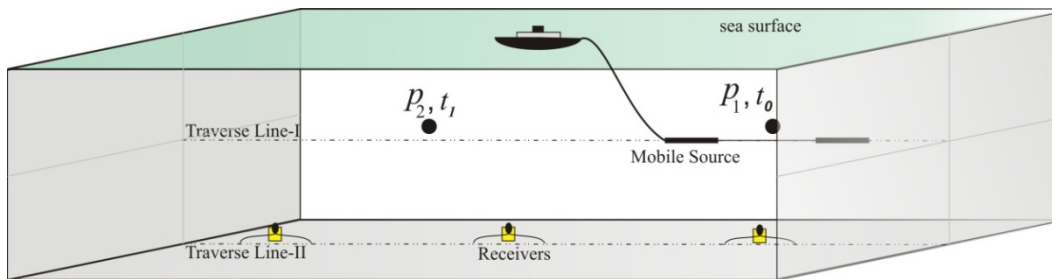


Figure 5.11–Plane view of inline profiling technique.

At time t_1 the dipole source would be at a new arbitrary position denoted by p_2 . The distance between point p_1 and p_2 is covered by the dipole in time t_d . In order to

calculate the source position when the radiated field from point p_1 at time t_0 , the source should be at same position until reflected signal is received by field receivers after time t_d . However, in practice the moving dipole source will not be at same position and this causes irregularities in source positioning for the received signal at time t_1 . The irregularities can be minimized if the covered distance of the dipole is shorter during time t_d . It is necessary calculate the optimal speed of mobile dipole source in marine CSEM survey. In order to calculate optimal speed of mobile dipole source, the numerical modeling will be done by using the field governing equations in spatial and temporal domain. The field governing equations are derived in next section.

5.5 FD Scheme in Spatial and Temporal Domain

The 1D forward modeling is an important tool for optimal survey design. It's used to find optimal frequency ranges for specific depth. However the effects of dipole speed on survey data can only be studied by using numerical modeling in spatial and time domain. In such case low frequency signal will be considered for the application of marine CSEM survey.

The basis of EM field used in geophysical surveys is provided by the *Quasi-static* equations. The numerical solutions for this type of partial differential equation are discussed by Ames [40], Cooper [41], Morton and Mayeres [42]. The field governing equations of 1D geological model for spatial and temporal domain can be written as,

$$\nabla^2 E_x + \sigma \mu \frac{\partial E_x}{\partial t} = 0 \quad t \geq 0, \quad (5.2)$$

Where $E_z = E(z, t)$ is the function of dependent variable on space and time. The coefficient with time derivative term in equation 5.2 expresses the medium properties. The given form of equation will be solved using Forward Time Centered Space (FTCS) scheme as [16];

$$\left. \frac{\partial E_x}{\partial t} \right|_{(t_n+1, x_i)} = \frac{E_i^{n+1} - E_i^n}{\delta t} + \mathcal{O}(\delta t), \quad (5.3)$$

where above equation is temporal derivative form, δt is the step size in time domain. Similarly the center difference approximation in spatial domain is

$$\left. \frac{\partial^2 E_x}{\partial z^2} \right|_{(x_i)} = \frac{E_{i+1}^n - 2E_i^n + E_{i-1}^n}{(\Delta z)^2} + \mathcal{O}(\Delta z^2). \quad (5.4)$$

The FTCS scheme is used for discrete approximation in time and space domain. The FTCS is preferred because of performance and ease of implementation in finite difference model [16]. The Equation 5.2 can be rewritten in temporal and spatial domain as,

$$E_x^{n+1} = E_x^n + \eta(E_{i+1}^n - 2E_i^n + E_{i-1}^n) + \mathcal{O}(\delta t) + \mathcal{O}(\Delta z^2), \quad (5.5)$$

where coefficient $\eta = \frac{\Delta t}{\sigma \mu (\Delta z)^2}$ is known as the stability factor. The improper value of stability factor can cause instability, oscillation and amplitude will grow up for EM field at outer boundaries. To control the factors of oscillation and amplitude of EM field at boundaries, the magnitude of stability factor should be less than 0.5 [42].

In Equation 5.5, terms $\mathcal{O}(\delta t)$ and $\mathcal{O}(\Delta z^2)$ are assumed to be negligible and ignored, so above equation can be rewritten as,

$$E_x^{n+1} = E_x^n + \eta(E_{i+1}^n - 2E_i^n + E_{i-1}^n). \quad (5.6)$$

The Equation 5.6 is the formulation of FTCS to approximate the electric field in spatial and temporal domain. In Equation 5.6, $x = i$ and can be rearranged as,

$$E_i^{n+1} = E_i^n (1 - 2\eta) + \eta E_{i+1}^n + \eta E_{i-1}^n, \quad (5.7)$$

The solution of the equations involves the boundary condition at the end point of spatial domain and can be written as;

$$E_x(\pm l, t) = E_{\pm l} \quad E_x(z, 0) = E(z) \quad (5.8)$$

The stability factor can be achieved only when $\eta \leq 0.5$. The suitable value of η can be determined using of skin depth Equation 2.38 and phase velocity Equation 2.44.

The electrical conductivity is assumed to be 3.2 S/m, 1.0 S/m and 0.5 S/m for seawater, sediments and hydrocarbons respectively. The penetration depth of EM field in conducting mediums of seawater, sediments and hydrocarbon are given in Table 5.2 at frequency of 0.25 Hz.

Table 5.2 - Maximum penetration depth of EM wave in conducting medium.

Multiple Skin depth	Penetration Depth in conductive medium		
	Sea water	Sediments	Hydrocarbon
$1\delta(d_1)$	562 m	1006 m	1423 m
$2\delta(d_2)$	1125 m	2012 m	2847 m
$3\delta(d_3)$	1688 m	3018 m	4270 m
$4\delta(d_4)$	2250 m	4024 m	5694 m
$5\delta(d_5)$	2813 m	5030 m	7117 m

The given values in Table 5.2 show the penetration depth of wave in conducting medium at certain multiple skin depth. Furthermore, the magnitude of the wave is reduced to less than 1% after the wave have penetrated the distance of 2813 m, 5030 m and 7117 m in the medium of seawater, sediments and hydrocarbon respectively.

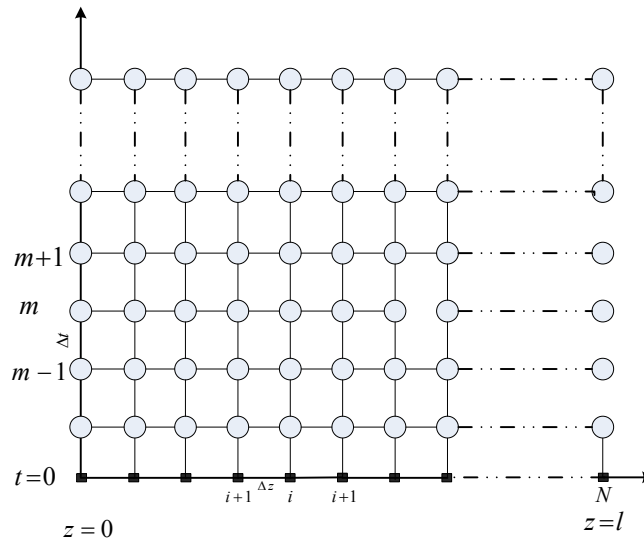


Figure 5.12 - Meshes used for solution to the 1D equation of electric polarization

The phase velocity of wave into conducting medium is dependent on electrical conductivity and its frequency. The velocity of wave by which it penetrates into conductive medium can be determined by using Equation 2.44. The phase velocity of EM signal in seawater, sediments and hydrocarbon is 883 m/Sec, 1581 m/Sec and 2236 m/Sec respectively at frequency of 0.25 Hz. On the other end, the calculated distances of 2813 m, 5030 m and 7117 m of wave can be traveled in time 3.186 Sec using phase velocities of 883 m/Sec, 1581 m/s and 2236 m/s respectively.

The main idea in FTSC method is to replace continuous derivative terms to discrete formulas. In Figure 5.12 the *mesh* is the set of locations to compute a numerical solution. The parameters Δz and Δt are the finite difference between adjacent point in spatial and time domain. These parameters are uniform for different medium throughout the entire domain. From the figure the parameters Δz and Δt can be obtained as,

$$\Delta z = \frac{l}{N-1}, \quad (5.9)$$

$$\Delta t = \frac{t_{\max}}{M-1} \quad (5.10)$$

where l is the length of 1D media and t_{\max} is maximum length of time. As indicated earlier the magnitude of EM field is reduced to less than 1% of its actual value at the surface of conducting host medium in time 3.186 Sec. The value of t_{\max} should be less than 3.186 Sec and will be considered 3 Sec in this modeling.

In FTCS scheme, the solution is obtained only when it reaches the condition of stability, i.e. $(\eta = \frac{\Delta t}{\mu\sigma(\Delta z^2)})$. The ranges of Δt is given in Table 5.3 while the value of z is assumed to be 500 m.

Table 5.3- Stability Factor

Parameters	Seawater	Sediments	Hydrocarbon
$\mu\sigma$	4.02125E-06	1.25664E-06	6.2832E-07
$\mu\sigma(\Delta z^2)$	0.994716068	3.183091418	6.366182837
Δt	$0 < t \leq 0.4918$	$0 < t \leq 1.4$	$0 < t \leq 3$

In Table 5.3, the value of permeability is considered to be same as in vacuum for EM geophysical surveys. The ranges of temporal step size Δt are also given for different conductive medium. Furthermore, to quantify electric field in space and time domain is done by solving the Equation 5.7 for each node of Figure 5.11. The resulting system of linear algebraic equations can be written in matrix form and its notion can be expressed as,

$$E^{m+1} = ME^m. \quad (5.11)$$

where M is $n \times n$ tri-diagonal matrix given as below. The E^{m+1} and E^m are the column matrix $m + 1$ and m respectively.

$$M = \begin{pmatrix} D_1 & d_{1,1} & 0 & \dots & \dots & 0 \\ d_{2,1} & D_2 & d_{1,2} & \ddots & & \vdots \\ 0 & d_{2,2} & D_3 & d_{1,3} & \ddots & \vdots \\ \vdots & \ddots & \ddots & \ddots & \ddots & 0 \\ \vdots & & \ddots & \ddots & \ddots & d_{1,n-1} \\ 0 & \dots & \dots & 0 & d_{2,n-1} & D_n \end{pmatrix}$$

5.6 Isotropic Media for Modeling in Temporal Domain

An isotropic geological structure will be used to find the optimal speed of mobile dipole source in marine CSEM survey. The selected model contains three different isotropic layers labeled as I, II and III. The electrical conductivity of layer I, II and III are assumed to be the same as of hydrocarbon, sediments and seawater respectively. In selected model the length of each layer is 10 km along z -axis and constant along other all directions. The electrical conductivity for layers of hydrocarbon, sediments and seawater are 0.5 S/m, 1.0 S/m and 3.2 S/m respectively.

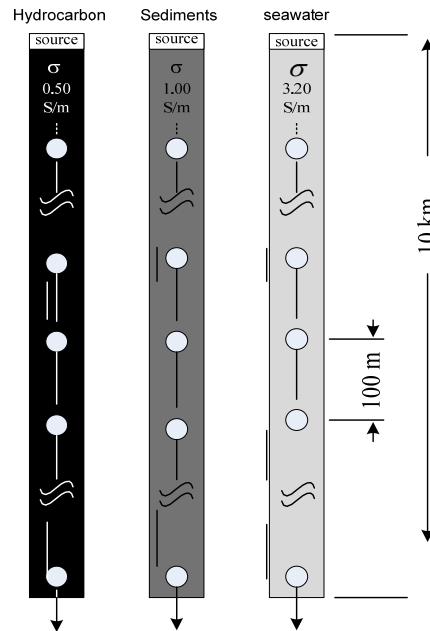


Figure 5.13 - 1D isotropic geological model

5.7 Numerical Results

The numerical solutions of FTCS schemes were implemented in MATLAB and are given in **APPENDIX-F**. The stability factor of FTCS method as discussed earlier can be achieved by using the larger step size in spatial domain. The FTCS scheme is implemented for three different isotropic layers with the frequency of 0.25 Hz. The electrical conductivity of given layers are 0.5 S/m, 1.0 S/m and 3.2 S/m. The simulation results are shown in Figure 5.14.

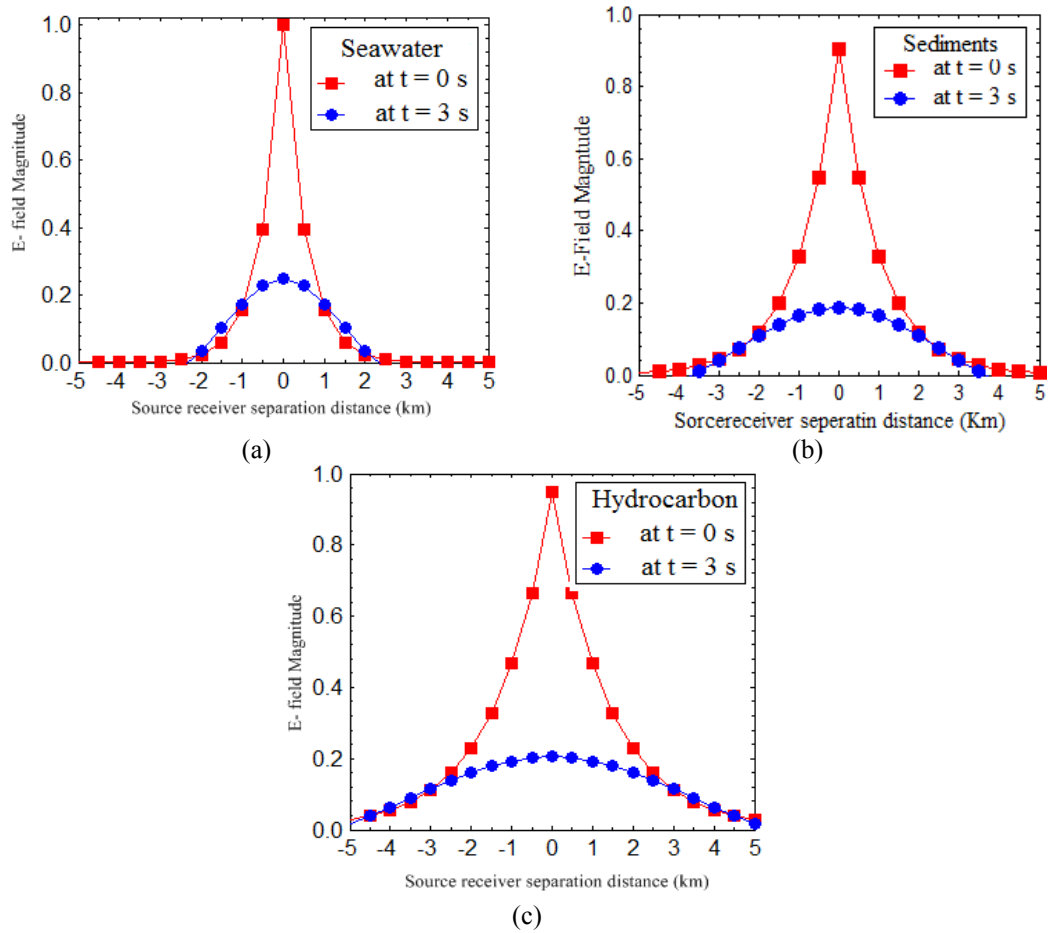


Figure 5.14- Modeling results for the magnitude of electric field in space and temporal domain

Results of Figure 5.14, illustrates the magnitude of electric field in spatial and time domain. It shows the magnitude of electric field reduces to less than 0.2 of its original value in time 3 Sec. In marine environment the major part of the diffused EM energy will be vanished along the strike direction or reflected back to the receiver end. Furthermore, in reference to Figure 5.11 the separation distance d_s between points p_1 and p_2 is a function of vessel speed as shown in Table 5.4. It shows the

uncertainties in the position of dipole source will increase when its moving speed is more. These uncertainties can be minimized by using less moving speed for water vessel.

Table 5.4 – separation distance between p_1 and p_2 at certain speed of dipole source

Vessel Speed	10 Km/h	20 Km/h	40 km/h	60 km/h	80 km/h
d_s	8.85 m	17.7 m	35.4 m	53.1 m	70.8 m

5.8 Summary

This chapter involves the study of dipping effects on received field using 2D layered media and optimal speed of mobile dipole source in marine CSEM survey. The formulation to quantify the electric field for dipping effects is obtained by solving the TE polarization using Equation 4.11. To implement forward modeling, there are different lengths of infinitesimal dipole with various zenith angles are considered. Similarly, to find the optimal velocity of moving HED above seafloor is done by using *forward time centered space* method. In both models the resulting equations of TE mode are implemented and it is simplified in the form at a system matrix with boundary conditions. The resulting matrix form is solved to calculate electric field for different geological models. The results for dipping model shows the anomalies in survey data occur when source is oriented improperly. On the other end the numerical modeling of 1D model using *forward time centered space* scheme shows the radiated signal will attenuated and its magnitude dropped to less than 1% of actual value after time 3.186 Sec for penetration depth of 5δ . If the mobile dipole is traveling at a speed higher than 20 km/h the uncertainty in the source position will be large.

CHAPTER 6

CONCLUSION AND FUTURE WORK

The main objective of marine CSEM/SBL survey is to explore petroleum reserves in deep water. The development of CSEM method was relatively slow in comparison to other techniques because of inadequate instrumentation and effective methods for interpretations. In recent years, marine CSEM/SBL has gained wide acceptance as a viable geophysical exploration tool. This method provides high data quality rate for interpretation than usual passive geophysical surveys. The irregularities of survey data are affected by the improper selection of source-receiver setup. Furthermore, the scenarios in real geological structure are extremely varied and only a few cases can be described in terms of simple geometric forms. So there are rare possibilities to feasibly convert the field measurements into a reliable earth model using an automatic interpretation process. Thus a human interpreter is still needed to guide the interpretation process and for that a qualitative understanding of the fundamentals EM field behavior for layered earth media is necessary. As a result, it is necessary to improve the survey procedure by using some logistical restrictions.

The study of most technical improvement in EM geophysical surveys is possible by using numerical modeling rather than real time survey. In this study there is a need to construct geological models of extremely varied conditions and to calculate electric and magnetic field. This field is considered to pass through the interior of the selected model. For numerical modeling the second order EM wave equations are evaluated for selected layered media in terms of system matrix. This system matrix is a function of medium conductivity and source parameters. The anomalous electric field at interface can be calculated by using the eigen values of system matrix. Many improvements have been implemented by conducting different experiments and simulation.

In this research, the study of 1D forward modeling allows the use of different frequencies and range combinations in order to find a parameter for marine CSEM. It demonstrated that the lower frequencies can penetrate at depth into the layered earth model. It also shows that the EM field behavior is sensitive to the electrical conductivity of physical earth materials. In high conductive medium the diffused EM energy attenuates rapidly and its penetration depth is also less than that of the resistive medium. The low frequency signal allows for the study of EM field behavior in horizontal layered media when reservoir is saturated with resistive hydrocarbon or conductive saline fluids.

The study of 2D forward modeling allows the understanding of EM field behavior in layered media. The field equations for TE and TM mode of polarizations can be obtained by using Maxwell's equations. The TE polarization is used to calculate the electric field and this is achieved by discretizing the whole solution region into a number of elements using *staggered-grid* scheme. The final systems of equations are solved to quantify electric field for different geological models and expressed in matrix form with boundary conditions. The results obtained of forward modeling for single model allows the understanding of EM field behavior at interface. The obtained results for multi interface model shows, the total electric field will reduce over the body if reservoir is filled with saline conductive fluids and enhanced if reservoir is filled with resistive hydrocarbons. The 2D forward modeling is important when looking for the effects of improper source orientation on measured EM field.

The irregularities in the orientation of mobile dipole source create the effects of dipping and rotation. The effect of both dipping and rotation can only be studied using 3D modeling. However in this research only 2D numerical modeling was used, that allows to study the behavior of EM field due to source dipping in real time survey data. The dipping effects are recreated by using different source orientation and using the equations of TE. In this work the different dimensions of mobile dipole source were used to understand the effects of dipole dimensions on dipping.

One major study was to find the optimal speed of moving source in marine environment. To find this, the numerical modeling is done using *forward time centered space* method. In this case, field governing equations are used to quantify

electric field in spatial domain than it propagates in temporal domain. The TE mode of polarization was used to obtain system matrix with boundary conditions. The numerical modeling of 1D model using *forward time centered space* scheme shows the radiated signal will attenuated and its magnitude dropped to less than 1% of actual value after time 3.186 s. The optimal suggested speed is 20 km/h or less because it allows less covered distance d_s as discussed in earlier chapter.

The real geological scenarios are extremely varied and are difficult to design in a simulation environment. In typical simulation environment simplified geological models are deemed sufficient. In this study, the geological structure is formed as plane horizontal layers. The obtained results provide a good understanding of how EM wave behave in different models of earth layers.

The results obtained through 1D forward modeling are used to find the optimal frequency for specified target depths. The results from 2D numerical modeling also provide the fundamentals of EM field behavior in hydrocarbon and saline fluid saturated geological structures. Furthermore effects of inaccurate source orientation (dipping) and various source dipole speeds on survey data are also analyzed.

The Earth's real geological structure consists of non-linear, anisotropic and non-homogeneous mediums. In numerical solution the values for electrical properties of various media are assumed to be constants for each grid of discretized solution region. These limitations may affect accuracy and stability of the numerical solution. However accuracy and stability can be increased using small grids to understand EM field behavior in layered earth using fundamentals of EM behavior rather than real time survey. In future we intend to enhance the proposed algorithm for 3D inversion.

REFERENCES

- [1] S. Ellingsrud, M. C. Sinha, et al. Remote sensing of hydrocarbon layers by seabed logging (SBL): Results from a cruise offshore Angola. *The Leading Edge*: 972-982. 2002,
- [2] A. D. Chave, and C. S. Cox. "Controlled Electromagnetic Sources for Measuring Electrical Conductivity Beneath the Oceans 1. Forward Problem and Model Study." *Journal of Geophysical Research* 87(B7): 5327-5338, 1982
- [3] A. D. Chave, S. Constable, et al.. *Electrical Exploration Methods for the Seafloor. Electromagnetic Methods in Applied Geophysics*. M. N. Nambighian, Society of Exploration Geophysicists. 2: 931-966, 1991.
- [4] L. S. Georgsson, and R. Karlsdóttir, *Resistivity Methods - DC And TEM With Examples And Comparison From the Reykjanes Peninsula And Öxarfjörður, Iceland*. [Online]. Available: <http://www.os.is/gogn/unu-gtp-sc/>. 2007,
- [5] K. L. Zonge, L. J. Hughes. *Electrical Exploration Methods for the Seafloor. Electromagnetic Methods in Applied Geophysics*. M. N. Nambighian, Society of Exploration Geophysicists. 2: 713-879, 1991.
- [6] T. Eidesmo, S. Ellingsrud, L. M. MacGregor, S. Constable, M. C. Sinha, S. Johansen, F. N. Kong and H. Westerdahl. *Sea Bed Logging (SBL), A New Method For Remote And Direct Identification Of Hydrocarbon Filled Layers In Deepwater Areas*. ElectroMagnetic GeoServices, Trondheim, Norway, 2000
- [7] B. R. Spies and F.C. Frischknecht , *Electromagnetic Sounding. Electromagnetic Methods in Applied Geophysics*. M. N. Nambighian, Society of Exploration Geophysicists. 2: 285-421, 1991.
- [8] T. M. Boyd. *Geophysical Surveying Using DC Resistivity*. [online]. Available: <http://www.earthsci.unimelb.edu.au>, 1998.
- [9] K.Vozoff. *Electrical Exploration Methods for the Seafloor. Electromagnetic Methods in Applied Geophysics*. M. N. Nabighian, Society of Exploration Geophysicists. 2: 641-966, 1991.

- [10] F. Simpson, K. Bahr. "Introduction", in *Practical Magnetotellurics*. Cambridge, United Kingdom: SYNDICATE, 2005, pp. 1-14, 2005.
- [11] L. O. Løseth. "Modeling of Controlled Source Electromagnetic Data," Ph.D Dissertation. Dept. of Phy. Norwegian University of Science and Technology., 2007
- [12] G. F. West, J.C. Macnae. Electrical Exploration Methods for the Seafloor. Electromagnetic Methods in Applied Geophysics. M. N. Nabighian, Society of Exploration Geophysicists. 2: 1- 45, 1991.
- [13] M. S. Zhdanov. "Forward and inverse Problem in Geophysics", *Geophysical Inverse Theory and Regularization Problems*, Salt Lake City: Elsevier, 2002, pp. 1-24, 2002.
- [14] D. L. Alumbaugh, A. Abubakar, et al. Fast 2D Forward and Inversion Algorithms for Interpreting Marine CSEM Data. Offshore Technology Conference, Houston, Texas, USA, 1-4 May 2006
- [15] K. A. Weitemeyer, "Marine Electromagnetic Methods for Gas Hydrate Characterization," Ph.D. dissertation, Dept. of Earth Science. Univ. of California, San Diego, 2008.
- [16] G. W. Recktenwald, "Finite-Difference Approximations to the Heat Equation," Portland. 2004
- [17] K. L. Zonge, L. J. Hughes. Electrical Exploration Methods for the Seafloor. Electromagnetic Methods in Applied Geophysics. M. N. Nambighian, Society of Exploration Geophysicists. 2: 713-879, 1991.
- [18] D.S. Parasnis, Large Layout Harmonic Field System. Electromagnetic Methods in Applied Geophysics. M. N. Nambighian, Society of Exploration Geophysicists. 2: 271-283, 1991.
- [19] R. N. Edward, M. N. Nabighian. Electrical Exploration Methods for the Seafloor. Electromagnetic Methods in Applied Geophysics. M. N. Nabighian, Society of Exploration Geophysicists. 2:47- 104, 1991.
- [20] J. R. Reitz, F. J. Milford. "Electromagnetic Induction", *Foundation of Electromagnetic Theory* (1st Edition). Massachusetts: ADDISON 1959, pp. 170-177, 1960
- [21] J. A. Stratton. "Maxwell's Equations", *Electromagnetic Theory*. (1st Edition). New York: MacGraw, 1941, pp. 1-13.

- [22] M. S. Zhdanov. "Foundation of Electromagnetic Theory in Geophysics", *Geophysical Inverse Theory and Regularization Problems*, Salt Lake City: Elsevier, 2002, pp. 201-227, 2002.
- [23] B. S. Guru and H. Hiziroglu. "Vector Analysis", *Electromagnetic field theory fundamentals*. Cambridge, UK: PWS, 2004, pp. 14-66, 2004.
- [24] B. S. Guru and H. Hiziroglu. "Plane Wave Propagation", *Electromagnetic field theory fundamentals*. Cambridge, UK: PWS, 2004, pp. 351-416, 2004.
- [25] T. Rosten, L. Ammendson, "Electromagnetic Data Processing" U.S. Patent 0065330, 2008.
- [26] R.S. Elliott. "The far field integrals-Reciprocity, Directivity", *Antenna Theory and Design* (Revised Edition). Hoboken: Willey, 2003, pp. 1-53, 2003.
- [27] C. A. Balanis, "Fundamental parameters of Antenna", *Antenna Theory Analysis and Design*, (3rd Edition) Hoboken: Wiley, 2005, pp. 1-24.
- [28] B.S. Nair, S. R. Deepa. "Reflection and Refraction of Plane wave", *Applied Electromagnetic Theory: Analysis Problem and Application*. New Delhi, India: Prentice pp. 210-220, 2008.
- [29] M. N. O. Sadiku, "Finite Difference Method", *Numerical Techniques in Electromagnetic*. Florida : CRC 2000 pp. 120-208
- [30] M. S. Zhdanov. "Integral Presentation in Electromagnetic Forward Modeling", *Geophysical Inverse Theory and Regularization Problems*, Salt Lake City: Elsevier, 2002, pp. 231-281.
- [31] M. S. Zhdanov. "Differential methods in Electromagnetic Modeling and Inversion" Forward and inverse Problem in Geophysics", *Geophysical Inverse Theory and Regularization Problems*, Salt Lake City: Elsevier, 2002, pp. 361-386. 2002
- [32] L. M. MacGregor, S. Constable, and M. C. Sinha. The RAMESSES experiment-III. Controlled-source electromagnetic sounding of the Reykjanes Ridge at 57° 45'N, *Geophys. J. Int.*, 135, 773-789, 1998.
- [33] L.M. MacGregor, D. Andreis, J. Tomlinson, N. Barker, Controlled-source electromagnetic imaging on the Huggets-1 reservoir, *The Leading Edge*, 984-992, 2006.

- [34] L. J. Srnka, Method and Apparatus for Offshore Electromagnetic Sounding Utilizing Wavelength Effects to Determine Optimum Source and Detector Positions” U.S.Patent 4617518, Oct 14, 1986.
- [35] S. D. Pawar, P. Murugavel, D. M. Lal . “Effect of relative humidity and sea level pressure on electrical conductivity of air over Indian Ocean” Journal Of Geophysical Research, VOL. 114, D02205, 2009, 8 PP
- [36] C. A. Balanis, “Linear Wire Antenna”, *Antenna Theory Analysis and Design*, (3rd Edition) Hoboken: Wiley, 2005, pp. 151-231.
- [37] L. O. Løseth, B. Ursin. “Electromagnetic fields in planarly layered anisotropic media,” *Geophysical Journal International*, 170: 44–80. doi: 10.1111/j.1365-246X.2007.03390.x, 2007.
- [38] G. R. Jirack. “Near Surface and Topographic Distortions in Electromagnetic Induction,” Department of Geological Science, san Diego state University, CA92182, USA, 1990.
- [39] K. A. Weitemeyer, “Marine Electromagnetic Methods for Gas Hydrate Characterization,” Ph.D. dissertation, Dept. of Earth Science. Univ. of California, San Diego, 2008.
- [40] William F. Ames. *Numerical Methods for Partial Differential Equations*. Academic Press, Inc., Boston, third edition, 1992.
- [41] Jeffery Cooper. *Introductin to Partial Differential Equations with MATLAB*. Birkh auser, Boston, 1998.
- [42] K.W. Morton and D.F. Mayers. *Numerical Solution of Partial Differential Equations: An Introduction*. Cambridge University Press, Cambridge, England, 1994.

APPENDIX A

ALGORITHM FOR 1D GEOLOGICAL MODEL

APPENDIX A

%:-----1D Forward Modelling (staggered grid scheme with FDM)

```
format long; clear all; clc; clf;
%:----- Model Parameters.
freq_1 = 0.25;           % Frequency 0.25 & 1.0 Hz
cond_1 = 0.02;           % Conductivity 0.25 & 1.0 Hz
perm    = pi*4e-7;
tol      = 1e-20; maxit   = 200; % Tolerance & Iteration
var_length = 10000;
i = sqrt(-1);
omega = 2*pi*freq_1;
%:-----Sparse Matrix
var_dis = 100;
var_unk = var_dis + 2;
var_stp = var_length/var_unk;
var_dig = -2/((var_stp)^2);
var_dig1 = (var_dig + i*omega*perm*cond_1)*ones(var_unk,1);
var_sub = ones(var_unk,1)/((var_stp)^2);
Main_mtx_1 = spdiags([var_sub,var_dig1,...
[var_sub]],[-1 0 1], var_unk, var_unk);
Main_mtx_1(1,2) = (1/var_stp);
Main_mtx_1(1,1) = -(1/var_stp);
var_rvm = zeros(var_unk,1);
var_rvm(1,1) = -i*1000*perm*omega;
%:----- Solution of Vector Matrix
Elect_1 = qmr(Main_mtx_1,var_rvm,tol,maxit);
for j = 1:var_unk
    var_1(j,1) = imag(Elect_1(j));
    var_2(j,1) = real(Elect_1(j));
end
for k = 1:var_unk
    if k==1
        x(k) = 0;
    else
        x(k)= var_stp + x(k-1);
    end
end
end
```

APPENDIX –B

ALGORITHM FOR SINGLE INTERFACE GEOLOGICAL MODEL

APPENDIX –B

%:-----2D Forward Modelling (Single Interface Model)

%:----- program Initializing

```
clear all;
clf
clc
format long
```

%:----- program Parameters

```
var1_1 = 0.25;           % Frequency in Hz
var1_2 = 2*pi*var1_1;    % Angular Frequency
var1_3 = pi*4e-007;      % Permeability
var1_4 = sqrt(-1);       % Imaginary part
var1_5 = 1e-99;          % Tolerance of QMR
var1_6 = 600;            % Maximum Iteration of QMR
```

%:----- Medium Electrical Properties

```
var2_1 = 3.20;           % con of sea water
var2_2 = 1.00;           % con of overburden and bottom half-space
var2_3 = 0.50;           % con of resistive hydrocarbons
var2_4 = 0.01;           % con of conductive hydrocarbons
var2_5 = 5.00;           % con of Moderate saline water
var2_6 = 1e-8;           % con of Air
var2_k1_6 = sqrt(var1_4*var1_2*var1_3*var2_2 + var1_2^2*var1_3);
var2_k2_7 = sqrt(var1_4*var1_2*var1_3*var2_3 + var1_2^2*var1_3);
var2_k3_8 = sqrt(var1_4*var1_2*var1_3*var2_5 + var1_2^2*var1_3);
var2_k3_9 = sqrt(var1_4*var1_2*var1_3*var2_6 + var1_2^2*var1_3);
```

%:----- program Parameters

```
var3_1 = 20000;          % Domain length in meters
var3_2 = 100;            % Water depth from HOD
var3_3 = 1500;           % Over burden Sediments
var3_4 = 1000;           % Hydrocarbon containing layer
var3_5 = 400;            % Under burden Sediments
```

%:----- Medium Properties in Matrix Form

```
var4_1 = var3_1/200;     % Horizontal step size
var4_2 = (var3_2 + var3_3 + var3_4 + var3_5)/50; % Vertical step size
% Matrix size var4_3 x var4_3
var4_3 = var4_1 * var4_2;
% Seawater
var4_4 = ((2/(var4_1^2)) + (2/(var4_2^2))) - var1_4*var1_2*var1_3*var2_1;
% Sediments
var4_5 = ((2/(var4_1^2)) + (2/(var4_2^2))) - var1_4*var1_2*var1_3*var2_2;
% Hydrocarbon
var4_6 = ((2/(var4_1^2)) + (2/(var4_2^2))) - var1_4*var1_2*var1_3*var2_3;
% Saline water
var4_7 = ((2/(var4_1^2)) + (2/(var4_2^2))) - var1_4*var1_2*var1_3*var2_5;
% Free space Air
var4_8 = ((2/(var4_1^2)) + (2/(var4_2^2))) - var1_4*var1_2*var1_3*var2_6;
```

%:----- Discretization

```
var5A_1 = ones(var4_3,1);
%:----- Interface (Domain Air)
for i1 = 1:1000
    Dia5A_2(i1,1) = var4_8;
end
```

%:----- Interface (Domain Water)----- SPARSE MATRIX A

```
for i2 = 1001:6000
    Dia5A_2(i2,1) = var4_4;
end
```

```

        Dig5A12 = ones(var4_3,1)/(var4_1^2);
        Dig5A13 = ones(var4_3,1)/(var4_2^2);
        Dig5A21 = ones(var4_3,1)/(var4_1^2);
        Dig5A31 = ones(var4_3,1)/(var4_2^2);
% Applying Matrix Upper and Lower Diagonal Conditions
for i5 = 0:100:var4_3
    if i5 == 0
    else
        Dig5A12(i5,1) = 0;
    end
end
for i6 = 0:100:var4_3
    if i6 == 0
    else
        Dig5A21(i6,1) = 0;
    end
end
%:----- Interface (Water domain)----- SPARSE MATRIX B
for j1 = 1:1000
    Dia5B_2(j1,1) = var4_5;
end
% Interface (Sediments Domain)
for j2 = 1001:6000
    Dia5B_2(j2,1) = var4_5;
end
%:----- Interface (Sediments Domain) )----- SPARSE MATRIX C
for k1 = 1:1000
    Dia5C_2(k1,1) = var4_5;
end
% Over burden Sediments Layer
for k2 = 1001:6000
    Dia5C_2(k2,1) = var4_6;
end
%:----- Interface (Water domain)----- SPARSE MATRIX D
for m1 = 1:1000
    Dia5D_2(m1,1) = var4_4;
end
% Interface (Saline Water domain)
for m2 = 1001:6000
    Dia5D_2(m2,1) = var4_5;
end
Main_mtxA = spdiags([Dig5A31,Dig5A21,Dia5A_2,Dig5A12,Dig5A13],...
    [-100 -1 0 1 100],var4_3,var4_3);
Main_mtxB = spdiags([Dig5A31,Dig5A21,Dia5B_2,Dig5A12,Dig5A13],...
    [-100 -1 0 1 100],var4_3,var4_3);
Main_mtxC = spdiags([Dig5A31,Dig5A21,Dia5C_2,Dig5A12,Dig5A13],...
    [-100 -1 0 1 100],var4_3,var4_3);
Main_mtxD = spdiags([Dig5A31,Dig5A21,Dia5D_2,Dig5A12,Dig5A13],...
    [-100 -1 0 1 100],var4_3,var4_3);
var7_1 = zeros(6000,1);
for var7_2 = 1:100
    var7_1(var7_2)= -var1_4*var1_3*var1_2;

```

```

end
for j = 1:100
    var7_1(j) = -var1_4*var1_3*var1_2*1000*var2_1;
    var8_1 = qmr(Main_mtxA,var7_1,var1_5,var1_6);
    var8_2 = qmr(Main_mtxB,var7_1,var1_5,var1_6);
    var8_3 = qmr(Main_mtxC,var7_1,var1_5,var1_6);
    var8_4 = qmr(Main_mtxD,var7_1,var1_5,var1_6);
    % Direct Signal
    var_dir1(j)= abs(var8_1(1250));
    var_dir2(j)= abs(var8_2(1250));
    var_dir3(j)= abs(var8_3(1250));
    var_dir4(j)= abs(var8_4(1250));
    var_step = 200;
    for var10_1 = 1:100
        if var10_1 == 1
            var10_2(var10_1) = 0;
        else
            var10_2(var10_1)= var_step + var10_2(var10_1-1);
        end
    end
end
end
end

```

APPENDIX –C

ALGORITHM FOR MULTI INTERFACES GEOLOGICAL MODEL

APPENDIX –C

%:-----2D Forward Modelling (Multi Interface Model)

%:-----Program Initializing

```

clear all; clf; clc; format long;
% General Variables
var1_1 = 0.25; % Frequency in Hz
var1_2 = 2*pi*var1_1; % Angular Frequency
var1_3 = pi*4e-007; % Permeability.
var1_4 = sqrt(-1); % Imaginary part i
var1_5 = 1e-99; % Tolerance of QMR
var1_6 = 600; % Maximum Iteration of QMR
%Media Parameters
var2_1 = 3.20; % con of sea water
var2_2 = 1.00; % con of overburden and bottom half space
var2_3 = 5.00; % con of resistive hydrocarbons
var2_4 = 0.01; % con of conductive hydrocarbons
var2_5 = 5.00; % con of Moderate saline water
var2_k1_6 = sqrt(var1_4*var1_2*var1_3*var2_2 + var1_2^2*var1_3);
var2_k2_7 = sqrt(var1_4*var1_2*var1_3*var2_3 + var1_2^2*var1_3);
var2_k3_8 = sqrt(var1_4*var1_2*var1_3*var2_5 + var1_2^2*var1_3);
% Discretization
var3_1 = 20000; % Domain length in meters
var3_2 = 100;
var3_3 = 1500; % Over burden Sediments
var3_4 = 1000; % Hydrocarbon containing layer
var3_5 = 400; % Under burden Sediments
var4_1 = var3_1/200; % Horizontal step size
var4_2 = (var3_2 + var3_3 + var3_4 + var3_5)/50; % Vertical step size
var4_3 = var4_1 * var4_2; % Matrix size var4_3 x var4_3
% sea water
var4_4 = ((2/(var4_1^2)) + (2/(var4_2^2))) - var1_4*var1_2*var1_3*var2_1;
% Sediments
var4_5 = ((2/(var4_1^2)) + (2/(var4_2^2))) - var1_4*var1_2*var1_3*var2_2;
% Hydrocarbon
var4_6 = ((2/(var4_1^2)) + (2/(var4_2^2))) - var1_4*var1_2*var1_3*var2_3;
% Saline water
var4_7 = ((2/(var4_1^2)) + (2/(var4_2^2))) - var1_4*var1_2*var1_3*var2_5;
%:----- Defining SPARSE MATRIX A
var5A_1 = ones(var4_3,1);
% Sea Water Layer
for i1 = 1:200
    Dia5A_2(i1,1) = var4_4;
end
% Over burden Sediments Layer
for i2 = 201:4200
    Dia5A_2(i2,1) = var4_5;
end
% Hydrocarbon Containing Layer

```

```

for i3= 4201:5200
Dia5A_2(i3,1) = var4_6;
end
% Under burden Sediments Layer
for i4 = 5201:6000
    Dia5A_2(i4,1) = var4_5;
end
Dig5A12 = ones(var4_3,1)/(var4_1^2);
Dig5A13 = ones(var4_3,1)/(var4_2^2);
Dig5A21 = ones(var4_3,1)/(var4_1^2);
Dig5A31 = ones(var4_3,1)/(var4_2^2);
% Applying Matrix Upper and Lower Diagonal Conditions
for i5 = 0:100:var4_3
    if i5 == 0
    else
        Dig5A12(i5,1) = 0;
    end
end
for i6 = 0:100:var4_3
    if i6 == 0
    else
        Dig5A21(i6,1) = 0;
    end
end
end
%:----- SPARSE MATRIX B
% Sea Water Layer
for j1 = 1:200
    Dia5B_2(j1,1) = var4_4;
end
% Over burden Sediments Layer
for j2 = 201:4700
    Dia5B_2(j2,1) = var4_5;
end
% Hydrocarbon Containing Layer
for j3= 4701:5200
    Dia5B_2(j3,1) = var4_6;
end
% Under burden Sediments Layer
for j4 = 5201:6000
    Dia5B_2(j4,1) = var4_5;
end
end
%:----- SPARSE MATRIX C
% Sea Water Layer
for k1 = 1:200
    Dia5C_2(k1,1) = var4_4;
end
% Over burden Sediments Layer
for k2 = 201:4200
    Dia5C_2(k2,1) = var4_5;
end
% Hydrocarbon Containing Layer
for k3= 4201:5200

```

```

        if (k3 >= 4233) && (k3 <= 4268)
            Dia5C_2(k3,1) = var4_6;
        elseif (k3 >= 4333) && (k3 <= 4368)
            Dia5C_2(k3,1) = var4_6;
        elseif (k3 >= 4433) && (k3 <= 4468)
            Dia5C_2(k3,1) = var4_6;
        elseif (k3 >= 4533) && (k3 <= 4568)
            Dia5C_2(k3,1) = var4_6;
        elseif (k3 >= 4633) && (k3 <= 4668)
            Dia5C_2(k3,1) = var4_6;
        elseif (k3 >= 4733) && (k3 <= 4768)
            Dia5C_2(k3,1) = var4_6;
        elseif (k3 >= 4833) && (k3 <= 4868)
            Dia5C_2(k3,1) = var4_6;
        elseif (k3 >= 4933) && (k3 <= 4968)
            Dia5C_2(k3,1) = var4_6;
        elseif (k3 >= 5033) && (k3 <= 5068)
            Dia5C_2(k3,1) = var4_6;
        elseif (k3 >= 5133) && (k3 <= 5168)
            Dia5C_2(k3,1) = var4_6;
        else
            Dia5C_2(k3,1) = var4_5;
        end
    end
% Under burden Sediments Layer
for k4 = 5201:6000
    Dia5C_2(k4,1) = ((2/(var4_1^2)) + (2/(var4_2^2))) -
    var1_4*var1_2*var1_3*var2_2*var5A_1(k4);
end
%:----- SPARSE MATRIX D
% Sea Water Layer
for p1 = 1:200
    Dia5D_2(p1,1) = var4_4;
end
% Over burden Sediments Layer
for p2 = 201:4700
    Dia5D_2(p2,1) = var4_5;
end
% Hydrocarbon Containing Layer
for p3= 4701:5200
    if (p3 >= 4733) && (p3 <= 4768)
        Dia5D_2(p3,1) = var4_6;
    elseif (p3 >= 4833) && (p3 <= 4868)
        Dia5D_2(p3,1) = var4_6;
    elseif (p3 >= 4933) && (p3 <= 4968)
        Dia5D_2(p3,1) = var4_6;
    elseif (p3 >= 5033) && (p3 <= 5068)
        Dia5D_2(p3,1) = var4_6;
    elseif (p3 >= 5133) && (p3 <= 5168)
        Dia5D_2(p3,1) = var4_6;
    else

```

```

        Dia5D_2(p3,1) = var4_5;
    end
end
% Under burden Sediments Layer
for p4 = 5201:6000
    Dia5D_2(p4,1) = var4_5;
end
%:----- SPARSE MATRIX F
% Sea Water Layer
for m1 = 1:200
    Dia5E_2(m1,1) = var4_4;
end
% Over burden Sediments Layer
for m2 = 201:4200
    Dia5E_2(m2,1) = var4_5;
end
% Saline Water Saturated Containing Layer
for m3= 4201:5200
    if m3>= 4233 && m3<= 4268
Dia5E_2(m3,1) = var4_7;
    elseif m3>= 4333 && m3<= 4368
        Dia5E_2(m3,1) = var4_7;
    elseif m3>= 4433 && m3<= 4468
        Dia5E_2(m3,1) = var4_7;
    elseif m3>= 4533 && m3<= 4568
        Dia5E_2(m3,1) = var4_7;
    elseif m3>= 4633 && m3<= 4668
        Dia5E_2(m3,1) = var4_7;
    elseif m3>= 4733 && m3<= 4768
        Dia5E_2(m3,1) = var4_7;
    elseif m3>= 4833 && m3<= 4868
        Dia5E_2(m3,1) = var4_7;
    elseif m3>= 4933 && m3<= 4968
        Dia5E_2(m3,1) = var4_7;
    elseif m3>= 5033 && m3<= 5068
        Dia5E_2(m3,1) = var4_7;
    elseif m3>= 5133 && m3<= 5168
        else
        Dia5E_2(m3,1) = var4_5;
    end
end
% Under burden Sediments Layer
for m4 = 5201:6000
    Dia5E_2(m4,1) = var4_5;
end
%:----- SPARSE MATRIX F
% Sea Water Layer
for n1 = 1:200
    Dia5F_2(n1,1) = var4_4;
end
% Over burden Sediments Layer
for n2 = 201:4700

```

```

        Dia5F_2(n2,1) = var4_5;
    end
    % Hydrocarbon Containing Layer
    for n3= 4701:5200
        if (n3 >= 4733) && (n3 <= 4768)
            Dia5F_2(n3,1) = var4_7;
        elseif (n3 >= 4833) && (n3 <= 4868)
            Dia5F_2(n3,1) = var4_7;
        elseif (n3 >= 4933) && (n3 <= 4968)
            Dia5F_2(n3,1) = var4_7;
        elseif (n3 >= 5033) && (n3 <= 5068)
            Dia5F_2(n3,1) = var4_7;
        elseif (n3 >= 5133) && (n3 <= 5168)
            else
                Dia5F_2(n3,1) = var4_5;
            end
        end
    end
    % Under burden Sediments Layer
    for n4 = 5201:6000
        Dia5F_2(n4,1) = var4_5;
    end
    Main_mtxA = ...
    spdiags([Dig5A31,Dig5A21,Dia5A_2,Dig5A12,Dig5A13],...
        [-100 -1 0 1 100],var4_3,var4_3);
    Main_mtxB = ...
    spdiags([Dig5A31,Dig5A21,Dia5B_2,Dig5A12,Dig5A13],...
        [-100 -1 0 1 100],var4_3,var4_3);
    Main_mtxC = ... spdiags([Dig5A31,Dig5A21,Dia5C_2,Dig5A12,Dig5A13],...
        [-100 -1 0 1 100],var4_3,var4_3);
    Main_mtxD =... spdiags([Dig5A31,Dig5A21,Dia5D_2,Dig5A12,Dig5A13],...
        [-100 -1 0 1 100],var4_3,var4_3);
    Main_mtxE = ... spdiags([Dig5A31,Dig5A21,Dia5E_2,Dig5A12,Dig5A13],...
        [-100 -1 0 1 100],var4_3,var4_3);
    Main_mtxF = ... spdiags([Dig5A31,Dig5A21,Dia5F_2,Dig5A12,Dig5A13],...
        [-100 -1 0 1 100],var4_3,var4_3);
    %:----- Column Matrix
    var7_1 = zeros(6000,1);
    for var7_2 = 1:100
        var7_1(var7_2)= -var1_4*var1_3*var1_2;
    end
    for var78_3 = 1:100
        if var78_3 > 1
            var7_1(var78_3-1,1)= -var1_4*var1_3*var1_2;
        end
        var7_1(var78_3,1) = -var1_4*var1_3*var1_2*1000*var2_1;
    end
    % System Matrix Solution
    var8_1 = qmr(Main_mtxA,var7_1,var1_5,var1_6);
    var8_2 = qmr(Main_mtxB,var7_1,var1_5,var1_6);
    var8_3 = qmr(Main_mtxC,var7_1,var1_5,var1_6);
    var8_4 = qmr(Main_mtxD,var7_1,var1_5,var1_6);
    var8_5 = qmr(Main_mtxE,var7_1,var1_5,var1_6);
    var8_6 = qmr(Main_mtxF,var7_1,var1_5,var1_6);

```

```

% Transmitter Distance from Corners
var_ref_1 = var78_3; % Declaring Var. moving Source
var_ref_2 = 100 - var_ref_1; % Declaring Dis. Var. Backward
var_ref_3 = 100 - var_ref_2; % Declaring Dis. Var. Backward

for var_ref_4 = 1:var_ref_3 % Backward Distance
    var_ref_5 = var_ref_3;
    if var_ref_5 == var_ref_4;
    else
        var_ref_6(var_ref_4) = (var_ref_5-var_ref_4)*200;
    end
end

%:----- Forward Distance
for var_ref_7 = 1:var_ref_2 % Forward distance
    var_ref_6(var_ref_3+var_ref_7) = var_ref_7*200;
end
var_ref_6(var_ref_1) = 0; % Zero angle at Source Position
%:----- Grazing Angle.
for var_ang_1 = 1:100
    var_ang_3(var_ang_1) = atan(2100/var_ref_6(var_ang_1));
    var_ang_4(var_ang_1) = atan(2350/var_ref_6(var_ang_1));
    var_ang_5(var_ang_1) = atan(2600/var_ref_6(var_ang_1));
end
var_ang_6 = var_ang_3;
var_ang_7 = var_ang_4;
var_ang_8 = var_ang_5;
for var_ang_9 = 1:100
    if (var_ang_9 >= 34) && (var_ang_9 <= 67)
else
        var_ang_6(var_ang_9) = 0;
        var_ang_7(var_ang_9) = 0;

var_ang_8(var_ang_9) = 0;
    end
end
%:-----Refraction Angle.
for var_ref_8 = 1:100
    var_ref_9(var_ref_8) = asin((var2_k1_6/var2_k2_7)*...
        (sin(var_ang_6(var_ref_8))));
    var_ref_10(var_ref_8) = asin((var2_k1_6/var2_k2_7)*...
        (sin(var_ang_7(var_ref_8))));
    var_ref_11(var_ref_8) = asin((var2_k1_6/var2_k2_7)*...
        (sin(var_ang_8(var_ref_8))));
end
for var_ang12 = 1:100
    if (var_ang_9 >= 34) && (var_ang_9 <= 67)
    else
        var_ang_12(var_ang12) = 0;
        var_ang_13(var_ang12) = 0;
        var_ang_14(var_ang12) = 0;
    end
end

```

```

end
%----- Anomalous Field b/c of Reflection
for var_ref_15 = 1:100

% ***** Model 1A & 1B
var_ele_ref_modA1(var_ref_15) =...
    (((var1_3*var2_k1_6*sin(var_ang_3(var_ref_15)))...
    -(var1_3*var2_k2_7*sin(var_ref_9(var_ref_15))))...
    /((var1_3*var2_k1_6*sin(var_ang_3(var_ref_15)))...
    +(var1_3*var2_k2_7*sin(var_ref_9(var_ref_15))))...
    * var8_1(3100 + var_ref_15);
var_ele_ref_modB1(var_ref_15) = ...
    (((var1_3*var2_k2_7*sin(var_ang_5(var_ref_15)))...
    -(var1_3*var2_k1_6*sin(var_ref_11(var_ref_15))))...
    /((var1_3*var2_k2_7*sin(var_ang_5(var_ref_15)))...
    +(var1_3*var2_k1_6*sin(var_ref_11(var_ref_15))))...
    * var8_1(5100 + var_ref_15);

% ***** Model 2A & 2B
var_ele_ref_modA2(var_ref_15) =...
    (((var1_3*var2_k1_6*sin(var_ang_4(var_ref_15)))...
    (var1_3*var2_k2_7*sin(var_ref_10(var_ref_15))))...
    /((var1_3*var2_k1_6*sin(var_ang_4(var_ref_15)))...
    +(var1_3*var2_k2_7*sin(var_ref_10(var_ref_15))))...
    *var8_2(2100 + var_ref_15);
var_ele_ref_modB2(var_ref_15) =...
    (((var1_3*var2_k2_7*sin(var_ang_5(var_ref_15)))...
    -(var1_3*var2_k1_6*sin(var_ref_11(var_ref_15))))...
    /((var1_3*var2_k2_7*sin(var_ang_5(var_ref_15)))...
    +(var1_3*var2_k1_6*sin(var_ref_11(var_ref_15))))...
    *var8_2(5100 + var_ref_15);
end
for var_ref_16 = 34:67

% ***** Model 3A & 3B
var_ele_ref_modA3(var_ref_16) = ...
    (((var1_3*var2_k1_6*sin(var_ang_3(var_ref_16)))...
    -(var1_3*var2_k2_7*sin(var_ref_9(var_ref_16))))...
    /((var1_3*var2_k1_6*sin(var_ang_3(var_ref_16)))...
    +(var1_3*var2_k2_7*sin(var_ref_9(var_ref_16))))...
    *var8_3(3100 + var_ref_16);
var_ele_ref_modB3(var_ref_16) =...
    (((var1_3*var2_k2_7*sin(var_ang_5(var_ref_16)))...
    -(var1_3*var2_k1_6*sin(var_ref_11(var_ref_16))))...
    /((var1_3*var2_k2_7*sin(var_ang_5(var_ref_16)))...
    +(var1_3*var2_k1_6*sin(var_ref_11(var_ref_16))))...
    *var8_3(5100 + var_ref_16);

% ***** Model 4A & 4B
var_ele_ref_modA4(var_ref_16) =...
    (((var1_3*var2_k1_6*sin(var_ang_4(var_ref_16)))...
    -(var1_3*var2_k2_7*sin(var_ref_10(var_ref_16))))...
    /((var1_3*var2_k1_6*sin(var_ang_4(var_ref_16)))...
    +(var1_3*var2_k2_7*sin(var_ref_10(var_ref_16))))...
    *var8_4(2100 + var_ref_16);

```

```

var_ele_ref_modB4(var_ref_16) =...
(((var1_3*var2_k2_7*sin(var_ang_5(var_ref_16)))...
-(var1_3*var2_k1_6*sin(var_ref_11(var_ref_16)))...
/((var1_3*var2_k2_7*sin(var_ang_5(var_ref_16)))...
+(var1_3*var2_k1_6*sin(var_ref_11(var_ref_16))))...
*var8_4(5100 + var_ref_16);

% ***** Model 5A & 5B
var_ele_ref_modA5(var_ref_16) =...
(((var1_3*var2_k1_6*sin(var_ang_3(var_ref_16)))...
-(var1_3*var2_k3_8*sin(var_ref_9(var_ref_16)))...
/((var1_3*var2_k1_6*sin(var_ang_3(var_ref_16)))...
+(var1_3*var2_k3_8*sin(var_ref_9(var_ref_16))))...
*var8_5(3100 + var_ref_16);

var_ele_ref_modB5(var_ref_16) =...
(((var1_3*var2_k3_8*sin(var_ang_5(var_ref_16)))...
-(var1_3*var2_k1_6*sin(var_ref_11(var_ref_16)))...
/((var1_3*var2_k3_8*sin(var_ang_5(var_ref_16)))...
+(var1_3*var2_k1_6*sin(var_ref_11(var_ref_16))))...
*var8_5(5100 + var_ref_16);

% ***** Model 6A & 6B
var_ele_ref_modA6(var_ref_16) =...
(((var1_3*var2_k1_6*sin(var_ang_4(var_ref_16)))...
-(var1_3*var2_k3_8*sin(var_ref_10(var_ref_16)))...
/((var1_3*var2_k1_6*sin(var_ang_4(var_ref_16)))...
+(var1_3*var2_k3_8*sin(var_ref_10(var_ref_16))))...
*var8_6(2100 + var_ref_16);

var_ele_ref_modB6(var_ref_16) =...
(((var1_3*var2_k3_8*sin(var_ang_5(var_ref_16)))...
-(var1_3*var2_k1_6*sin(var_ref_11(var_ref_16)))...
/((var1_3*var2_k3_8*sin(var_ang_5(var_ref_16)))...
+(var1_3*var2_k1_6*sin(var_ref_11(var_ref_16))))...
*var8_6(5100 + var_ref_16);
end
    var_rhm_1B = zeros(5800,1);
    var_rhm_2B = zeros(5800,1);
    var_rhm_3B = zeros(5800,1);
    var_rhm_4B = zeros(5800,1);
    var_rhm_5B = zeros(5800,1);
    var_rhm_6B = zeros(5800,1);
    for var_ref_16 = 1:100
var_rhm_1B(var_ref_16+800) =... var_ele_ref_modB1(var_ref_16)*(-
var1_4*var1_3*var1_2);

var_rhm_2B(var_ref_16+800) =...
var_ele_ref_modB2(var_ref_16*(-var1_4*var1_3*var1_2));
    end
    for var_ref_17 = 34:67
var_rhm_3B(var_ref_17+800) = ...

```



```

var_ele_ref_modB3(var_ref_17)*(-var1_4*var1_3*var1_2);

var_rhm_4B(var_ref_17+800) =.....var_ele_ref_modB4(var_ref_17)*(-
var1_4*var1_3*var1_2);

var_rhm_5B(var_ref_17+800) = ... var_ele_ref_modB5(var_ref_17)*(-
var1_4*var1_3*var1_2);

var_rhm_6B(var_ref_17+800) = ... var_ele_ref_modB6(var_ref_17)*(-
var1_4*var1_3*var1_2);
    end
    for var_ref_16 = 1:100
var_rhm_1B(var_ref_16+1300) = ... var_ele_ref_modB1(var_ref_16)*(-
var1_4*var1_3*var1_2);

var_rhm_2B(var_ref_16+1800) = ... var_ele_ref_modB2(var_ref_16)*(-
var1_4*var1_3*var1_2);
    end
    for var_ref_17 = 34:67
var_rhm_3B(var_ref_17+1300) = ... var_ele_ref_modB3(var_ref_17)*(-
xvar1_4*var1_3*var1_2);
var_rhm_4B(var_ref_17+1800) = ... var_ele_ref_modB4(var_ref_17)*(-
var1_4*var1_3*var1_2);
var_rhm_5B(var_ref_17+1300) = ... var_ele_ref_modB5(var_ref_17)*(-
var1_4*var1_3*var1_2);
var_rhm_6B(var_ref_17+1800) = ... var_ele_ref_modB6(var_ref_17)*(-
var1_4*var1_3*var1_2);
    end
%----- Sparse Matrix for Reflection
    var_81A_3 = 5800;
% MODEL 1B
        var81A_25 = ones(var_81A_3,1);
        for var_81A_4 = 1:var_81A_3
            if (var_81A_4 >= 800) && (var_81A_4 <= 1800)
                var_81A_mod1_6(var_81A_4,1) = var4_6;
            else
                var_81A_mod1_6(var_81A_4,1) = var4_5;
            end
        end
        var_81A_mod1_7 = ones(var_81A_3,1)/(var4_1^2);
        var_81A_mod1_8 = ones(var_81A_3,1)/(var4_1^2);
        var_81A_mod1_9 = ones(var_81A_3,1)/(var4_2^2);
        var_81A_mod1_10 = ones(var_81A_3,1)/(var4_2^2);
        for var81A_3 = 0:100:var_81A_3
            if var81A_3 == 0
            else
                var_81A_mod1_7(var81A_3,1) = 0;
            end
        end
        for var81A_4 = 0:100:var_81A_3
            if var81A_4 == 0
            else

```

```

        var_81A_mod1_8(var81A_4,1) = 0;
    end
end
%MODEL 1B
    for var_81A_5 = 1:var_81A_3
        if (var_81A_5 >= 800) && (var_81A_5 <= 1300)
            var_81A_mod2_6(var_81A_5,1) = var4_6;
        else
            var_81A_mod2_6(var_81A_5,1) = var4_5;
        end
    end
    var_81A_mod2_7 = ones(var_81A_3,1)/(var4_1^2);
    var_81A_mod2_8 = ones(var_81A_3,1)/(var4_1^2);
    var_81A_mod2_9 = ones(var_81A_3,1)/(var4_2^2);
    var_81A_mod2_10 = ones(var_81A_3,1)/(var4_2^2);

    for var81A_7 = 0:100:var_81A_3
        if var81A_7 == 0
            else
                var_81A_mod2_7(var81A_7,1) = 0;
            end
        end
    for var81A_8 = 0:100:var_81A_3
        if var81A_8 == 0
            else
                var_81A_mod2_8(var81A_8,1) = 0;
            end
        end
    end

%MODEL 3B
    for var_81A_6 = 1:var_81A_3
        if (var_81A_6 >= 833) && (var_81A_6 <= 868)
            var_81A_mod3_6(var_81A_6,1) = var4_6;
        elseif (var_81A_6 >= 933) && (var_81A_6 <= 968)
            var_81A_mod3_6(var_81A_6,1) = var4_6;
        elseif (var_81A_6 >= 1033) && (var_81A_6 <= 1068)
            var_81A_mod3_6(var_81A_6,1) = var4_6;
        elseif (var_81A_6 >= 1133) && (var_81A_6 <= 1168)
            var_81A_mod3_6(var_81A_6,1) = var4_6;
        elseif (var_81A_6 >= 1233) && (var_81A_6 <= 1268)
            var_81A_mod3_6(var_81A_6,1) = var4_6;
        elseif (var_81A_6 >= 1333) && (var_81A_6 <= 1368)
            var_81A_mod3_6(var_81A_6,1) = var4_6;
        elseif (var_81A_6 >= 1433) && (var_81A_6 <= 1468)
            var_81A_mod3_6(var_81A_6,1) = var4_6;
        elseif (var_81A_6 >= 1533) && (var_81A_6 <= 1568)
            var_81A_mod3_6(var_81A_6,1) = var4_6;
        elseif (var_81A_6 >= 1633) && (var_81A_6 <= 1668)
            var_81A_mod3_6(var_81A_6,1) = var4_6;
        elseif (var_81A_6 >= 1733) && (var_81A_6 <= 1768)
            var_81A_mod3_6(var_81A_6,1) = var4_6;
        else

```

```

        var_81A_mod3_6(var_81A_6,1) = var4_5;
    end
end

var_81A_mod3_7 = ones(var_81A_3,1)/(var4_1^2);
var_81A_mod3_8 = ones(var_81A_3,1)/(var4_2^2);
var_81A_mod3_9 = ones(var_81A_3,1)/(var4_1^2);
var_81A_mod3_10 = ones(var_81A_3,1)/(var4_2^2);

    for var81A_11 = 0:100:var_81A_3
        if var81A_11 == 0
else

        var_81A_mod3_7(var81A_11,1) = 0;
    end
end
for var81A_12 = 0:100:var_81A_3
    if var81A_12 == 0
    else
        var_81A_mod3_8(var81A_12,1) = 0;
    end
end
%----- MODEL 4B
    for var_81A_7 = 1:var_81A_3
        if (var_81A_7 >= 833) && (var_81A_7 <= 868)
            var_81A_mod4_6(var_81A_7,1) = var4_6;
elseif (var_81A_7 >= 933) && (var_81A_7 <= 968)
            var_81A_mod4_6(var_81A_7,1) = var4_6;
elseif (var_81A_7 >= 1033) && (var_81A_7 <= 1068)
            var_81A_mod4_6(var_81A_7,1) = var4_6;
elseif (var_81A_7 >= 1133) && (var_81A_7 <= 1168)
            var_81A_mod4_6(var_81A_7,1) = var4_6;
elseif (var_81A_7 >= 1233) && (var_81A_7 <= 1268)
            var_81A_mod4_6(var_81A_7,1) = var4_6;
        else
            var_81A_mod4_6(var_81A_7,1) = var4_5;
        end
    end

    var_81A_mod4_7 = ones(var_81A_3,1)/(var4_1^2);
    var_81A_mod4_8 = ones(var_81A_3,1)/(var4_2^2);
    var_81A_mod4_9 = ones(var_81A_3,1)/(var4_1^2);
    var_81A_mod4_10 = ones(var_81A_3,1)/(var4_2^2);
    for var81A_15 = 0:100:var_81A_3
        if var81A_15 == 0
        else
            var_81A_mod4_7(var81A_15,1) = 0;
        end
    end
    for var81A_16 = 0:100:var_81A_3
        if var81A_16 == 0
        else
            var_81A_mod4_8(var81A_16,1) = 0;

```

```

end
    end
%----- MODEL 5B
    for var_81A_8 = 1:var_81A_3
        if (var_81A_8 >= 833) && (var_81A_8 <= 868)
            var_81A_mod5_6(var_81A_8,1) = var4_7;
        elseif (var_81A_8 >= 933) && (var_81A_8 <= 968)
            var_81A_mod5_6(var_81A_8,1) = var4_7;
        elseif (var_81A_8 >= 1033) && (var_81A_8 <= 1068)
            var_81A_mod5_6(var_81A_8,1) = var4_7;
        elseif (var_81A_8 >= 1133) && (var_81A_8 <= 1168)
            var_81A_mod5_6(var_81A_8,1) = var4_7;
        elseif (var_81A_8 >= 1233) && (var_81A_8 <= 1268)
            var_81A_mod5_6(var_81A_8,1) = var4_7;
        elseif (var_81A_8 >= 1333) && (var_81A_8 <= 1368)
            var_81A_mod5_6(var_81A_8,1) = var4_7;
        elseif (var_81A_8 >= 1433) && (var_81A_8 <= 1468)
            var_81A_mod5_6(var_81A_8,1) = var4_7;
        elseif (var_81A_8 >= 1533) && (var_81A_8 <= 1568)
            var_81A_mod5_6(var_81A_8,1) = var4_7;
        elseif (var_81A_8 >= 1633) && (var_81A_8 <= 1668)
            var_81A_mod5_6(var_81A_8,1) = var4_7;
        elseif (var_81A_8 >= 1733) && (var_81A_8 <= 1768)
            var_81A_mod5_6(var_81A_8,1) = var4_7;
        else
            var_81A_mod5_6(var_81A_8,1) = var4_5;
        end
    end
    var_81A_mod5_7 = ones(var_81A_3,1)/(var4_1^2);
    var_81A_mod5_8 = ones(var_81A_3,1)/(var4_2^2);
    var_81A_mod5_9 = ones(var_81A_3,1)/(var4_1^2);
    var_81A_mod5_10 = ones(var_81A_3,1)/(var4_2^2);

    for var81A_19 = 0:100:var_81A_3
        if var81A_19 == 0
            else
                var_81A_mod5_7(var81A_19,1) = 0;
            end
        end
    for var81A_20 = 0:100:var_81A_3
        if var81A_20 == 0
            else
                var_81A_mod5_8(var81A_20,1) = 0;
            end
        end
    end
%----- MODEL 6B
    for var_81A_9 = 1:var_81A_3
        if (var_81A_9 >= 833) && (var_81A_9 <= 868)
            var_81A_mod6_6(var_81A_9,1) = var4_7;
        elseif (var_81A_9 >= 933) && (var_81A_9 <= 968)
            var_81A_mod6_6(var_81A_9,1) = var4_7;
        elseif (var_81A_9 >= 1033) && (var_81A_9 <= 1068)

```

```

        var_81A_mod6_6(var_81A_9,1) = var4_7;
elseif (var_81A_9 >= 1133) && (var_81A_9 <= 1168)
        var_81A_mod6_6(var_81A_9,1) = var4_7;
elseif (var_81A_9 >= 1233) && (var_81A_9 <= 1268)
        var_81A_mod6_6(var_81A_9,1) = var4_7;

else
        var_81A_mod6_6(var_81A_9,1) = var4_5;
end
end
var_81A_mod6_7 = ones(var_81A_3,1)/(var4_1^2);
var_81A_mod6_8 = ones(var_81A_3,1)/(var4_2^2);
var_81A_mod6_9 = ones(var_81A_3,1)/(var4_1^2);
var_81A_mod6_10 = ones(var_81A_3,1)/(var4_2^2);

for var81A_23 = 0:100:var_81A_3
    if var81A_23 == 0
    else
        var_81A_mod6_7(var81A_23,1) = 0;
    end
end
for var81A_24 = 0:100:var_81A_3
    if var81A_24 == 0
    else
        var_81A_mod6_8(var81A_24,1) = 0;
    end
end
end
%----- Sparse Matrix Generation
spa_ref_modB1 =...
    spdiags([var_81A_mod1_10,var_81A_mod1_8,var_81A_mod1_6,...
        var_81A_mod1_7,var_81A_mod1_9],[-100,1,0,1,100],...
        var_81A_3,var_81A_3);

% ***** Model 2A & 2B
spa_ref_modB2 =...
    spdiags([var_81A_mod2_10,var_81A_mod2_8,var_81A_mod2_6,...
        var_81A_mod2_7,var_81A_mod2_9],[-100,1,0,1,100],...
        var_81A_3,var_81A_3);

% ***** Model 3A & 3B
spa_ref_modB3 =...
    spdiags([var_81A_mod3_10,var_81A_mod3_8,var_81A_mod3_6,
...
        var_81A_mod3_7,var_81A_mod3_9],[-100,1,0,1,100],...
        var_81A_3,var_81A_3);

% ***** Model 4A & 4B
spa_ref_modB4 =...
    spdiags([var_81A_mod4_10,var_81A_mod4_8,var_81A_mod4_6,
...
        var_81A_mod4_7,var_81A_mod4_9],[-100,1,0,1,100],...
        var_81A_3,var_81A_3);

% ***** Model 5A & 5B
spa_ref_modB5 =...

```

```

spdiags([var_81A_mod5_10,var_81A_mod5_8,var_81A_mod5_6,...
var_81A_mod5_7,var_81A_mod5_9],[-100,1,0,1,100],...
var_81A_3,var_81A_3);
% ***** Model 1A & 1B
spa_ref_modB6 =...
    spdiags([var_81A_mod6_10,var_81A_mod6_8,var_81A_mod6_6,...
var_81A_mod6_7,var_81A_mod6_9],[-100,1,0,1,100],...
var_81A_3,var_81A_3);
% Matrices Solution of Model A1 & B1
var9_1 = qmr(spa_ref_modB1,var_rhm_1B,var1_5,var1_6);
var9_2 = qmr(spa_ref_modB2,var_rhm_2B,var1_5,var1_6);
var9_3 = qmr(spa_ref_modB3,var_rhm_3B,var1_5,var1_6);
var9_4 = qmr(spa_ref_modB4,var_rhm_4B,var1_5,var1_6);
var9_5 = qmr(spa_ref_modB5,var_rhm_5B,var1_5,var1_6);
var9_6 = qmr(spa_ref_modB6,var_rhm_6B,var1_5,var1_6);
% The Signal @ Receiver
var10_ele1(var78_3) = abs(var9_1(5750));
var10_ele2(var78_3) = abs(var9_2(5750));
var10_ele3(var78_3) = abs(var9_3(5750));
var10_ele4(var78_3) = abs(var9_4(5750));
var10_ele5(var78_3) = abs(var9_5(5750));
var10_ele6(var78_3) = abs(var9_6(5750));
end
%Source Receiver Separation Distance
var_step = 200;
for var10_1 = 1:100
    if var10_1 == 1
        var10_2(var10_1) = 0;
    else
        var10_2(var10_1)= var_step + var10_2(var10_1-1);
    end
end
for var_fin1 = 1:50
    var10_ele1(50 + var_fin1)= var10_ele1(51 - var_fin1);
    var10_ele2(50 + var_fin1)= var10_ele2(51 - var_fin1);
    var10_ele3(50 + var_fin1)= var10_ele3(51 - var_fin1);
    var10_ele4(50 + var_fin1)= var10_ele4(51 - var_fin1);
    var10_ele5(50 + var_fin1)= var10_ele5(51 - var_fin1);
    var10_ele6(50 + var_fin1)= var10_ele6(51 - var_fin1);
end

```

APPENDIX –D

ALGORITHM FOR DIPPING EFFECTS IN 2D GEOLOGICAL MODEL

APPENDIX –D

%:-----2D Forward Modelling (Dipping Model)

%:-----Programs initializing

```
clear all; clf; clc; format long;
```

%----- General Variables

```
var1_1 = 0.25; % Frequency in Hz
var1_2 = 2*pi*var1_1; % Angular Frequency
var1_3 = pi*4e-007; % Permeability.
var1_4 = sqrt(-1); % Imaginary part
var1_5 = 1e-99; % Tolerance of QMR
var1_6 = 600; % Maximum Iteration of QMR
```

%----- Media Parameters

```
var2_1 = 3.20; % con of sea water
var2_2 = 1.00; % con of overburden and bottom half space
var2_3 = 0.50; % con of resistive hydrocarbons
var2_4 = 0.01; % con of conductive hydrocarbons
var2_5 = 5.00; % con of Moderate saline water
var2_k1_6 = sqrt(var1_4*var1_2*var1_3*var2_2 + var1_2^2*var1_3);
var2_k2_7 = sqrt(var1_4*var1_2*var1_3*var2_3 + var1_2^2*var1_3);
var2_k3_8 = sqrt(var1_4*var1_2*var1_3*var2_5 + var1_2^2*var1_3);
```

%----- Field Region

```
var3_1 = 20000; % Domain length in meters
var3_2 = 200; % Water depth from HOD
var3_3 = 1400; % Over burden Sediments
var3_4 = 1000; % Hydrocarbon containing layer
var3_5 = 400; % Under burden Sediments
```

%----- Discretization

```
var4_1 = var3_1/200; % Horizontal step size
var4_2 = (var3_2 + var3_3 + var3_4 + var3_5)/50; % Vertical step size
var4_3 = var4_1 * var4_2; % Matrix size var4_3 x var4_3
```

%-----

```
var4_1A1 = ((2/(var4_1^2)) + (2/(60*63.14))) - ...
    var1_4*var1_2*var1_3*var2_1;
var4_1A2 = ((2/(var4_1^2)) + (2/(63.14*56.86))) - ...
    var1_4*var1_2*var1_3*var2_1;
var4_1A3 = ((2/(var4_1^2)) + (2/(56.86*60))) - ...
    var1_4*var1_2*var1_3*var2_2;
```

%-----

```
var4_2A1 = ((2/(var4_1^2)) + (2/(60*66.31))) - ...
    var1_4*var1_2*var1_3*var2_1;
var4_2A2 = ((2/(var4_1^2)) + (2/(66.31*53.69))) - ...
    var1_4*var1_2*var1_3*var2_1;
var4_2A3 = ((2/(var4_1^2)) + (2/(53.69*60))) - ...
    var1_4*var1_2*var1_3*var2_2;
```

%-----

```
var4_3A1 = ((2/(var4_1^2)) + (2/(60*69.5))) - ...
    var1_4*var1_2*var1_3*var2_1;
var4_3A2 = ((2/(var4_1^2)) + (2/(69.5*50.5))) - ...
    var1_4*var1_2*var1_3*var2_1;
var4_3A3 = ((2/(var4_1^2)) + (2/(50.5*60))) - ...
```



```

        var1_4*var1_2*var1_3*var2_2;
%-----
    var4_4A1 = ((2/(var4_1^2)) + (2/(60*72.75))) - ...
        var1_4*var1_2*var1_3*var2_1;
    var4_4A2 = ((2/(var4_1^2)) + (2/(72.75*47.25))) - ...
        var1_4*var1_2*var1_3*var2_1;
    var4_4A3 = ((2/(var4_1^2)) + (2/(47.25*60))) - ...
        var1_4*var1_2*var1_3*var2_2;
% sea water
var4_4 = ((2/(var4_1^2)) + (2/(var4_2^2))) - var1_4*var1_2*var1_3*var2_1;
% Sediments
var4_5 = ((2/(var4_1^2)) + (2/(var4_2^2))) - var1_4*var1_2*var1_3*var2_2;
% Hydrocarbon
var4_6 = ((2/(var4_1^2)) + (2/(var4_2^2))) - var1_4*var1_2*var1_3*var2_3;
% Saline water
var4_7 = ((2/(var4_1^2)) + (2/(var4_2^2))) - var1_4*var1_2*var1_3*var2_5;
% Sea Water Layer
var5A_1 = ones(var4_3,1);
for i1 = 1:400
    Dia5A_2(i1,1) = var4_4;
End
%----- Sparse Matrix A
% Over burden Sediments Layer
for i2 = 401:4200
    Dia5A_2(i2,1) = var4_5;
end
% Hydrocarbon Containing Layer
for i3 = 4201:5200
    Dia5A_2(i3,1) = var4_6;
end
% Under burden Sediments Layer
for i4 = 5201:6000
    Dia5A_2(i4,1) = var4_5;
end
Dig5A12 = ones(var4_3,1)/(var4_1^2);
Dig5A13 = ones(var4_3,1)/(var4_2^2);
Dig5A21 = ones(var4_3,1)/(var4_1^2);
Dig5A31 = ones(var4_3,1)/(var4_2^2);
% Applying Matrix Upper and Lower Diagonal Conditions
for i5 = 0:100:var4_3
    if i5 == 0
        else
            Dig5A12(i5,1) = 0;
        end
    end
end
for i6 = 0:100:var4_3
    if i6 == 0
        else
            Dig5A21(i6,1) = 0;
        end
    end
end
%----- Sparse Matrix B

```

```

var5A_1 = ones(var4_3,1);
% Sea Water Layer
for j1 = 1:400
    if j1 <= 200
        Dia5B_2(j1,1) = var4_4;
    elseif j1 >= 200 && j1 <= 300
        Dia5B_2(j1,1)= var4_1A1;
    else
        Dia5B_2(j1,1)= var4_1A2;
    end
end
% Over burden Sediments Layer
for j2 = 401:4200
    if j2 >= 401 && j2 <= 500
        Dia5B_2(j2,1) = var4_1A3;
    else
        Dia5B_2(j2,1) = var4_5;
    end
end
% Hydrocarbon Containing Layer
for j3= 4201:5200
    Dia5B_2(j3,1) = var4_6;
end
% Under burden Sediments Layer
for j4 = 5201:6000
    Dia5B_2(j4,1) = var4_5;
end
%----- Sparse Matrix C
% Sea Water Layer
for k1 = 1:400
    if k1 <= 200
        Dia5C_2(k1,1) = var4_4;
    elseif k1 >= 200 && k1 <= 300
        Dia5C_2(k1,1)= var4_2A1;
    else
        Dia5C_2(k1,1)= var4_2A2;
    end
end
% Over burden Sediments Layer
for k2 = 401:4200
    if k2 >= 401 && k2 <= 500
        Dia5C_2(k2,1) = var4_2A3;
    else
        Dia5C_2(k2,1) = var4_5;
    end
end
% Hydrocarbon Containing Layer
for k3= 4201:5200
    Dia5C_2(k3,1) = var4_6;
end
% Under burden Sediments Layer
for k4 = 5201:6000

```

```

        Dia5C_2(k4,1) = var4_5;
    end
%----- Sparse Matrix D
    % Sea Water Layer
    for l1 = 1:400
        if l1 <= 200
            Dia5D_2(l1,1) = var4_4;
        elseif l1 >= 200 && l1 <= 300
            Dia5D_2(l1,1)= var4_3A1;
        else
            Dia5D_2(l1,1)= var4_3A2;
        end
    end
    % Over burden Sediments Layer
    for l2 = 401:4200
        if l2 >= 401 && l2 <= 500
            Dia5D_2(l2,1) = var4_3A3;
        else
            Dia5D_2(l2,1) = var4_5;
        end
    end
    % Hydrocarbon Containing Layer
    for l3= 4201:5200
        Dia5D_2(l3,1) = var4_6;
    end
    % Under burden Sediments Layer
    for l4 = 5201:6000
        Dia5D_2(l4,1) = var4_5;
    end
%----- Sparse Matrix D
    % Sea Water Layer
    for m1 = 1:400
        if m1 <= 200
            Dia5E_2(m1,1) = var4_4;
        elseif m1 >= 200 && m1 <= 300
            Dia5E_2(m1,1)= var4_4A1;
        else
            Dia5E_2(m1,1)= var4_4A2;
        end
    end
    % Over burden Sediments Layer
    for m2 = 401:4200
        if m2 >= 401 && m2 <= 500
            Dia5E_2(m2,1) = var4_4A3;
        else
            Dia5E_2(m2,1) = var4_5;
        end
    end
    % Hydrocarbon Containing Layer
    for m3= 4201:5200
        Dia5E_2(m3,1) = var4_6;
    end

```

```

% Under burden Sediments Layer
for m4 = 5201:6000
    Dia5E_2(m4,1) = var4_5;
end
Main_mtxA = spdiags([Dig5A31,Dig5A21,Dia5A_2,Dig5A12,Dig5A13],...
    [-100 -1 0 1 100],var4_3,var4_3);
Main_mtxB = spdiags([Dig5A31,Dig5A21,Dia5B_2,Dig5A12,Dig5A13],...
    [-100 -1 0 1 100],var4_3,var4_3);
Main_mtxC = spdiags([Dig5A31,Dig5A21,Dia5C_2,Dig5A12,Dig5A13],...
    [-100 -1 0 1 100],var4_3,var4_3);
Main_mtxD = spdiags([Dig5A31,Dig5A21,Dia5D_2,Dig5A12,Dig5A13],...
    [-100 -1 0 1 100],var4_3,var4_3);
Main_mtxE = spdiags([Dig5A31,Dig5A21,Dia5E_2,Dig5A12,Dig5A13],...
    [-100 -1 0 1 100],var4_3,var4_3);
var_step = 100;
for var10_1 = 1:100
    if var10_1 == 1
        var10_2(var10_1) = 0;
    else
        var10_2(var10_1)= var_step + var10_2(var10_1-1);
    end
end
for k2 = 1:100
    var7_1(6000,1)= 0 ;
    var7_1(k2+200)= -var1_4*var1_3*var1_2*1000;

    if k2 >= 55 && k2 <= 65
        var_Elec_1 = qmr(Main_mtxA,var7_1,var1_5,var1_6);
        var_Elec_2 = qmr(Main_mtxB,var7_1,var1_5,var1_6);
        var_Elec_3 = qmr(Main_mtxC,var7_1,var1_5,var1_6);
        var_Elec_4 = qmr(Main_mtxD,var7_1,var1_5,var1_6);
        var_Elec_5 = qmr(Main_mtxE,var7_1,var1_5,var1_6);

    else

        var_Elec_1 = qmr(Main_mtxA,var7_1,var1_5,var1_6);
        var_Elec_2 = qmr(Main_mtxA,var7_1,var1_5,var1_6);
        var_Elec_3 = qmr(Main_mtxA,var7_1,var1_5,var1_6);
        var_Elec_4 = qmr(Main_mtxA,var7_1,var1_5,var1_6);

        var_Elec_5 = qmr(Main_mtxA,var7_1,var1_5,var1_6);

    end
    var_real1(k2)= real(var_Elec_1(2250));
    var_imag1(k2)= imag(var_Elec_1(2250));
    var_real2(k2)= real(var_Elec_2(2250));
    var_imag2(k2)= imag(var_Elec_2(2250));
    var_real3(k2)= real(var_Elec_3(2250));
    var_imag3(k2)= imag(var_Elec_3(2250));
    var_real4(k2)= real(var_Elec_4(2250));
    var_imag4(k2)= imag(var_Elec_4(2250));
    var_real5(k2)= real(var_Elec_5(2250));
    var_imag5(k2)= imag(var_Elec_5(2250));
    PhaseA1(k2)= abs(atan((var_imag1(k2)/var_real1(k2))));

```

```
PhaseA2(k2)= abs(atan((var_imag2(k2)/var_real2(k2))));  
PhaseA3(k2)= abs(atan((var_imag3(k2)/var_real3(k2))));  
PhaseA4(k2)= abs(atan((var_imag4(k2)/var_real4(k2))));  
PhaseA5(k2)= abs(atan((var_imag4(k2)/var_real5(k2))));  
end
```

APPENDIX –E

ALGORITHM FOR 1D FTCS SCHEME

APPENDIX –E

%:-----Forward Time Centre Space Model

%:-----Programs initializing

```

format long;clear; clc;clf
var_tol = 1e-20;
var_max = 200;
var_dsz = 10000;
var_com = sqrt(-1);
var_per = pi*4e-7;
var_fre = 0.25;
var_omg = 2*pi*var_fre;
var_con = 1.0;
var_unk = 22;
var_stp = 500;
% Solve equation in Temporal Domain.
var_t01 = 0;
var_t02 = 3;
var_nts = 40;          % Number of Time Step. M
var_nmp = 44;          % NUmber of Mesh Points.N
%Define the Mesh in Space.
var_nab6 = var_dsz/(var_nmp - 1);
var_nab7 = -1000:500:20500;
var_nab7 = var_nab7';
%Define the Mesh in Time.
var_nab8 = (var_t02-var_t01)/var_nts;
var_nab9 = var_t01:var_nab8:var_t02;
var_nab10 = var_nab8/(var_con*var_per*(var_stp^2));
%-----
var_nab1 = -2/((var_stp)^2);
var_nab2 = (var_nab1 + i*var_omg*var_per*var_con)*ones(var_unk,1);
var_nab3 = zeros(var_unk,1);
var_diag = ones(var_unk,1)/((var_stp)^2);
var_nab4 = var_unk;
var_nab5 = var_nab4;
Main_mtx_1 = spdiags([[var_diag],var_nab2,[var_diag]],[-1 0 1],
var_nab4, var_nab5);
Main_mtx_1(1,2) = (1/var_stp);
Main_mtx_1(1,1) = -(1/var_stp);
Main_mtx_1(var_nab4,var_nab5) = 1;
Main_mtx_1(var_nab4,var_nab5-1) = 0;
var_clmr = zeros(var_unk,1);
var_clmr(1,1) = -i*1000*var_per*var_omg;
Elect_2 = abs(qmr(Main_mtx_1,var_clmr,var_tol,var_max));
Elect_1 = zeros(44,1);
for m = 1:22
    Elect_1(22 + m)= Elect_2(m);
    Elect_1(m+1) = Elect_2(23-m);
end
hold on
plot(var_nab7, Elect_1)
for j=1:var_nts
    Elect_1(1,j+1) = Elect_1(1,j) + var_nab10*(Elect_1(2,j)-
2*Elect_1(1,j)+Elect_1(var_nmp-1,j));

for i=2:var_nmp-1
    Elect_1(i,j+1) = Elect_1(i,j) + var_nab10*(Elect_1(i+1,j)-

```

```

2*Elect_1(i,j)+Elect_1(i-1,j));
end
    Elect_1(var_nmp,j+1) = Elect_1(var_nmp,j) +
var_nab10*(Elect_1(2,j)-2*Elect_1(var_nmp,j)+Elect_1(var_nmp-1,j));
end
for x = 1:44
    var_nad(1,x) = Elect_1(x,var_nts+1);
end

plot(var_nab7, var_nad-0.1)

```


INDEX

Anisotropic, 9, 33, 35, 40, 46, 49, 88
Attenuation Constant, 18
Auxiliary potential function for Electric Field, 24
Auxiliary potential function for Magnetic Field, 23
Broadside survey Geometry, 6
Central Difference, 37, 38, 41, 54
Constitutive relation, 14, 24, 51
Current Density, 13, 14
Dipping, 68, 69, 70, 71, 73, 77
Electric Permittivity, 36,
EM geophysical data, 3
EM Geophysical Surveys, 1, 2
Far-Field Region, 30, 50
Finite Difference, 7, 12, 36, 38, 39, 49, 55, 74, 80, 82
Forward Modeling, 3, 6, 8, 12, 14, 16, 31, 36, 41, 47, 50, 63, 68
Forward time Central Space (FTCS), 7, 79
Geophysical Surveys, 1, 11, 15, 31, 50, 79, 82
Helmholtz Equation, 24,
Horizontal Electric dipole (HED), 5, 21, 23, 26
Horizontal magnetic Dipole (HMD), 5
Infinitesimal Dipole, 9, 21, 58, 68, 85
Inline Survey Geometry, 6
Inversion, 3, 8, 33, 41, 88
Isotropic, 9, 14, 33, 40,
Lorentz Conditions, 24, 25
Magnetic Permeability, 18, 36, 42, 61, 71
Magneto-hydrodynamic, 2
Magneto-telluric, 2, 3, 6, 21
Maxwell Equations, 2, 8, 9, 12, 14, 26, 28, 30, 36, 40, 50, 57, 67
Near Field Region, 50
Ohm's law, 14
Omni-directional Antenna, 29, 33, 58
Penetration Depth, 46, 59, 80
Phase Constant, 18, 19,
Phase Velocity, 15, 20, 78, 80
Phasor Diagram, 17
Poynting Vector, 21
Propagation Constant, 17,
Quasi-Static Equation, 8, 15, 32, 79
Reflection, 29, 30, 57
Reflected Electric Field, 31
Refracted Electric Field, 29,

Refraction, 9
Skin Depth, 8, 15, 17, 19, 49, 53
Stability factor in FTCS, 80
Staggered Grid, 7, 9, 36, 54, 67, 74
Taylor's Series, 36, 38, 41,
Telegraph equation, 16
Transverse Electric (TE), 5, 52
Transverse Magnetic (TM), 5, 52
Vertical Electric Dipole (VED), 5
Vertical Magnetic Dipole (VMD), 5
Volume Charge density, 13, 25
Wave Length, 15, 20